AD

AD 643 1

USAAVLABS TECHNICAL REPORT 66-1

TIP VORTEX CORE THICKENING FOR APPLICATION TO HELICOPTER ROTOR NOISE REDUCTION

CLEARINGHOUSE
FOR FEDERAL SCIENTIFIC AND TECHNICAL INFORMATION

Hardcopy	Microfiche		
$3.00	$ .65	89 pp	

ARCHIVE COPY

By

R. H. Spencer

H. Sternfeld, Jr.

B. W. McCormick

September 1966

U. S. ARMY AVIATION MATERIEL LABORATORIES
FORT EUSTIS, VIRGINIA

CONTRACT DA 44-177-AMC-215(T)
VERTOL DIVISION
THE BOEING COMPANY
MORTON, PENNSYLVANIA

Distribution of this document is unlimited

D D C
1967

Disclaimers

The findings in this report are not to be construed as an official Department of the Army position unless so designated by other authorized documents.

When Government drawings, specifications, or other data are used for any purpose other than in connection with a definitely related Government procurement operation, the United States Government thereby incurs no responsibility nor any obligation whatsoever; and the fact that the Government may have formulated, furnished, or in any way supplied the said drawings, specifications, or other data is not to be regarded by implication or otherwise as in any manner licensing the holder or any other person or corporation, or conveying any rights or permission, to manufacture, use, or sell any patented invention that may in any way be related thereto.

Disposition Instructions

Destroy this report when no longer needed. Do not return it to the originator.

ACCESSION for
CFSTI WHITE SECTION ☑
DDC BUFF SECTION ☐
UNANNOUNCED
JUSTIFICATION Per Statement on Doc
BY
DISTRIBUTION/AVAILABILITY CODES
DIST. AVAIL. and/or SPECIAL
1

DEPARTMENT OF THE ARMY
U. S ARMY AVIATION MATERIEL LABORATORIES
FORT EUSTIS, VIRGINIA 23604

This report, which is published for the exchange of information and the stimulation of ideas, has been reviewed by the U. S. Army Aviation Materiel Laboratories. The results, although technically sound, are considered qualitative in nature because the data do not reflect the influence of aspect ratio which changes with rotor tip configuration.

TASK 1P121401A14801
CONTRACT DA 44-177-AMC-215(T)
USAAVLABS TECHNICAL REPORT 66-1
September 1966

TIP VORTEX CORE THICKENING FOR APPLICATION TO HELICOPTER ROTOR NOISE REDUCTION

R-403A

by

R. H. SPENCER
H. STERNFELD, JR.
B. W. McCORMICK

Prepared by
VERTOL DIVISION
THE BOEING COMPANY
Morton, Pennsylvania

for
U.S. ARMY AVIATION MATERIEL LABORATORIES
FORT EUSTIS, VIRGINIA

Distribution of this
document is unlimited

ABSTRACT

Helicopter rotor noise levels are sharply increased when a rotor blade intercepts the rolled-up tip vortex trailed by a previous blade. This study deals with modification of the induced velocity structure of the vortex from both an analytical and an experimental standpoint. Ten tip configurations were evaluated in a wind tunnel, to determine the magnitude of velocity reduction achievable. Results indicated that the maximum velocities induced within the vortex core could be reduced to about 12 percent of those for a standard tip (formed by revolving the tip airfoil section about the chordline and typical for many present generation helicopters). Drag data measured on the model wing for each blade tip indicates that most configurations adversely affect performance.

FOREWORD

This report was prepared by R. H. Spencer and H. Sternfeld, Jr., Vertol Division, The Boeing Company, and Dr. B. W. McCormick, Aero Engineering Associates, State College, Pennsylvania, under Contract DA 44-177-AMC-215(T). It was sponsored by the U.S. Army Aviation Materiel Laboratories under the technical cognizance of Mr. J. Yeates and Mr. J. McGarvey.

The wind-tunnel study was conducted at Pennsylvania State University under the direction of Dr. McCormick, with the assistance of Mr. G. L. Sanders. Dr. McCormick was a major contributor to the final text.

CONTENTS

	Page
ABSTRACT	iii
FOREWORD	v
LIST OF ILLUSTRATIONS	viii
LIST OF SYMBOLS	xi
SUMMARY	1
INTRODUCTION	3
ANALYSIS OF PROBLEM	4
TEST PROGRAM	10
Design of a Wing To Simulate a Rotor Blade	10
Description of Tip Shapes	12
Instrumentation	19
Experimental Procedure	27
DISCUSSION OF RESULTS	29
Vortex Measurements	29
Photographic Tuft-Grid Studies	44
Evaluation of Vorticity from Test Data	58
Vortex Strengths	58
Performance Evaluation	62
Noise-Level Measurements	66
Interpretation of Results	66
CONCLUSIONS	73
REFERENCES	74
DISTRIBUTION	75

ILLUSTRATIONS

Figure		Page
1	Comparison of Maximum Induced Velocities . . .	2
2	Induced Velocity Distribution Through Vortex .	5
3	Vorticity Distribution Through Vortex	7
4	Intersection of Trailed Vortex Filament and Rotor Blade - Tandem Rotor Helicopter	9
5	Wing and Rotor Blade Bound-Circulation Distributions	11
6	Wing and Wing Tips	13
7	Test Setup	20
8	Probe-Positioning Mechanism	22
9	Vortex Probe	23
10	Vane Calibration	25
11	Effect of Finite Vane Size on Measured Angular Velocity	26
12	Vorticity Distributions in Trailing Vortex for Several Tip Configurations	30
13	Vorticity Distributions Through Vortex Sheet Measured 1 Inch Downstream From Standard Tip	30
14	Exponential Fit of Data	33
15	Comparison of Potential Vortex With Experiment and With Lamb's Solution	34
16	Effect of Angle of Attack on Vorticity Distribution for Standard Tip.	35
17	Variation of Maximum Vorticity With Angle of Attack	36

Figure		Page
18	Variation of Vortex Width With Angle of Attack	37
19	Measured Values of Exponent n	38
20	Influence of Tip-Cavity Fairing on Vorticity Distribution	39
21	Influence of Tip-Cavity Fairing on Maximum Vorticity.	40
22	Effect of Blowing on Vorticity Distribution ($\alpha = 12^{\circ}$)	42
23	Effect of Blowing on Vorticity Distribution ($\alpha = 6^{\circ}$)	43
24	Effect of Blowing on Velocity Distribution .	45
25	Comparison of Photographic Tuft-Grid Study With Vortex Measurements	46
26	Tuft-Grid Study: Standard, Honeycomb, and 40%-Porous Tips at 12° Angle of Attack, $z = 2c$, $V = 75$ mph	47
27	Tuft-Grid Study: Effect of Angle of Attack and Tip Shape on Vorticity (8 sheets). . . .	48
28	Tuft-Grid Study at Varying Distances Downstream From the Standard Tip (2 sheets). . .	56
29	Contours of Constant Rotational Speeds in Four Transverse Planes Downstream From Standard Tip	59
30	Contours of Constant Rotational Speeds 1 and 2 Inches Downstream From 40%-Porous Tip (Sheet 1 of 2)	60
	Contours of Constant Rotational Speeds 30 Inches Downstream From 40%-Porous Tip (Sheet 2 of 2)	61

Figure		Page
31	Circulation Determined From Vorticity Compared With Circulation Determined From Lift Measurements	63
32	Sound Levels in Wakes of Eight Tip Configurations	65
33	Effect of Angle of Attack on Noise Level of 20%-Porous Tip	67
34	Tangential Component of Induced Velocity Variation for Ten Tip Configurations	68
35	Maximum Induced Velocity as a Function of α .	69
36	Lift and Drag Data	71

LIST OF SYMBOLS

Dimensional Quantities

c	in.	Blade Chord
c_o	in.	Midspan Chord
ΔHP	hp	The Increment in Horsepower Required for a Helicopter to Hover with Blade Tip Configurations Other Than Standard
k	miles/hr	Constant of Proportionality
L	lb	Wing Lift
Q_v	in.-lb	Aerodynamic Torque Produced by Vanes
r	in.	Radius
r_v	in.	Tip Radius of Vanes
R	in.	Rotor Blade Radius
R_f	in.	Radius of Hypothetical Vortex at $\omega = 0$
R_j	lb	Jet Reaction of Blown Tip
S	in.^{2}	Wing Area
t	sec	Time
u	ft/sec	Velocity Component in Direction of r
V	ft/sec	Free-Stream Velocity
v	ft/sec	Velocity Component Normal to u
v_i	ft/sec	Tangential Component of Induced Velocity in Vortex
v_j	ft/sec	Velocity of Jet
w	in.	Width of Vortex
x,y,z	in.	Coordinates of Vortex Probe Location

q	lb/ft^2	Dynamic Pressure
α	deg	Angle of Attack
Γ	$in.^2/sec$	Strength of Circulation
Γ_o	$in.^2/sec$	Maximum Strength of Circulation
γ	$in.^2/sec$	Strength of Vortex
ζ	rad/sec	Vorticity
ζ_o	rad/sec	Maximum Vorticity
Δp	in.Hg	Gage Pressure of Blown Tip
ρ	$lb\text{-}sec^2/ft^4$	Density of Air
ρ_j	$lb\text{-}sec^2/ft^4$	Density of Air Jet
ω_f	rad/sec	Angular Velocity of Fluid
ω_v	rad/sec	Angular Velocity of Vanes
ω_o	rad/sec	Maximum Angular Velocity of Fluid at Vortex Center
Ω	rad/sec	Rotor Angular Velocity
ν	ft^2/sec	Kinematic Viscosity

Nondimensional Quantities

AR	Aspect Ratio
C_D	Drag Coefficient
C_{D_o}	Drag Coefficient at $C_L = 0$
C_L	Lift Coefficient
C_ℓ	Section Lift Coefficient
C_Q	Blowing Coefficient

b	Number of Rotor Blades
M_{cr}	Critical Mach Number
n	Exponential Constant
R_e	Reynolds Number
ε	Oswald's Span Efficiency Factor
η	Calibration Coefficient
θ	Polar Coordinate Notation

SUMMARY

The sheet of vorticity shed by a lifting wing rolls into a vortex at the tip with a large-magnitude induced velocity component. The system persists for long times and, in the case of a rotating wing, takes the form of an elongated helix. When intercepted by a trailing blade of sufficient tip speed, the resultant velocity can exceed the critical Mach number and produce shock waves periodically. The objective of this study was to modify the induced velocity distribution of the trailed vortex without any appreciable effect on the strength of the bound circulation on the blade, and to accomplish this for a minimum performance penalty.

The approach taken in this study was to achieve the desired reduction in velocity profile by changes to the configuration of the rotor blade tip, and a wind-tunnel study was conducted to investigate this approach. A measure of vorticity was used to determine the velocity profile behind 10 blade tip configurations. In addition, photographs were made of a tuft grid mounted downstream of the blade with each of the 10 tips mounted.

The results of the program demonstrate that the velocity induced within a trailed vortex system can be significantly reduced by modification of the tip configuration (Figure 1). This reduction can be achieved with no overall loss of vortex strength, although an increase in the overall drag force may result in appreciable performance penalties. For example, predictions indicate that an additional 4 percent of the power required to hover a medium transport helicopter is required for operation with a tip which has 20 percent of its planform area open.

Since the trailing vortex does not become a significant noise source until it is intersected by a rapidly moving body, both vortex velocity and space location must be defined in order to predict the generated noise. Where possible, the high-velocity vortex system should not intersect high-velocity rotor blades. However, when this condition is unavoidable, modification of the induced velocity profile of the vortex appears to be a feasible approach to rotor noise reduction.

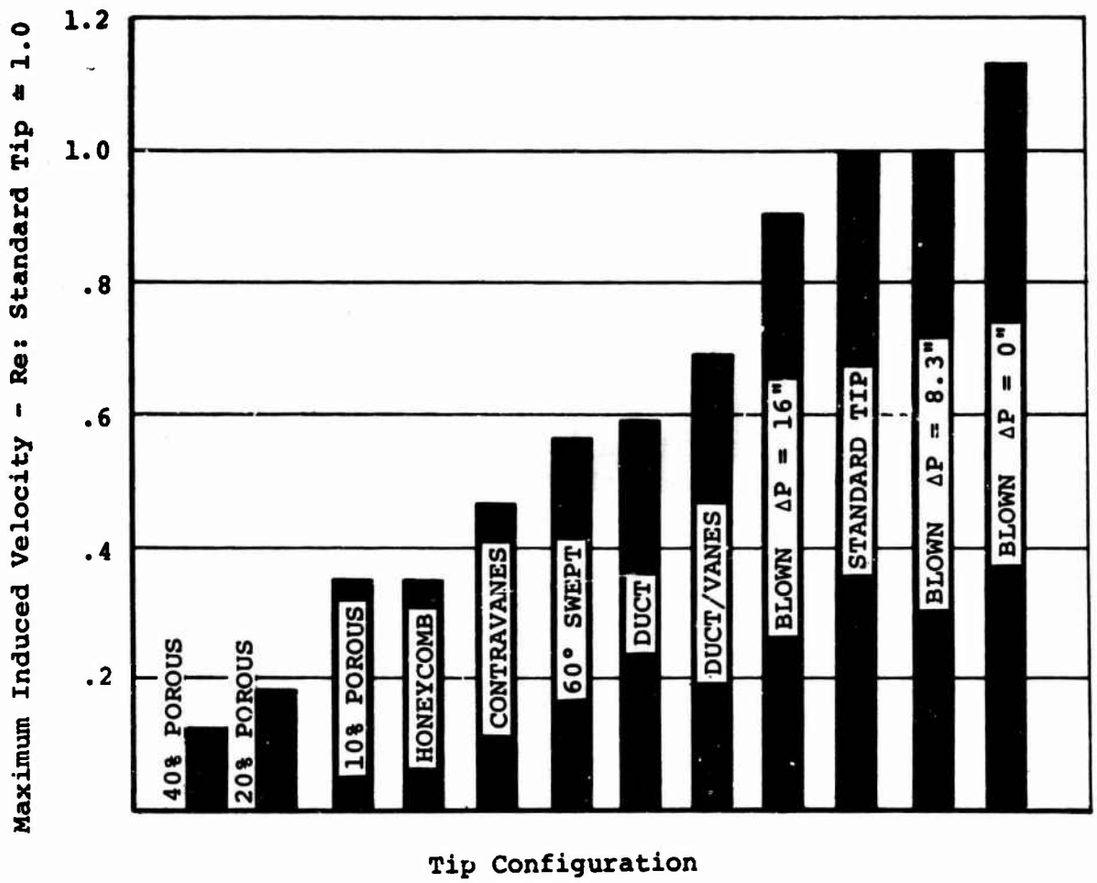

Figure 1. Comparison of Maximum Induced Velocities

INTRODUCTION

The subject study is part of a program to reduce helicopter rotor blade noise. The objective was to develop an optimum rotor tip shape aimed at thickening the tip vortex core, thus reducing the total flow over the blade to a value less than M_{cr} for that section.

Rotor noise can be considered to fall into four mai.. categories:

1. Rotational noise which is due to the pressure distribution associated with aerodynamic lift and which has time and space variation, with respect to a fixed observer, due to blade rotation.

2. Vortex induced noise which arises from viscous effects such as profile drag, boundary layer turbulence, flow instabilities, etc.

3. Blade slap which results from large angle-of-attack changes and flow separation. This noise is not associated with a specific azimuth location, but may occur over a range of stations.

4. Blade banging due to the pressure disturbance of a shock wave, resulting from the intersection of a trailed vortex filament and a rapidly moving body such as a rotor blade. This component of rotor noise is highly directional and occurs only at the rotor azimuth where a blade intercepts a trailed vortex filament.

This study deals with a solution for the last type of noise only. When it occurs, rotor bang becomes the predominant external noise associated with the aircraft and plays a major role in determining aircraft detectability and in setting the low-frequency end of the internal noise spectrum. One of the approaches to reducing this last source consists of reducing the induced velocity of the vortex. Since vortex strength is proportional to lift, no method which results in a weakening of the vortex can be considered. There remains, however, the possibility of enlarging the core diameter such that the velocity profile through the vortex is reduced in magnitude.

ANALYSIS OF THE PROBLEM

Any finite lifting surface produces a trailing system of vortices as a consequence of the lift distribution decreasing to zero at the tips. This system usually takes the form of a sheet immediately behind the surface which rolls up rapidly into discrete vortices. In the case of a wing, vortices trail from each tip, while for a rotor blade, the vortices trail from the hub and the tip.

In proximity to a trailing vortex, the resultant velocity is due to (1) the free-stream and (2) a tangential component produced by the circulation around the vortex. The tangential velocity can be appreciable in magnitude, i.e., of the order of the free-stream velocity. In fact, for two-dimensional potential flow, the tangential velocity varies inversely with the radius according to

$$v_i = \frac{\Gamma}{2\pi r} \tag{1}$$

where

v_i is the tangential component of induced velocity.
r is the radial dimension of the vortex.
Γ is the circulation.

Hence, at the center the velocity would be infinite. In a real fluid, however, v_i behaves as shown in Figure 2. Toward the center, the velocity increases almost inversely proportional to the radius. Nearer the center, however, the velocity begins to depart from potential theory, reaching a maximum, and then decreasing to zero precisely at the center. The central region where the velocity distribution departs from the potential distribution is referred to as the core. Like the thickness of a boundary layer, the size of the core is not well-defined since the actual velocity distribution approaches asymptotically to the potential distribution. Within the core, the velocity of the circulatory irrotational flow varies inversely with the radius, somewhat like a rigid body.

From Figure 2 it is seen that for the simplified core rotating as a rigid body,

$$v_1 = \omega r_1 = \frac{\Gamma}{2\pi r_1}$$

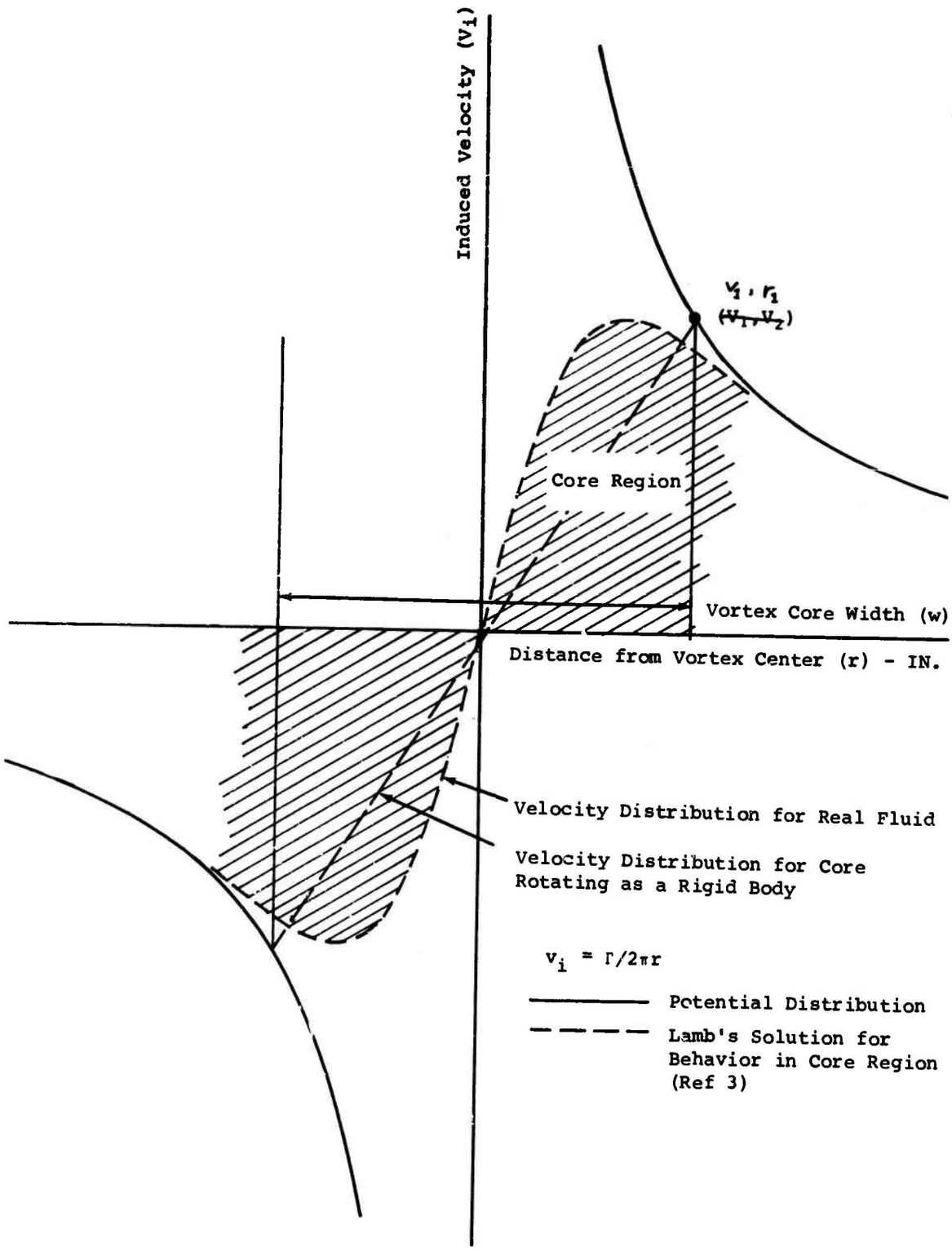

Figure 2. Induced Velocity Distribution Through Vortex

where ω is the core rotational speed. Thus, the circulation may be thought of as the area πr_1^2 rotating at an angular velocity of 2ω.

The variation of the vorticity through a vortex core is presented in Figure 3. The vorticity is defined as the curl of the velocity vector and in polar coordinates can be written as

$$\zeta = \frac{\partial v}{\partial r} + \frac{v}{r} - \frac{1}{r}\frac{\partial u}{\partial \theta} \tag{2}$$

where

u is the velocity component in the r direction.

v is the velocity component normal to u.

For axisymmetrical flow where $\frac{\partial u}{\partial \theta} = 0$, Equation 2 becomes

$$r\zeta dr = rdv + vdr$$

or

$$r\zeta dr = d(rv).$$

Integration yields

$$\int_0^R d(rv) = \int_0^R r\zeta dr$$

$$rv\Big|_0^R = \int_0^R r\zeta dr$$

$$Rv = \int_0^R r\zeta dr$$

$$v = \frac{1}{R}\int_0^R r\zeta dr \text{ where } v = f(R)$$

$$v(R) = \frac{1}{R}\int_0^R r\zeta dr . \tag{3}$$

The curve of Figure 2 is obtained from the curve of Figure 3 by applying Equation 3.

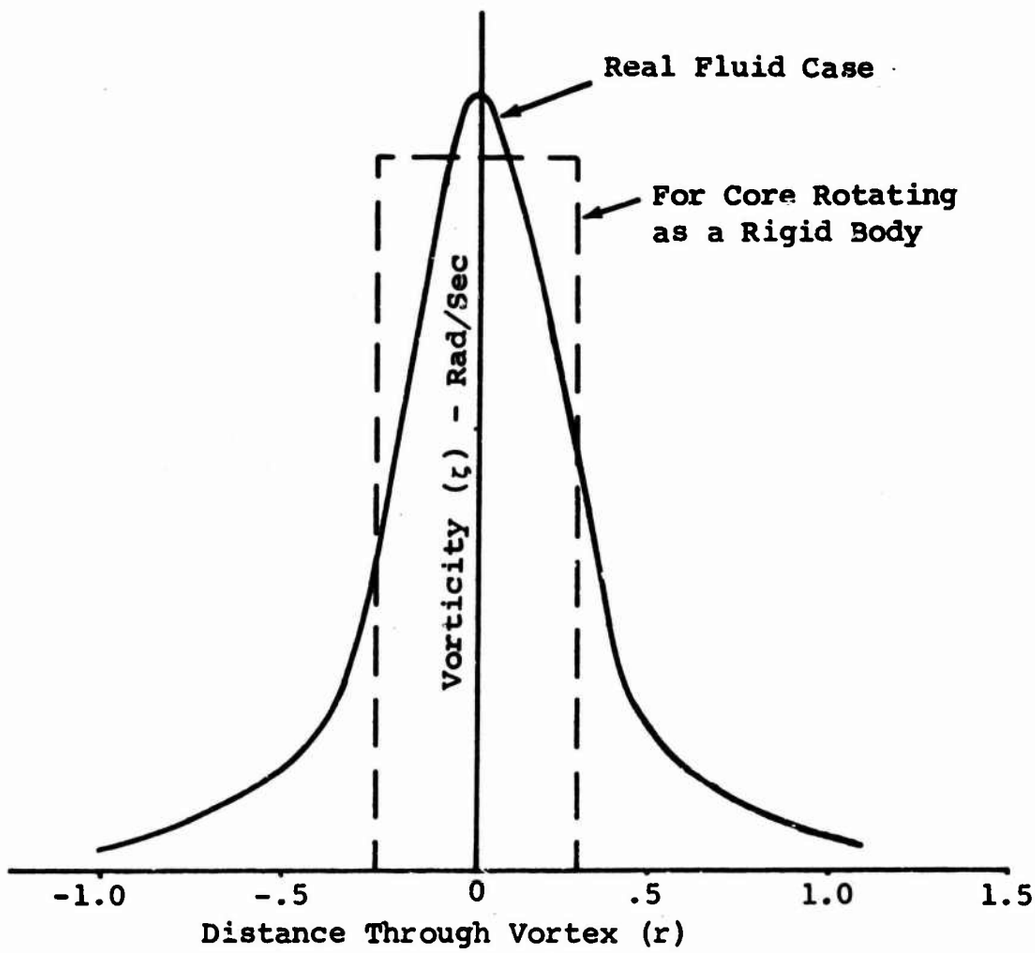

Figure 3. Vorticity Distribution Through Vortex

Typical test results show that for a free-stream velocity of 75 miles per hour (110 feet per second), the maximum tangential velocity around the vortex for a particular wing attains a maximum of about 52 feet per second, 47 percent of the free-stream velocity. A full-scale tip speed of 700 feet per second and a forward velocity component of 200 feet per second produce a resultant velocity of 900 feet per second for an advancing blade and would induce a tangential velocity within the vortex as high as 420 feet per second. A trailing blade piercing this vortex would momentarily experience a velocity as high as 1320 feet per second. This is illustrated schematically in Figure 4a. Furthermore, it will be shown later that the vortex interaction problem may be even more severe than this because the velocity induced by the vortex at higher Reynolds numbers may be equal to the free-stream velocity. Thus the relative wind over a rotor blade having a high tip speed can momentarily exceed the speed of sound if the blade tip intersects a vortex trailed from a previous rotor blade.

The result of exceeding Mach 1 would be an increase in the oscillating pressures and magnitude of unsteady aerodynamic forces. Also, depending on how the blade intersects the vortex, it could experience an appreciable change in the angle of attack as each section passes through the upwash and downwash of the core. Two possible paths intersecting a vortex, either of which would produce undesirable effects, are pictured in Figure 4b. If the section pierces the center of the vortex, its angle of attack changes ± 45 degrees with some increase in its resultant velocity. If the section cuts tangentially to the circle, for maximum velocity, it still experiences a substantial variation in angle of attack, but the primary effect is a change in the resultant velocity.

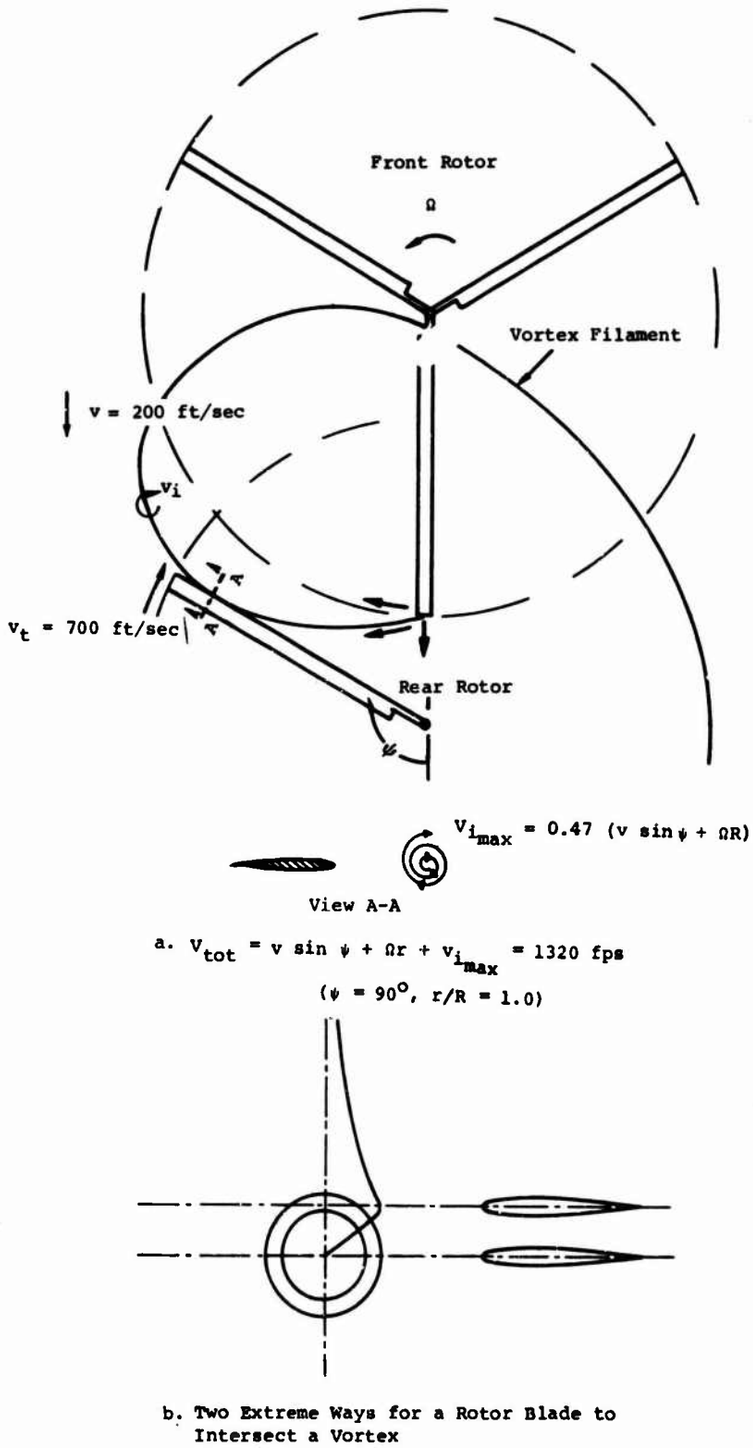

Figure 4. Intersection of Trailed Vortex Filament and Rotor Blade - Tandem Rotor Helicopter

TEST PROGRAM

DESIGN OF A WING TO SIMULATE A ROTOR BLADE

Since it was not practical to survey the geometry of the trailing vortex of a rotating blade, a fixed wing was designed to have the distribution of bound circulation similar in form to that calculated for a CH-46A rotor blade in hover. Only the circulation over the outer 14 percent of the rotor blade was simulated since calculations showed that the circulation was shed over this portion. This statement may be clarified by reference to Figure 5.

The rotor blade being simulated employs a 0012 airfoil section with a solidity of 0.0573, a 13.5-degree pitch angle at the root, and an 8.36-degree twist. Goldstein's vortex theory of propellers was used to predict the bound circulation distribution, Γ , along the blade. Initially, the distribution was numerically analyzed for its harmonic content and the Fourier coefficients were substituted into lifting-line theory to design the wing. However, this procedure was not satisfactory because the Fourier series converged very slowly. Instead, from the radius for maximum Γ outward, the circulation was assumed to be shed in the form of small but finite trailing vortices. This portion of the blade was divided into 2000 increments with a vortex shed from the center of each increment having a strength equal to the change in Γ over the increment. These vortices were then assumed to trail from a wing, and the induced velocities were calculated along the wing. In this way, the twist of the wing was calculated to produce the same Γ distribution as that of a rotor blade. The entire procedure was programmed through an IBM 7074 digital computer.

The geometry of the model wing was scaled from the outboard 14 percent of a full-scale CH-46A rotor blade - a span of 42 inches. Since the CH-46A has a rectangular planform with a blade radius and chord of 25 feet and 18 inches, respectively; the 42-inch outboard section to be simulated has an aspect ratio of 4.68. Because of wind tunnel size restrictions, the model wing semi-span was limited to 18 inches, with a corresponding chord of 7.7 inches.

$$AR = \frac{\text{Span}}{\text{Chord}} = \left(\frac{2\text{x}42}{18}\right)_{\substack{\text{Rotor}\\ \text{Tip}}} = \left(\frac{2\text{x}18}{7.7}\right)_{\substack{\text{Model}\\ \text{Wing}}} = 4.68$$

Since the twist of the model wing to simulate rotor loading would have been less than 1 degree over 80 percent of the span, the model wing was constructed with no twist.

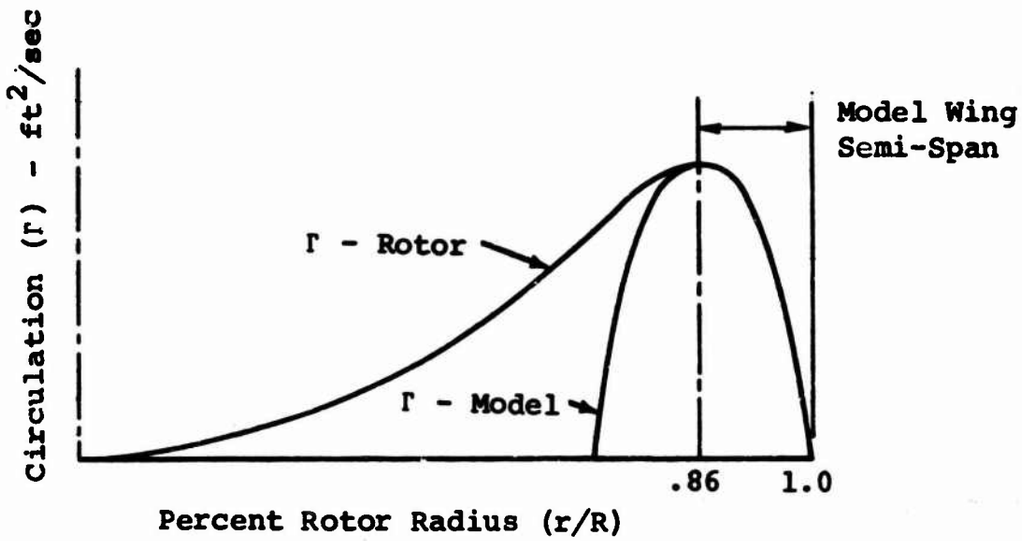

Figure 5. Wing and Rotor Blade Bound-Circulation Distributions

The velocity induced by an isolated vortex is given by Equation 1. From the Kutta-Joukowski law, this can be rewritten in the form

$$\frac{v_i}{V} = \frac{1}{4\pi} \frac{c}{r} C_L \tag{4}$$

where for the wing or rotor blade section having the maximum bound circulation,

C_L is the lift coefficient.

c is the chord.

V is the free-stream velocity.

v_i is the tangential component of the induced velocity at vortex radius, r.

Hence, if the geometry is scaled so that c/r for the model and rotor remains constant, then v_i/V would be proportional to C_L. One might thus expect that the maximum value of v_i/V which can be obtained with the model wing would equal the maximum value of v_i/V for the rotor. This would be true except that the size of the vortex core depends on the thickness of the boundary layer on the wing, which in turn is a function of the Reynolds number. The ratio c/r will thus not be a constant but will increase with increasing Reynolds number. Reference 1 presents strong experimental evidence showing v_i/V to vary with the two-tenths power of the Reynolds number. This implies that the core size increases with increasing boundary layer thickness (assuming the boundary layer to be turbulent). Since most of the experimental results reported herein are taken at 110 feet per second while the full-scale rotor blade tip speed is 690 feet per second, the ratio, c/r, should possibly be increased by a factor of

$$R_e^{0.2} \propto \left(\frac{V_{f.s}}{V_{mod}} \times \frac{C_{f.s.}}{C_{mod}} \right)^{0.2} = \left(\frac{690}{110} \times \frac{18}{7.7} \right)^{0.2} = 1.7.$$

DESCRIPTION OF TIP SHAPES

Figure 6 shows the wing and each of the 10 tips investigated.

Standard Tip - A tip with a shape generated by revolving an airfoil section around the blade tip chord.

60°-Sweptback Tip - A tip swept back 60 degrees from the leading edge was tested, since Reference 3 reported that delta wings have favorable tip-vortex cavitation characteristics.

Honeycomb Tip - A circular duct, 1.625 inches in diameter and 1.5 inches long, was positioned 1.128 inches behind the standard tip so that the tip vortex passed through its center. The duct was filled with an expanded honeycomb with approximately 0.1-inch cell size.

Duct Tip - A hollow duct, approximately 1 inch in diameter, was mounted on the tip of the wing. It was anticipated that the duct would have an end-plate effect and also enlarge the core radius.

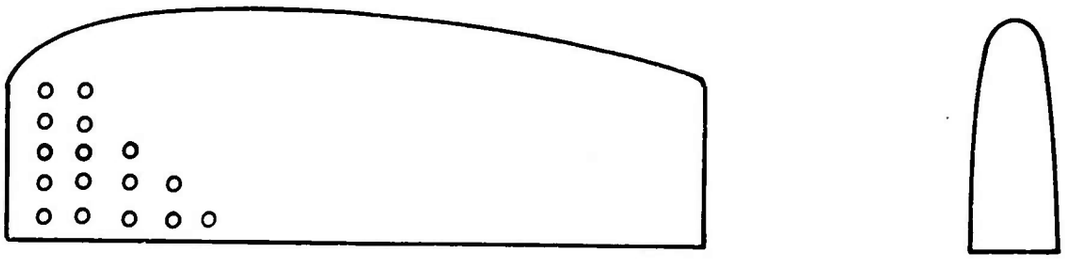

10%-Porous

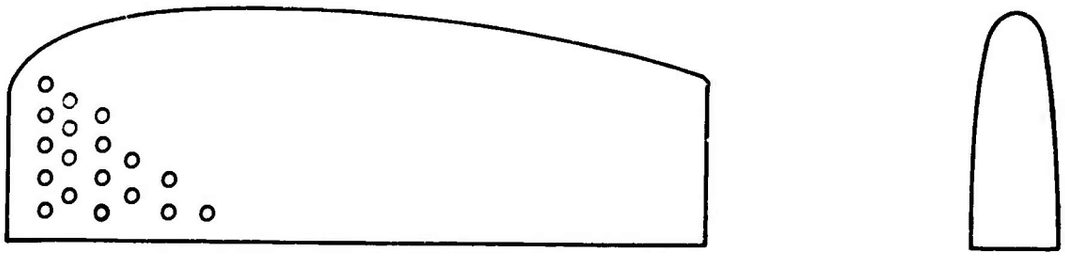

20%-Porous

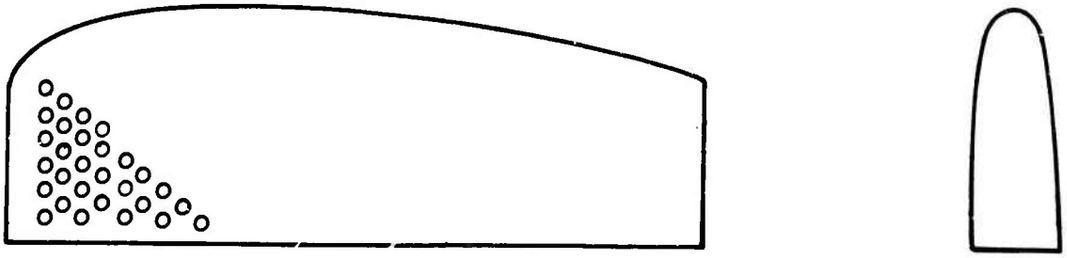

40%-Porous

Figure 6. Wing and Wing Tips (Sheet 1 of 6)

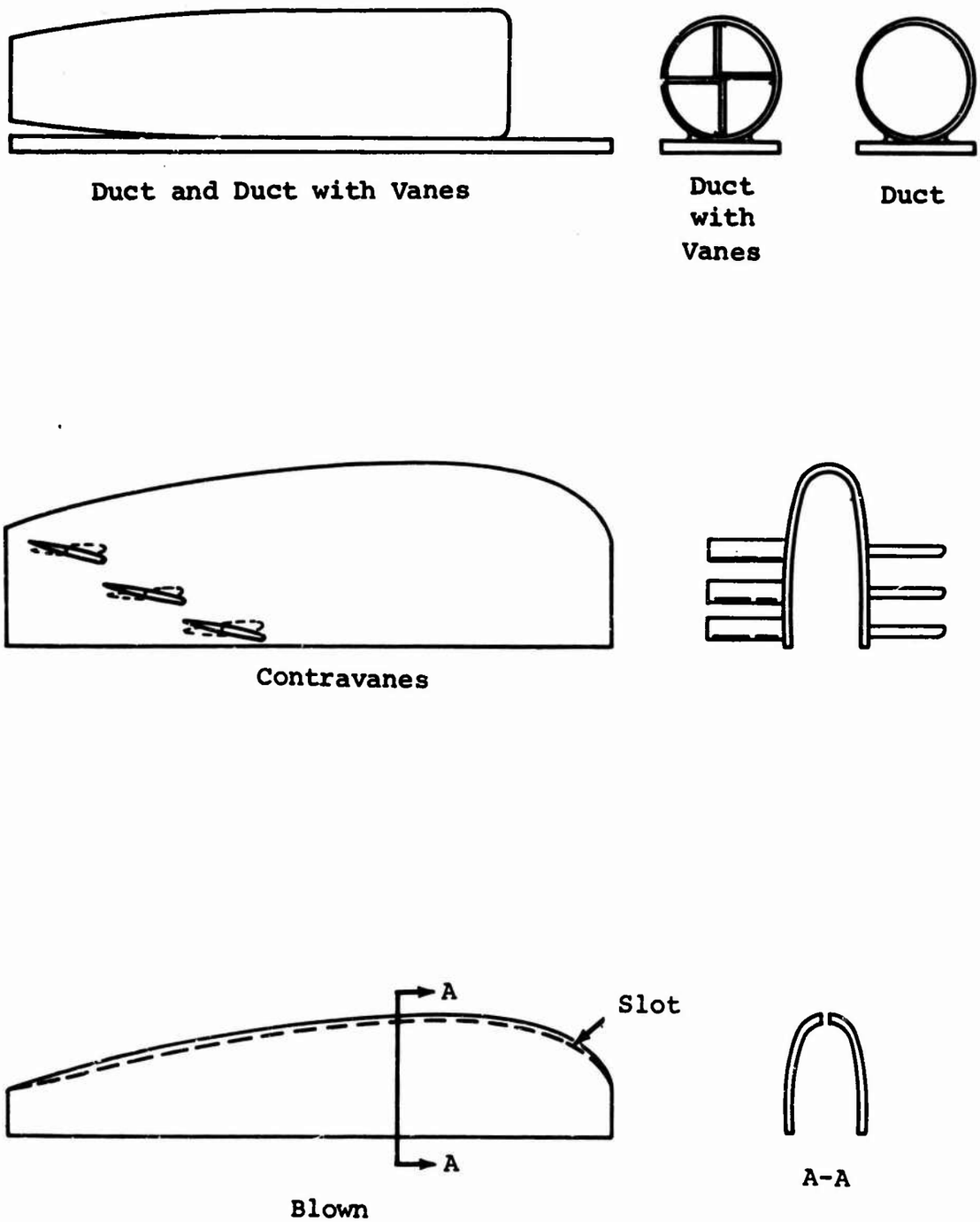

Figure 6. Wing and Wing Tips (Sheet 2 of 6)

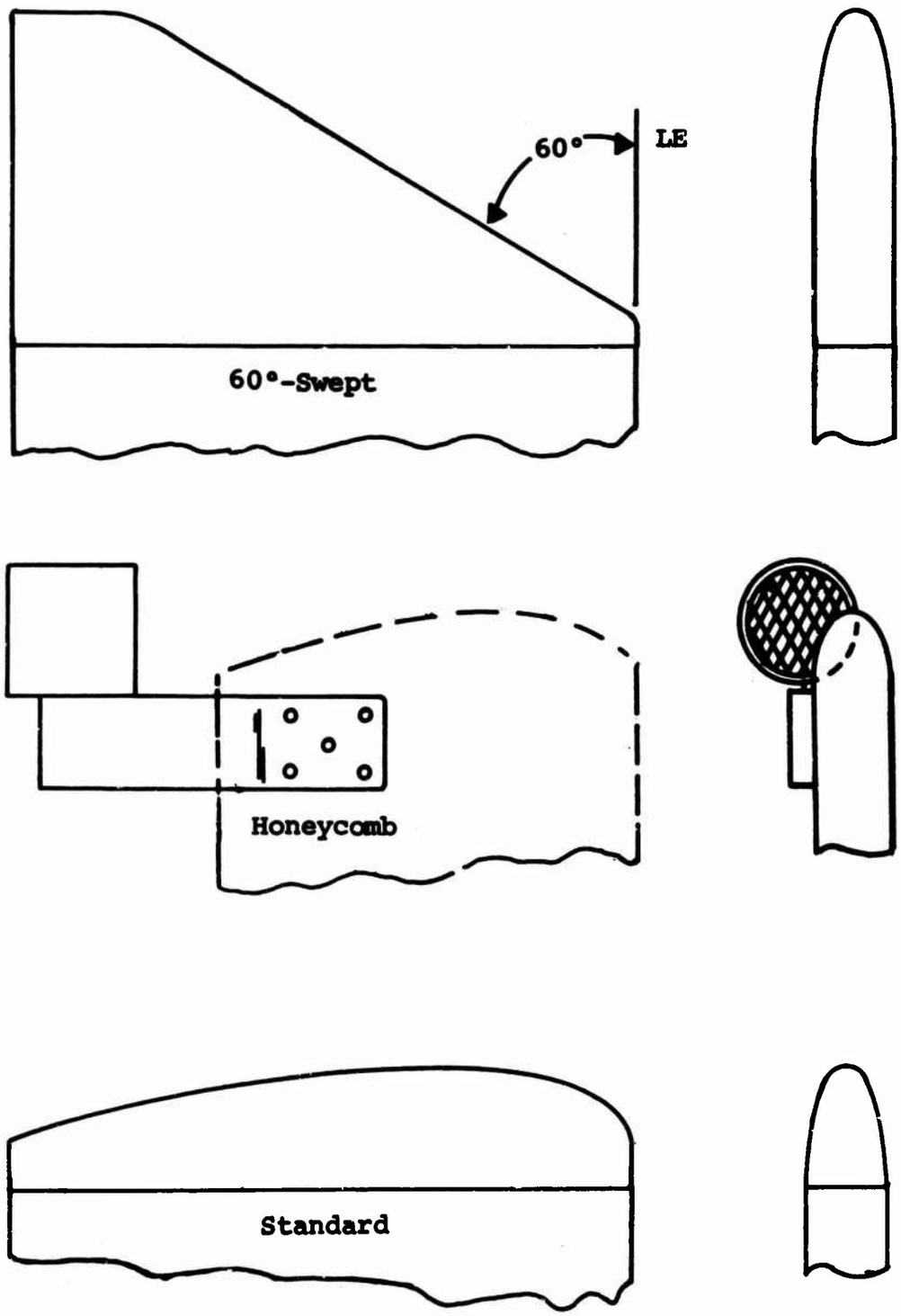

Figure 6. Wing and Wing Tips (Sheet 3 of 6)

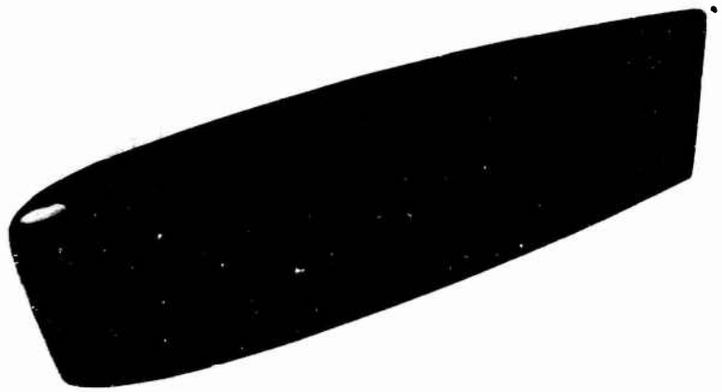

10%-Porous

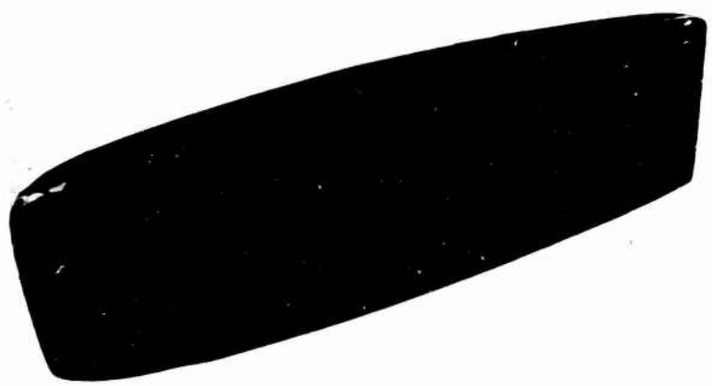

20%-Porous

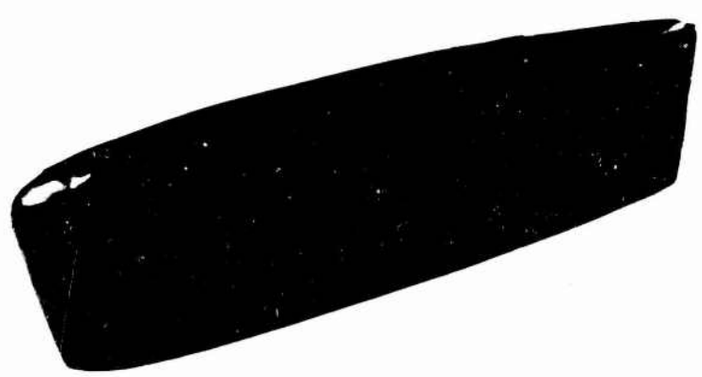

40%-Porous

Figure 6. Wing and Wing Tips (Sheet 4 of 6)

Duct/Duct with Vanes

Contravanes

Blown

Figure 6. Wing and Wing Tips (Sheet 5 of 6)

60°-Swept

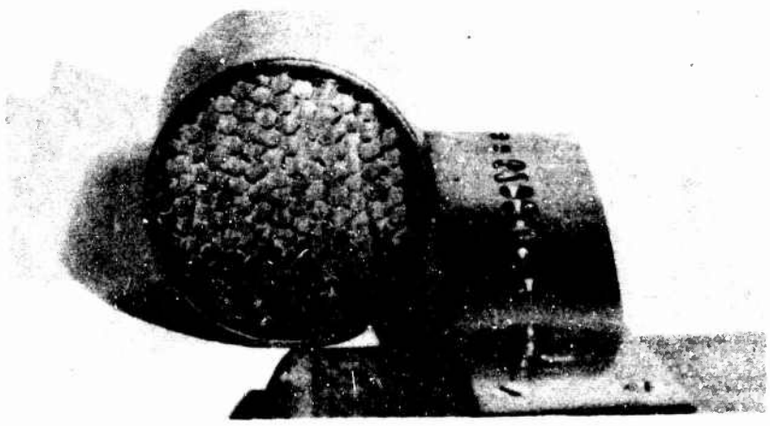

Honeycomb

Standard

Figure 6. Wing and Wing Tips. (Sheet 6 of 6)

Duct/Vanes Tip - Vanes were installed within the hollow duct noted above to produce a rotation of the flow through the duct opposite to that of the tip vortex.

Contravane Tip - A set of small vanes was mounted on each side of a tip projecting into the flow. An angle of attack was selected that would produce a rotation opposite to that of the tip vortex.

10%-Porous Tip - This is 2.75-inch extension of the standard tip. The extended portion was drilled with 0.0935-inch-diameter holes spaced at 0.25 inch on centers to give a porosity of 11 percent (actual) or 10 percent (nominal) of the planform area.

20%-Porous Tip - This is also a 2.75-inch-extension tip, but 0.1285-inch-diameter holes were drilled to give a porosity of 20.8 percent (actual) or 20 percent (nominal) of the planform area.

40%-Porous Tip - This is again a 2.75-inch-extension tip, but the holes were spaced closer to give a porosity of 41.6 percent (actual) or 40 percent (nominal) of the planform area.

Blown Tip - This has a 0.005-inch-wide chordwise slot along its outboard edge from which a jet of air is blown spanwise to thicken the core of the trailing vortex.

INSTRUMENTATION

Testing was performed in The Pennsylvania State University's subsonic wind tunnel operated by the Department of Aeronautical Engineering. The tunnel has a 3-by-3-foot test section, is equipped with a six-component strain-gage balance, and is capable of speeds up to 300 miles per hour. Most of the testing, however, was performed at 75 miles per hour. The semi-wing was mounted vertically and supported from the balance. The test setup is shown in Figure 7.

A probe-positioning mechanism designed and made specifically for this investigation (see Figure 8) was installed behind the wing so that the vortex probe could be positioned accurately in rectangular coordinates. With this mechanism, the position of the probe can be determined within 0.002 inch.

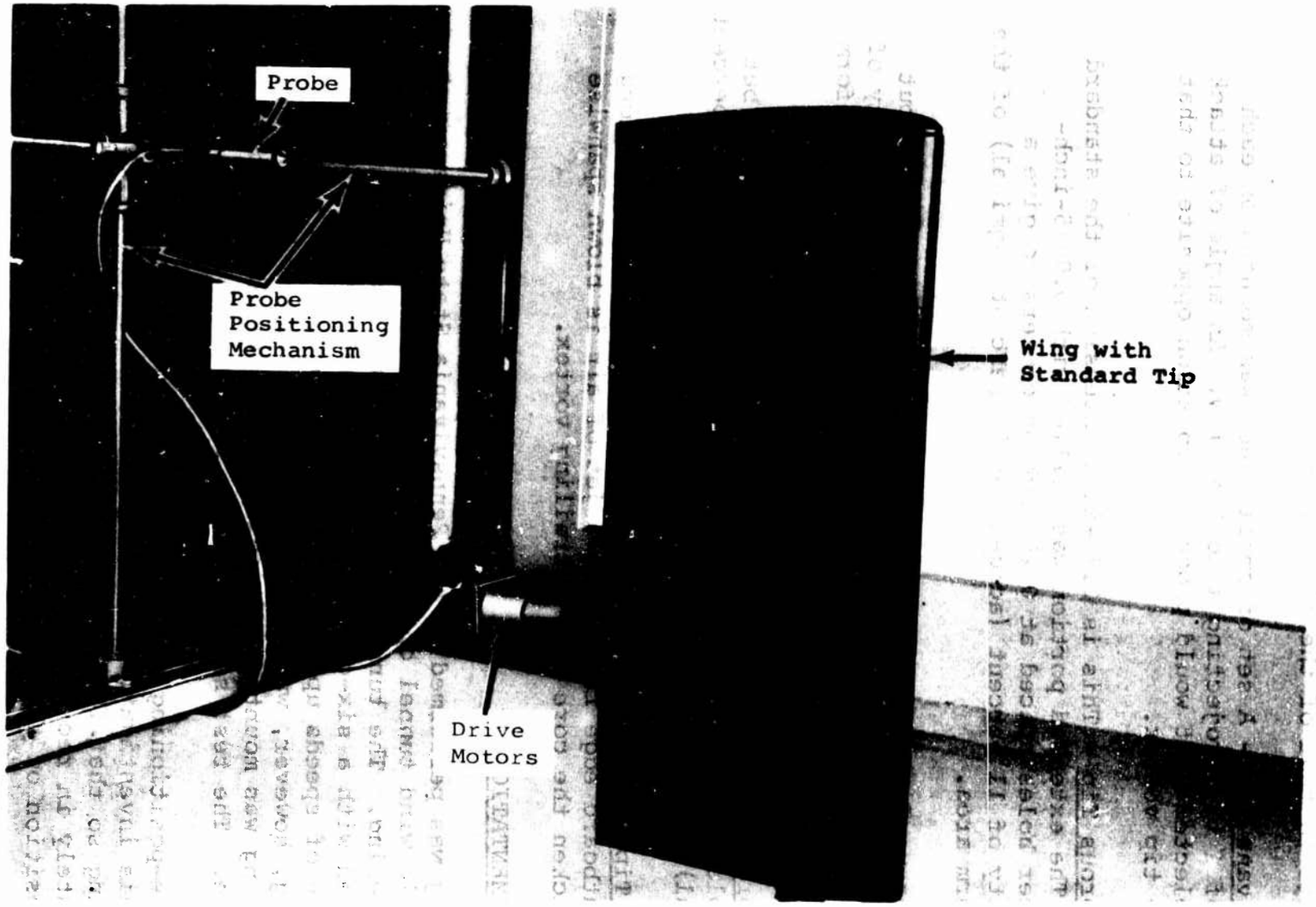

Figure 7. Test Setup

The vortex probe used to measure the vorticity in the trailing vortex system is shown in Figure 9. A set of unpitched vanes with 0.375-inch outside diameter is mounted on a shaft supported in jewel bearings. The shaft has a lucite-filled hole through it, permitting light transmission. On one side of the shaft, in line with the hole, is a grain-of-wheat bulb; on the other side is a photovoltaic detector similar to those used for punched-card readout. As the shaft rotates, a voltage pulse is generated twice every revolution. The pulses are counted electronically to give an accurate measurement of the rotational speed of the vanes. The probe is described in detail in Reference 2.

The vortex probe has given very satisfactory performance but must be corrected for two types of error in order to obtain absolute numbers: the error due to friction and windage losses, and the error due to its finite size. Unfortunately, changing the diameter of the vanes has an opposing effect on these two errors. The error due to friction and windage losses can be determined experimentally by calibrating the vane. Ideally this would mean generating a known vorticity field and inserting the probe into it, but this was too difficult. Instead, an attempt was made to calibrate the probe by rotating the probe mechanism in the wind tunnel. If there were no friction, the vanes would not rotate, and rotational speed of the vanes relative to that of the housing should be a measure of the error due to friction. However, even this procedure proved difficult to perform accurately. Because of the high rotational speeds required, very slight misalignments led to excessive centrifugal force on the bearings and, hence, excessive frictional losses. After considerable deliberation and interpretation of the data, the following relationship was arrived at. It was concluded that the aerodynamic torque produced by the rotating vanes will be proportional to

$$Q_v \propto (\omega_f - \omega_v) V$$

where

ω_f is the angular velocity of the fluid,

ω_v is the angular velocity of the vanes,

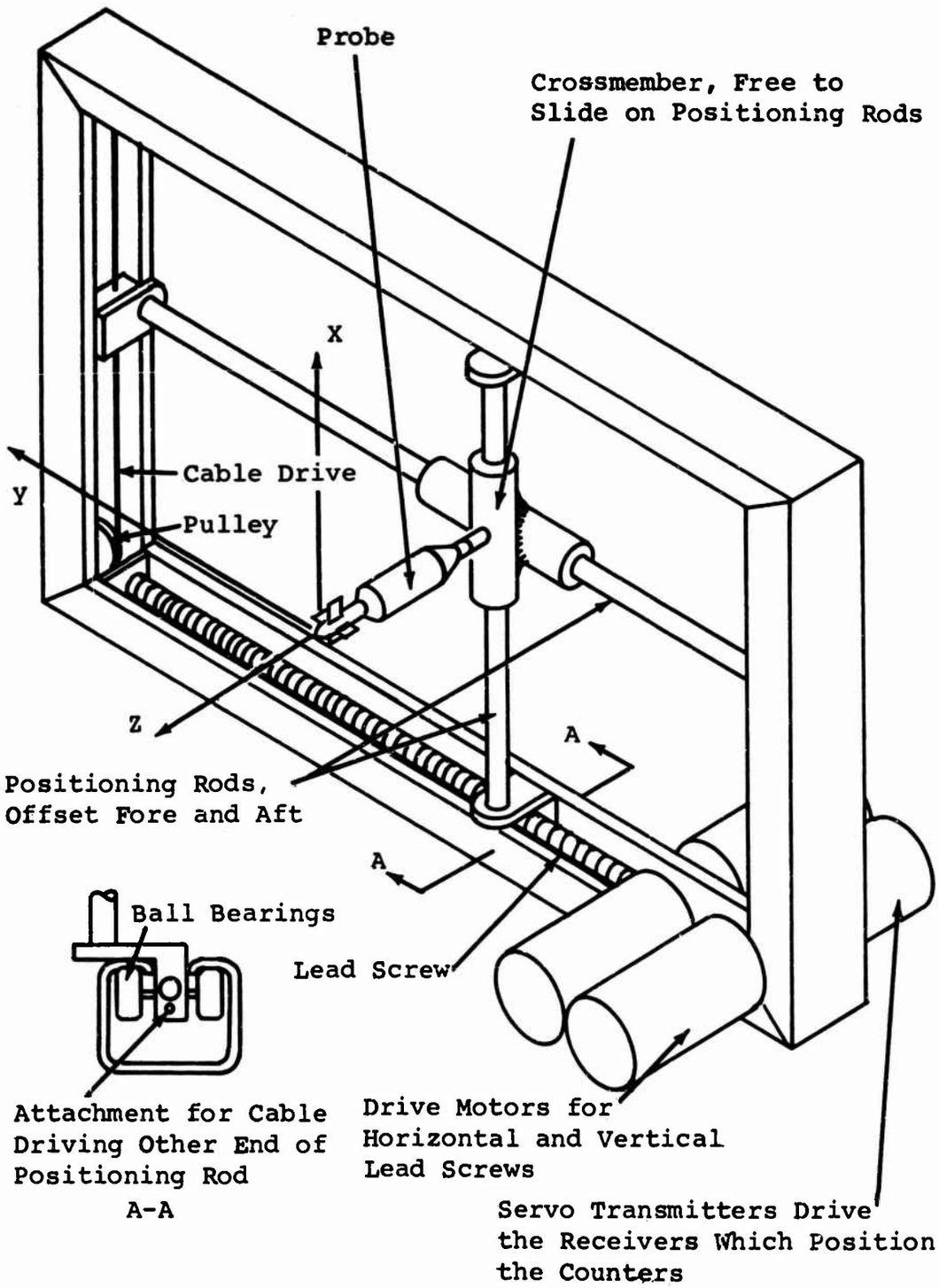

Figure 8. Probe-Positioning Mechanism

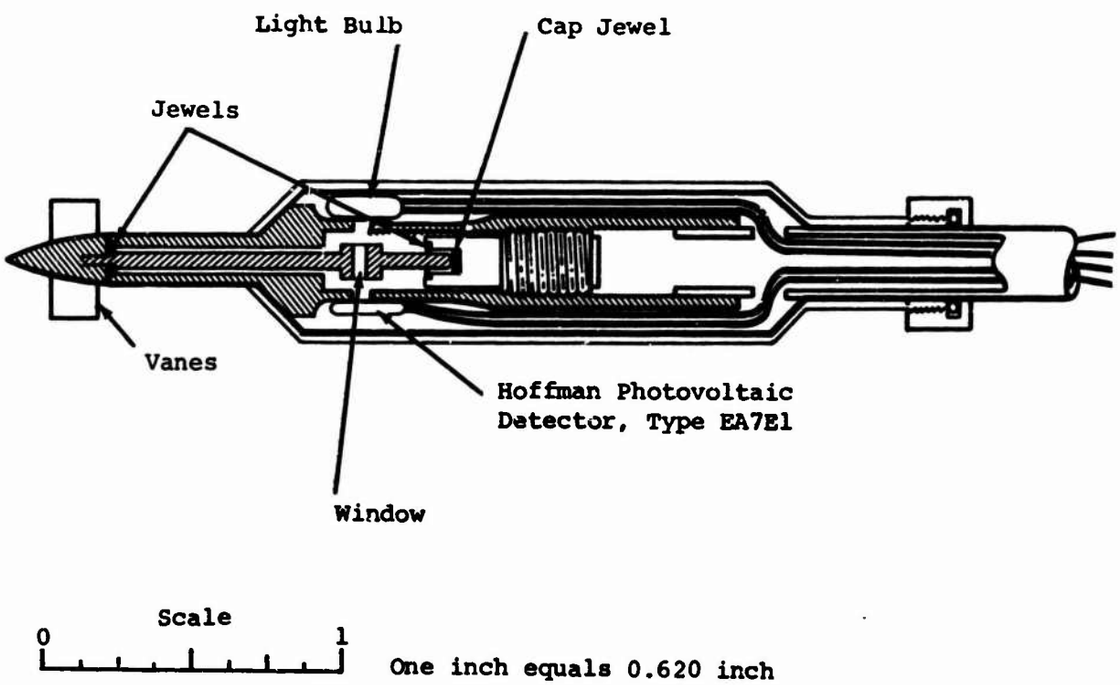

Figure 9. Vortex Probe

r_v is the tip radius of the vanes,

Q_v is the aerodynamic torque,

providing

$$(\omega_f - \omega_v) r_v << V.$$

The frictional torque opposing the rotation of the shaft will be proportional to ω_v. Hence, equating the two torques gives

$$\eta = \frac{\omega_v}{\omega_f} = \frac{1}{1 + k/V}$$

where

k is a constant of proportionality.

This constant has been determined experimentally to be approximately 18.8 with V in miles per hour, resulting in the vane calibration shown in Figure 10. This curve can be expected to hold for all the results of this experiment.

The error due to friction and windage losses is minimized in the design of the probe by (1) the use of jewel bearings lubricated periodically, (2) filling the window in the shaft with a clear plastic, (3) using as large a vane diameter as can be tolerated, and (4) allowing sufficient clearance between the shaft and the internal surfaces of the housing. At 75 miles per hour, the speed at which most of the testing was performed, the vane rotates at about 80 percent of the true angular velocity.

The error due to the finite size of the vane is illustrated in Figure 11. A hypothetical linear variation of ω_f with radius is shown. With the vane centered in the fluid rotation, the angular velocity of the vane will be less than the angular velocity of the fluid, ω_o. For an ideal frictionless vane, it can be shown that

$$\frac{\omega_v}{\omega_o} = 1 - \frac{1}{2}\frac{r_v}{R_f} \qquad (5)$$

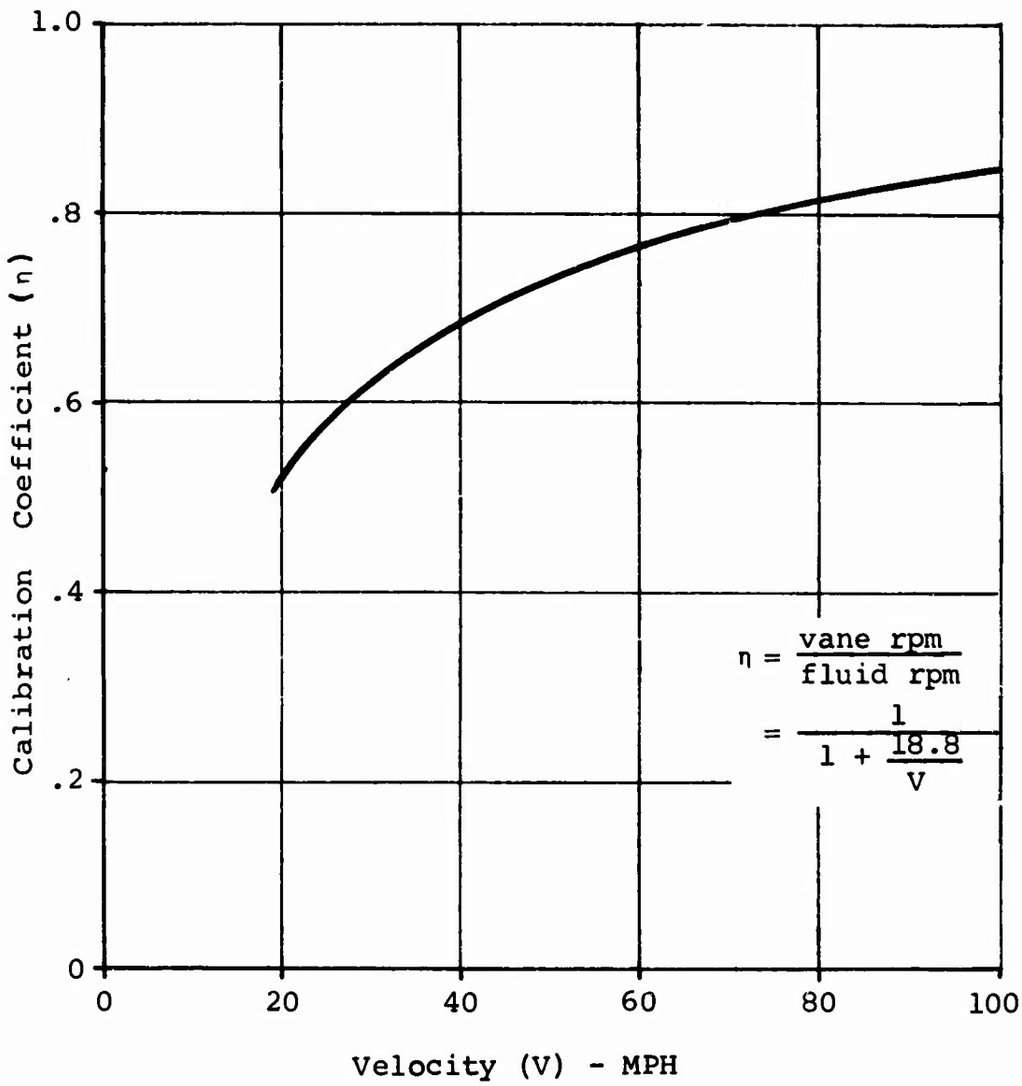

Figure 10. Vane Calibration

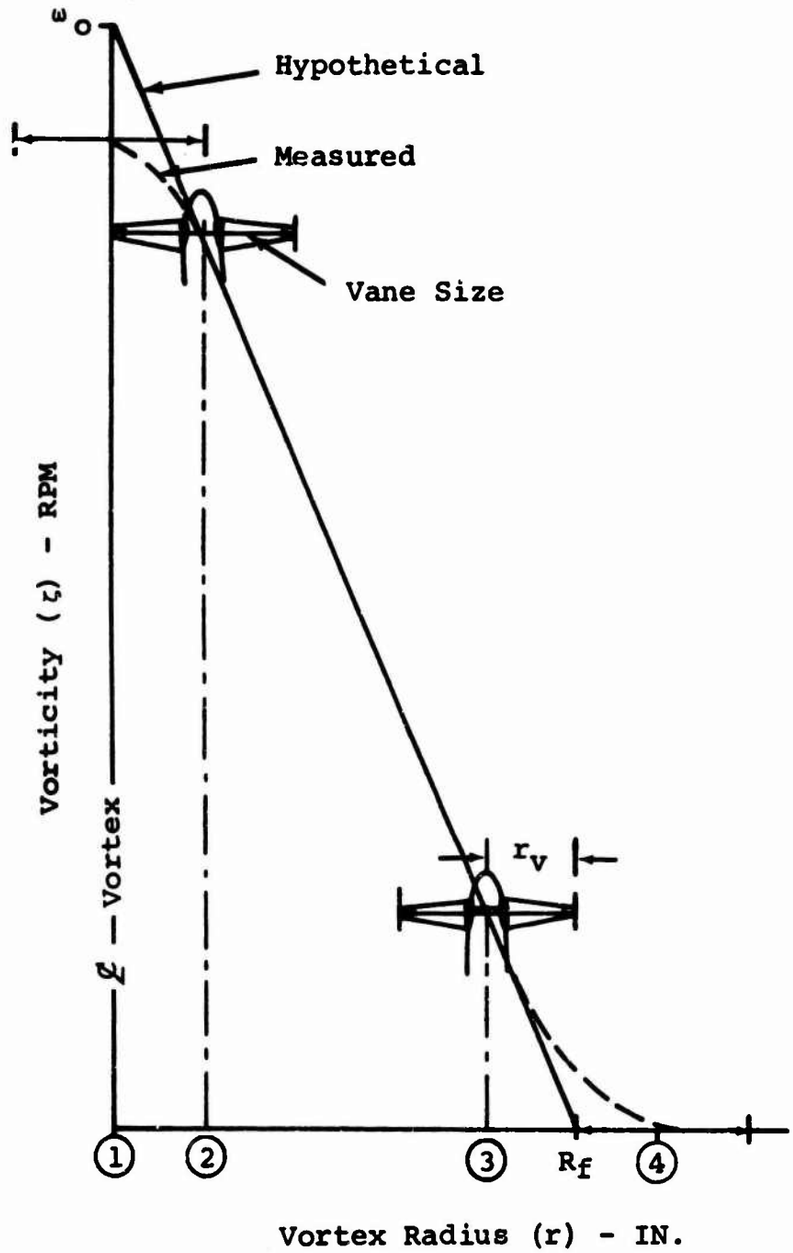

Figure 11. Effect of Finite Vane Size on Measured Angular Velocity

where

ω_v is the angular velocity of the vanes.

ω_o is the angular velocity of the fluid at vortex center.

r_v is the tip radius of the vanes.

R_f is as shown on Figure 11.

As the vane moves outward from 1 (Figure 11), its angular velocity approaches the true angular velocity of the fluid, attaining that value at a radius equal to the vane radius 2 where the vanes lie within the linear range of ω_f. It will continue to read the correct ω as r is increased until 3 is reached. For radii greater than this radius, e.g., 3 4, the angular velocity of the vanes will be greater than ω of the fluid.

The correction for finite size depends on the change of the slope of the ω versus r curve. If the slope is decreasing with radius, the vane ω will be low, as shown in Figure 11. Unfortunately, the correction for finite vane size can be calculated with assurance only for the condition of Equation 5.

In addition to the measurements made with the vortex probe, visual observations of the flow in the vortex system were made by means of a tuft grid behind each tip, and sound recordings were made using a microphone located downstream of the model.

EXPERIMENTAL PROCEDURE

After installing a wing and tip combination in the tunnel, lift and drag curves were obtained. Then, with the probe well clear of the wing, a calibrating device was installed on the probe. This device consisted of a fixed set of pitched vanes mounted ahead of the probe to impart a rotation to the flow. The tunnel speed was then brought up to 75 miles per hour, and the output from the vanes was noted. Calibrations were performed periodically as a check on the friction losses in the probe bearings. It was found that the calibration of the probe would remain unchanged for four or five hours of testing and then would suddenly, and noticeably, change by an appreciable amount. A drop of jeweler's oil on each bearing always returned the probe to its original calibration.

If the check on the probe calibration proved satisfactory, the calibrator was removed, the wing was positioned to the desired angle of attack, and the tunnel was again brought up to speed. For measurement downstream of the wing, where the vorticity had rolled up into a single vortex, it was sometimes difficult to locate the vortex. This was accomplished by tracing the path of the vortex with a tuft on the end of a rod from the trailing edge aft to the survey plane. The probe was then positioned sideways (y direction) and vertically (x direction) until a nearly maximum count was displayed on the electronic counter. Then holding y constant, a run was made by varying z in small increments, usually 0.075 inch.

The count per second (CPS) read from the electronic counter was then plotted against the z reading and, if far enough downstream, would give a curve symmetrical about a z value. This z value was then set, and another run made in the y direction would thus pass through the center of the vortex. For some tests, to be discussed later, the maximum rotational speed did not occur at the center. In runs where the vortex motion was not axisymmetrical, such as close behind the wing, it was necessary to survey varying y values for several fixed z values.

DISCUSSION OF RESULTS

VORTEX MEASUREMENTS

Unless specifically stated, all the data to be presented are uncorrected for probe calibration or finite probe size, with a few exceptions to be noted later. Since the data are compared on a relative basis between configurations, the validity of data interpretation is unaffected. An attempt was made to hold the lift values constant between wing configurations with different aspect ratios, although some variations did occur. It is nevertheless felt that the resulting effect on induced vorticity did not adversely affect the overall interpretation of results. A comparison of the measured vorticity distributions for several of the tips is presented in Figure 12. The data points have been omitted for clarity. Close behind the wing, it was necessary to make passes at each of several values of z from which contour maps for constant values of angular velocity could be constructed. Figure 13 presents typical results from such passes 1 inch behind the trailing edge of the wing equipped with the standard tip.

In view of the similarity of the data for the various tips presented in Figure 12, it was decided to fit the data taken through the rolled-up trailing vortices by a parametric family of curves. Lamb (Reference 3) presents a solution for a potential vortex in which viscosity is allowed to act for time $t > 0$. Rouse and Hsu (Reference 4) recently argued that Lamb's model requires an infinite amount of energy to establish the potential vortex. However, this objection is removed when one considers two equal and opposite rotating trailing vortices. Rouse and Hsu propose that the trailing vortex be visualized as having been generated by a rotating cylinder of finite circulation but zero radius. Considering the manner in which the tip vortex is actually generated, the choice of model on which to base reduction of the data is probably academic. This report will use Lamb's developments.

In terms of the vorticity for axisymmetrical flow, the Navier-Stokes equations of motion can be written in polar coordinates

$$\frac{\partial \zeta}{\partial t} = \nu\left(\frac{\partial^2 \zeta}{\partial r^2} + \frac{1}{r}\frac{\partial \zeta}{\partial r}\right) . \tag{6}$$

The above can be integrated for the vorticity to give

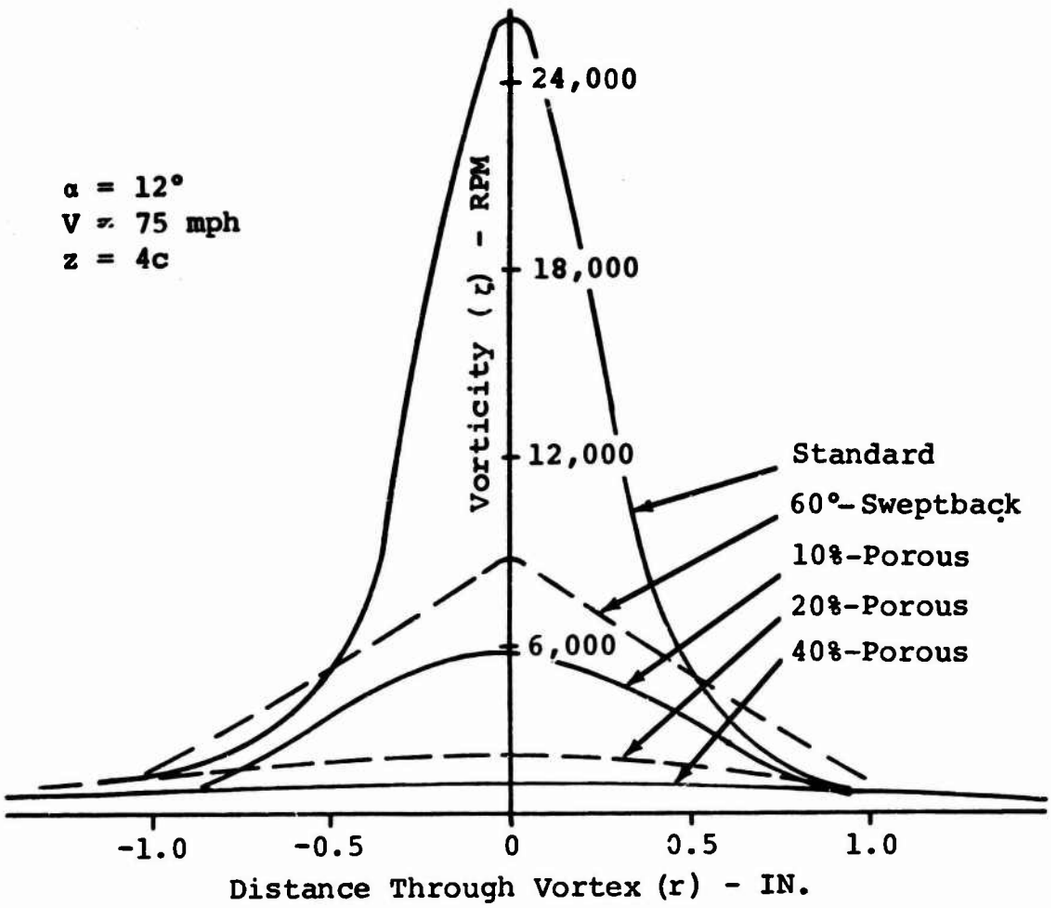

Figure 12. Vorticity Distributions in Trailing Vortex for Several Tip Configurations

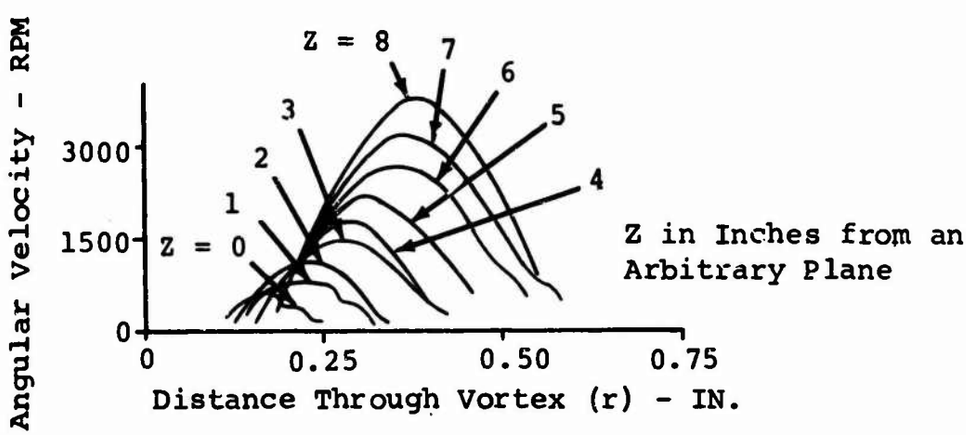

Figure 13. Vorticity Distributions Through Vortex Sheet Measured 1 Inch Downstream From Standard Tip

$$\zeta = \frac{\gamma}{4\pi\nu t} e^{-\frac{r^2}{4\nu t}} . \tag{7}$$

Substituting Equation 7 into Equation 3, the velocity around the vortex becomes

$$v = \frac{\gamma}{2\pi r}\left(1-e^{-\frac{r^2}{4\nu t}}\right) . \tag{8}$$

The above is Lamb's solution. To fit the data obtained here, it was decided to use an exponential similar to Equation 7; namely,

$$\zeta = \zeta_o e^{-(r/w)^n \log_e 2} \tag{9}$$

where

ζ_o is the maximum vorticity.

w is the "width" of the vortex, defined as twice the value of r for which $\zeta = \zeta_o/2$.

A computer program was written whereby, given ζ_o and values of ζ for two values of r, the constants w and n were obtained. These were then inserted by the computer into Equations 9 and 3 and numerically integrated to obtain v as a function of r. The circulatory strength of the vortex can be obtained by performing the following:

$$\gamma = \int_0^\infty 2\pi r\zeta dr. \tag{10}$$

Using Equation 9, this integral can be shown to reduce to

$$\gamma = \left(\frac{2\pi\zeta_o w^2}{n(\log_e 2)^{2/n}}\right) \Gamma\left(\frac{2}{n}\right) \tag{11}$$

where

$$\Gamma\left(\frac{2}{n}\right) = \text{gamma function of argument } \left(\frac{2}{n}\right).$$

For the particular case where n = 2.0,

$$\gamma = \frac{\pi w^2}{\log_e} \zeta_0 \tag{12}$$

and

$$v = \frac{w^2 \zeta_0}{2r \log_e} \left[1-e^{-(r/w)^2 \log_e 2}\right]. \tag{13}$$

With only a few exceptions, Equation 9 could be made to fit the experimental data closely by the proper choice of n. The maximum angular velocity at the vortex center ω_o is numerically equal to half of the maximum vorticity, ζ_0 . Figure 14 shows a typical fit of the exponential curve to the test data points, and Figure 15 illustrates the correlation of the induced velocities calculated from the test data by evaluating Equation 7 and substituting in Equation 3. Both the goodness of fit of Figure 14 and the excellent correlation between test points and calculated potential vortex velocity at the edge of the core confirm the validity of the test data.

The effect of angle of attack on ω_o, w, and n is shown in Figures 16 through 19 for the standard, porous, and 60-degree-sweptback tips. The nature of the variation of ω_o and α seems to depend on the tip shape. For the porous and 60-degree-sweptback tip, ω_o decreases with α at angles above 6 degrees. Because of this behavior, it is difficult to predict the vortex geometry for an arbitrary tip shape. Notice that w increases nearly linearly with α and that the values of n all lie between 1.5 and 2.0.

The critical dependence of the vortex geometry on irregularities in the tip shape is demonstrated by Figure 20. The two vorticity distributions were obtained with the same tip; but for the "cavities-faired" curve, the two attachment-screw holes were filled with clay. Unfaired holes reduce vorticity at the center of the vortex. This phenomenon seems to depend on both α and velocity. Figure 21 presents the maximum vorticity as a function of the tunnel velocity for the standard tip at 12 degrees. These data were obtained before the importance of fairing the tips was realized by searching for the maximum rpm

WING TIP	CONSTANTS FOR $\alpha = 6°$			CONSTANTS FOR $\alpha = 12°$		
	w (Inches)	ω_o (Rad/Sec)	n	w (Inches)	ω_o (Rad/Sec)	n
Standard	0.215	1940	1.51	0.302	2670	1.58
60°-Sweptback	0.200	1160	1.21	0.576	817	1.40
Honeycomb	0.468	220	2.22	0.688	402	1.70
Duct	0.217	864	1.28	0.227	1650	0.83
Duct/Vanes	0.294	770	1.66	0.303	1480	0.90
Contravanes	-----	----	----	0.447	748	1.02
10%-Porous	0.218	1290	1.41	0.550	534	1.71
20%-Porous	0.842	66	1.84	0.712	195	1.83
40%-Porous	0.917	63	2.20	0.866	104	2.27

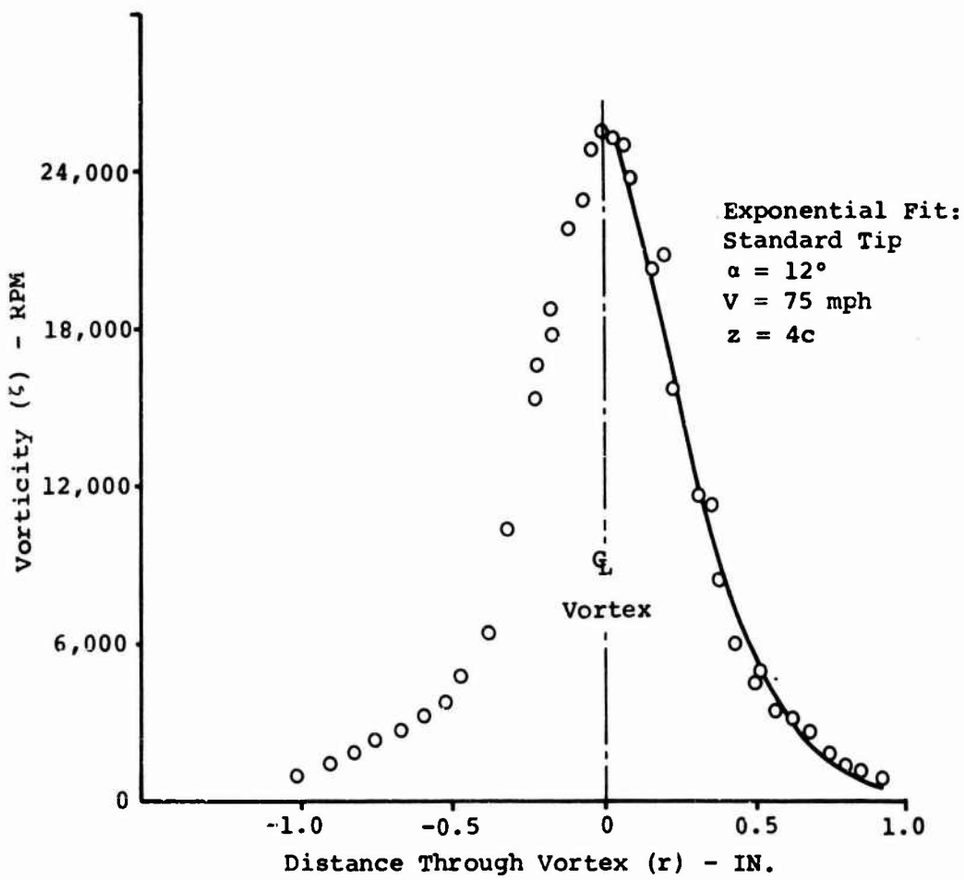

Figure 14. Exponential Fit of Data

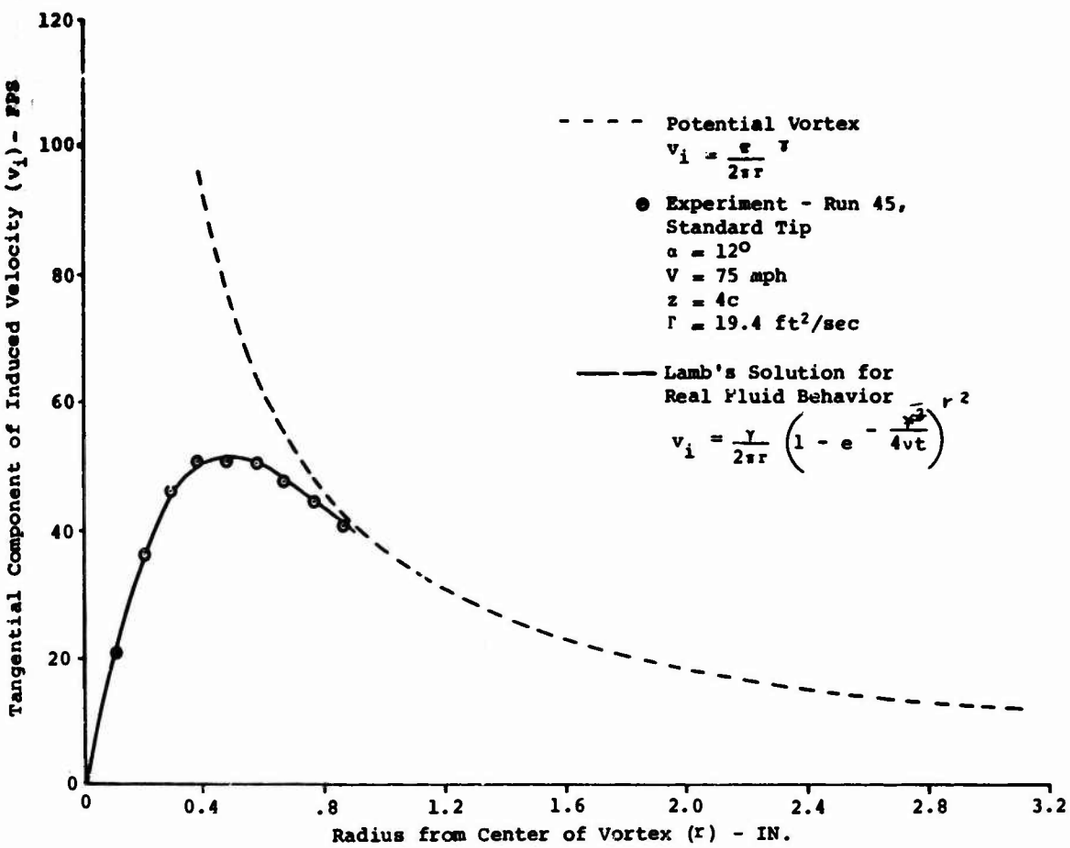

Figure 15. Comparison of Potential Vortex With Experiment and With Lamb's Solution

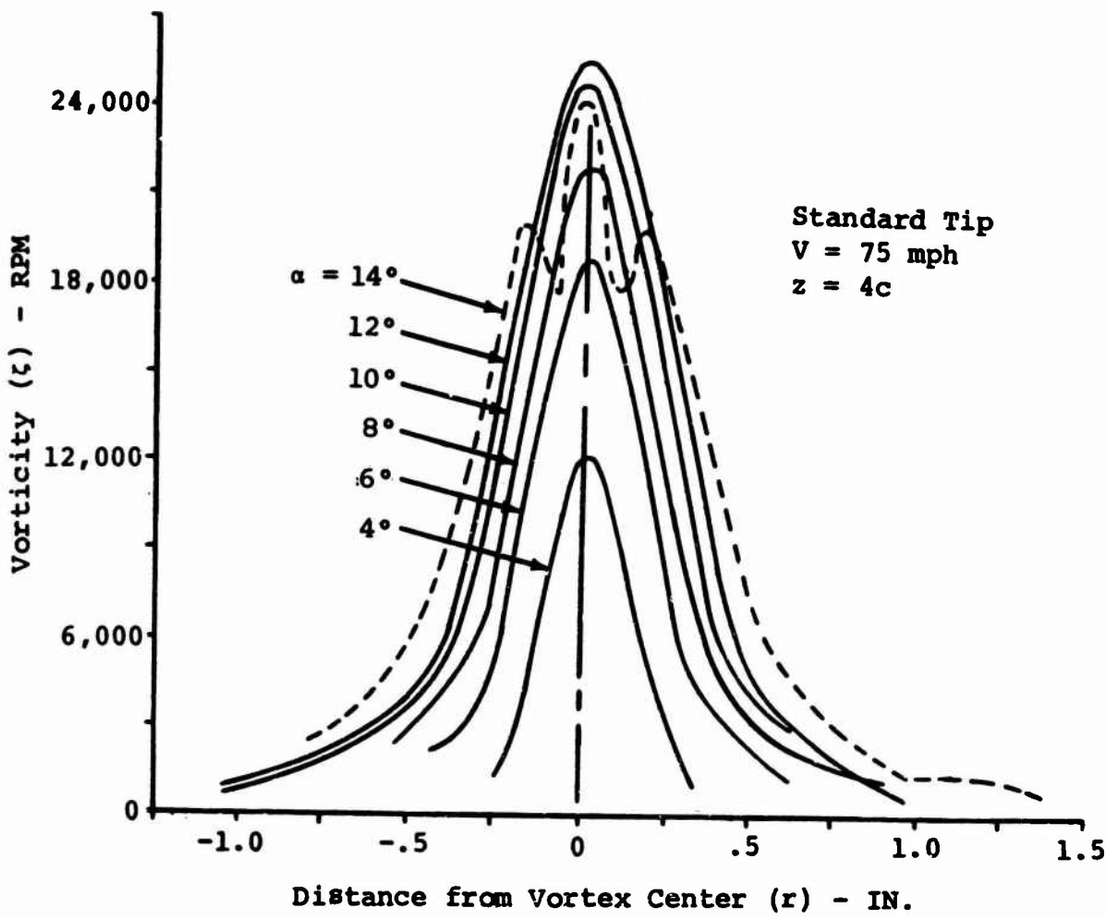

Figure 16. Effect of Angle of Attack on Vorticity Distribution for Standard Tip

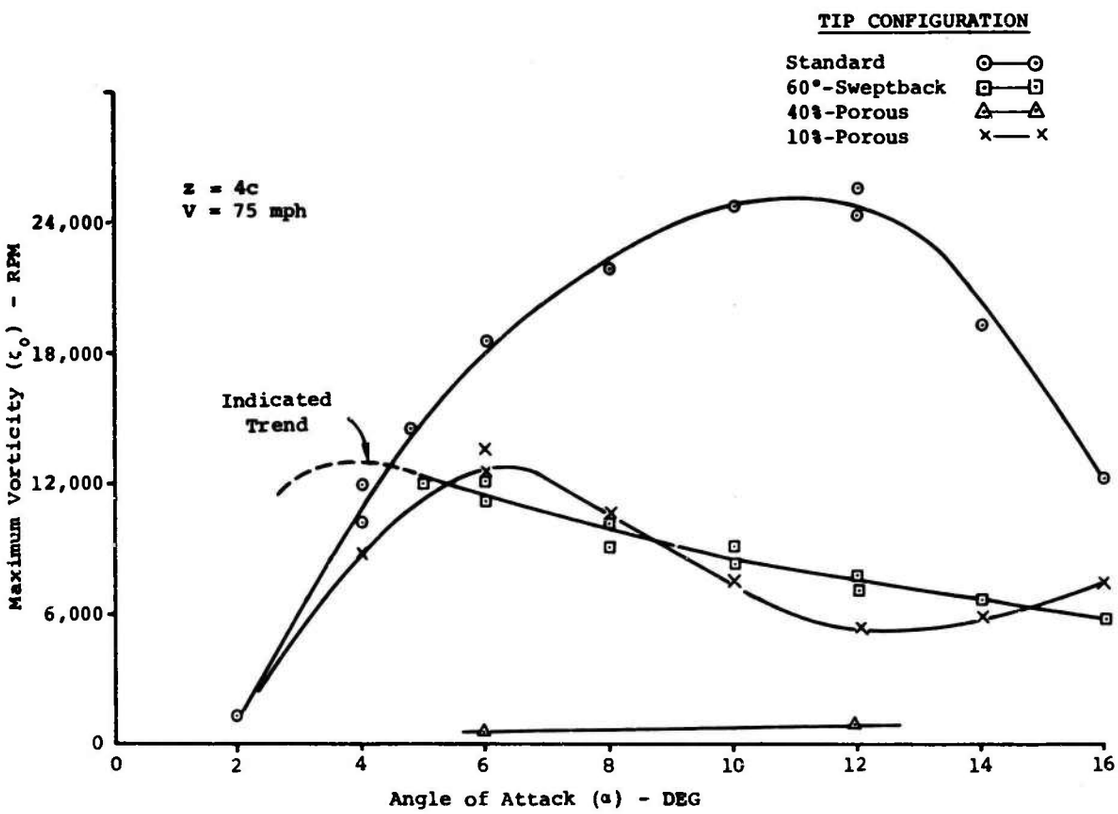

Figure 17. Variation of Maximum Vorticity With Angle of Attack

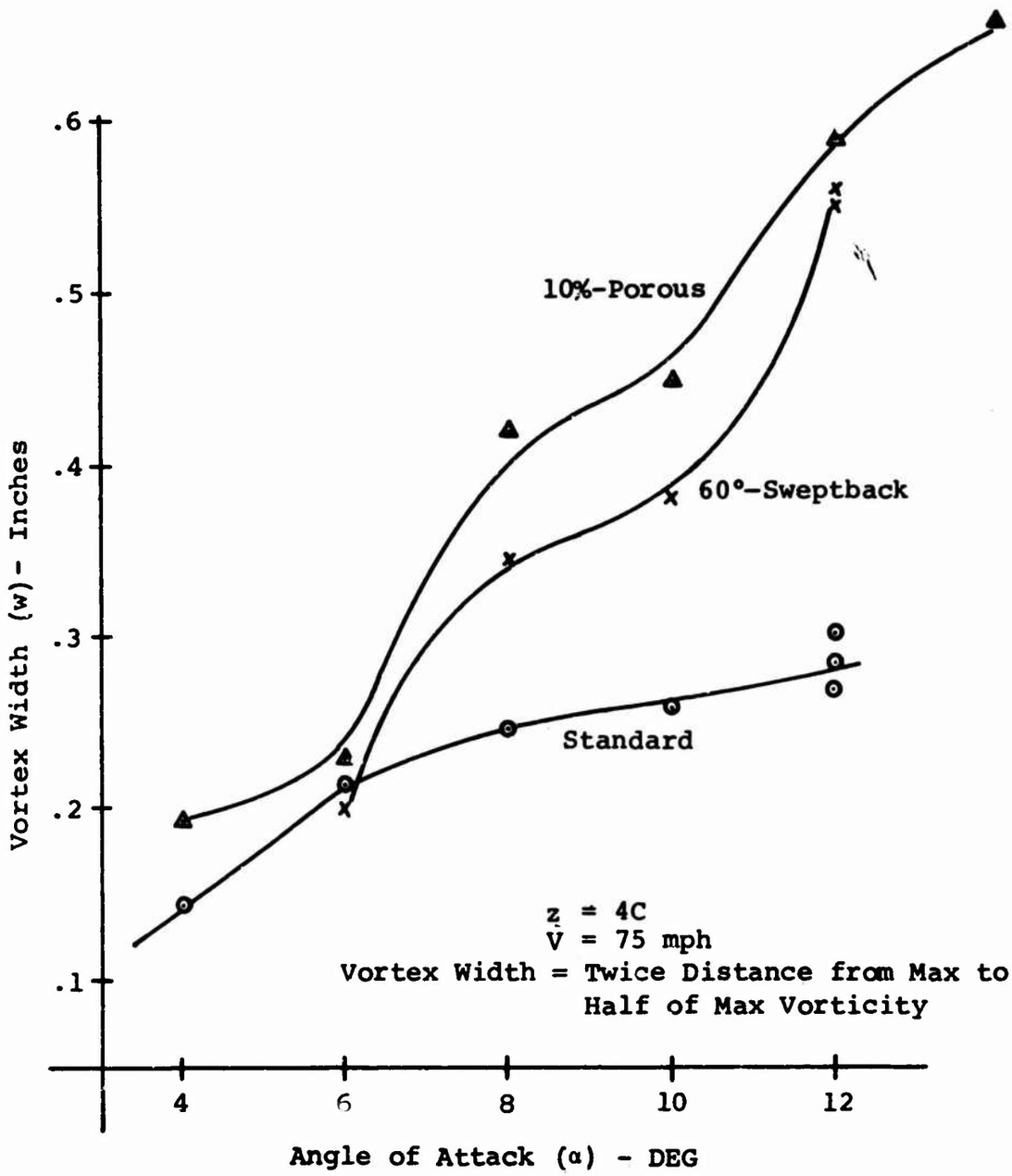

Figure 18. Variation of Vortex Width With Angle of Attack

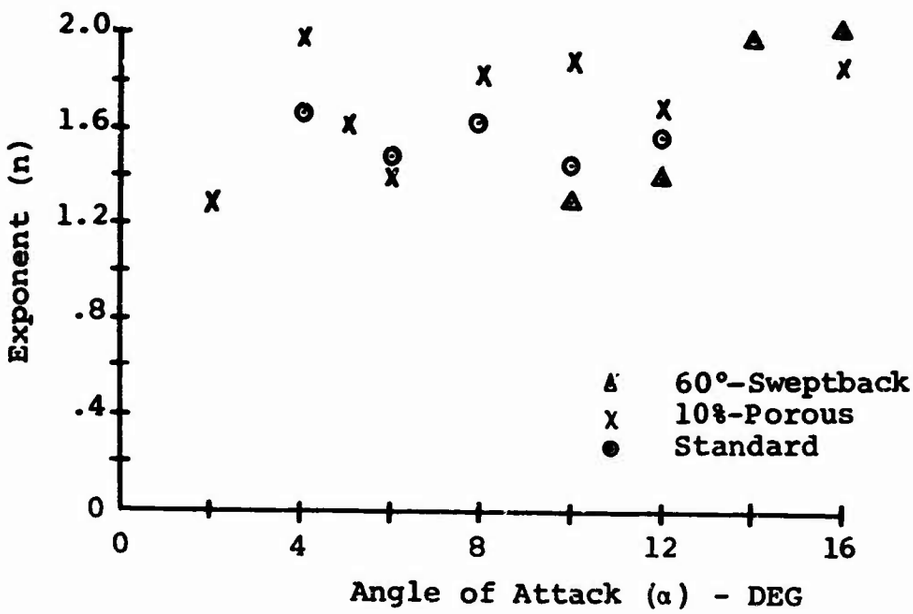

Figure 19. Measured Values of Exponent n

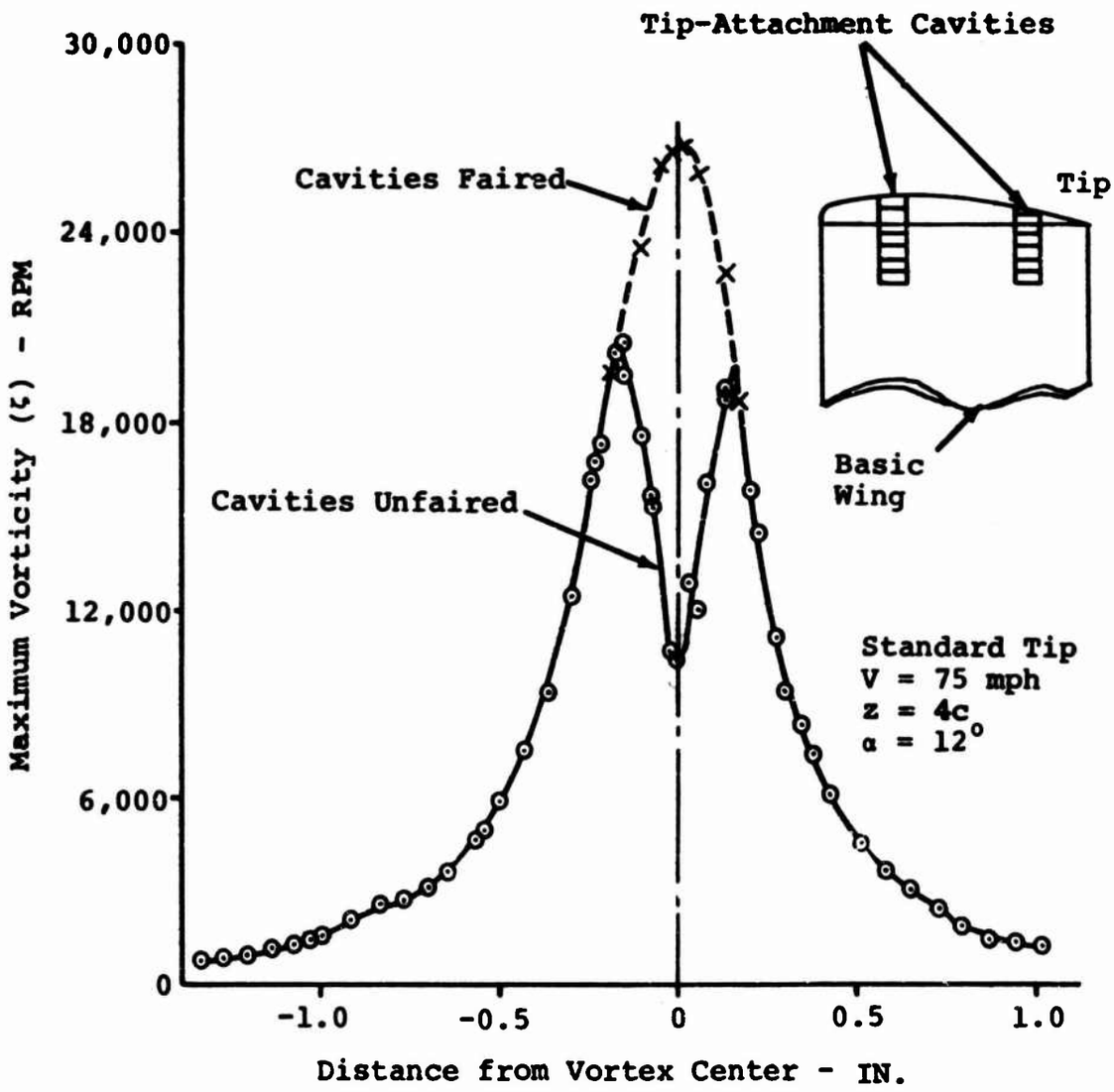

Figure 20. Influence of Tip-Cavity Fairing on Vorticity Distribution

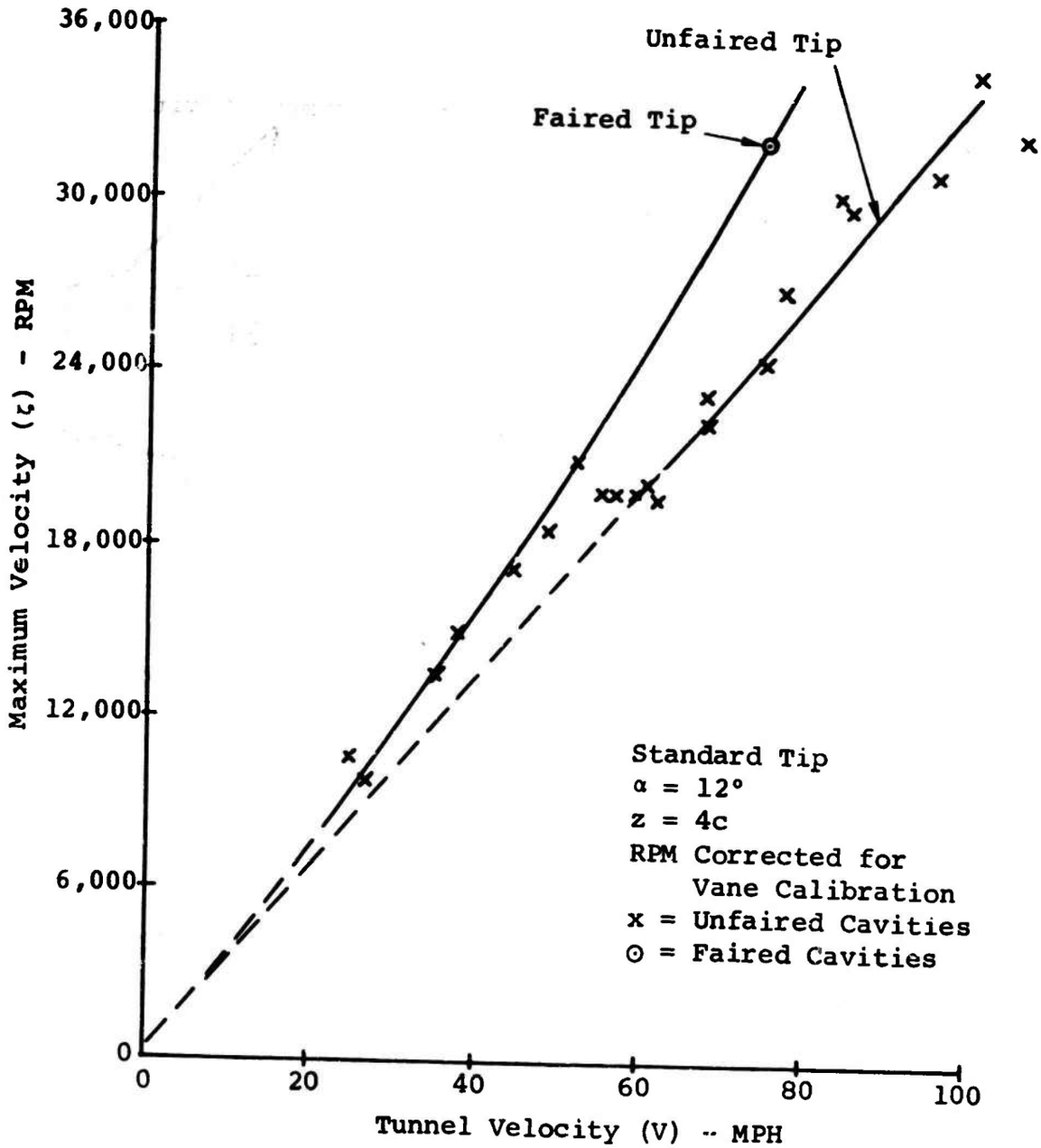

Figure 21. Influence of Tip-Cavity Fairing on Maximum Vorticity

reading at each V rather than by detailed surveys. The maximum vorticity, ζ_0, as indicated by the maximum recorded vane angular velocity, ω_v, increases linearly with tunnel velocity, V, from V=0 to V=50 miles per hour. From 50 to 60 miles per hour, the relation of maximum vorticity to tunnel velocity changes. Above 60 miles per hour, the maximum vorticity increases linearly with tunnel velocity but at a lower rate than when V<50 miles per hour. When the tip was faired, a maximum ω was obtained at 75 miles per hour in line with the points below 50 miles per hour. Hence, the unfaired tip seems to have changed the form of the vorticity distribution between 50 to 60 miles per hour peak to a dip in the middle of the curve. Figure 16 illustrates the same sort of behavior for an α of 14 degrees. The dip may be caused by a localized separation which depends on Reynolds number, surface condition, and angle of attack, or it may be related to the so-called "vortex breakdown" phenomenon.

The performance of the blown tip was similar to the unfaired tip. At a 12-degree angle of attack, a small amount of blowing air caused the vorticity distribution curve (Figure 22) to dip in the center; for 6 degrees (Figure 23), however, the greatest blowing available produced only a general flattening of the vorticity curve. The curves were integrated graphically to obtain the velocity distributions shown on Figure 24. These curves are for different values of the blowing coefficient defined by

$$C_Q = \frac{\rho_j v_j^2 tc}{\frac{1}{2}\rho V^2 S} \tag{14}$$

or

$$C_Q = \left(\frac{R_j}{L}\right) C_L \tag{15}$$

where

R_j is the jet reaction.

L is the wing lift.

C_L is the wing lift coefficient.

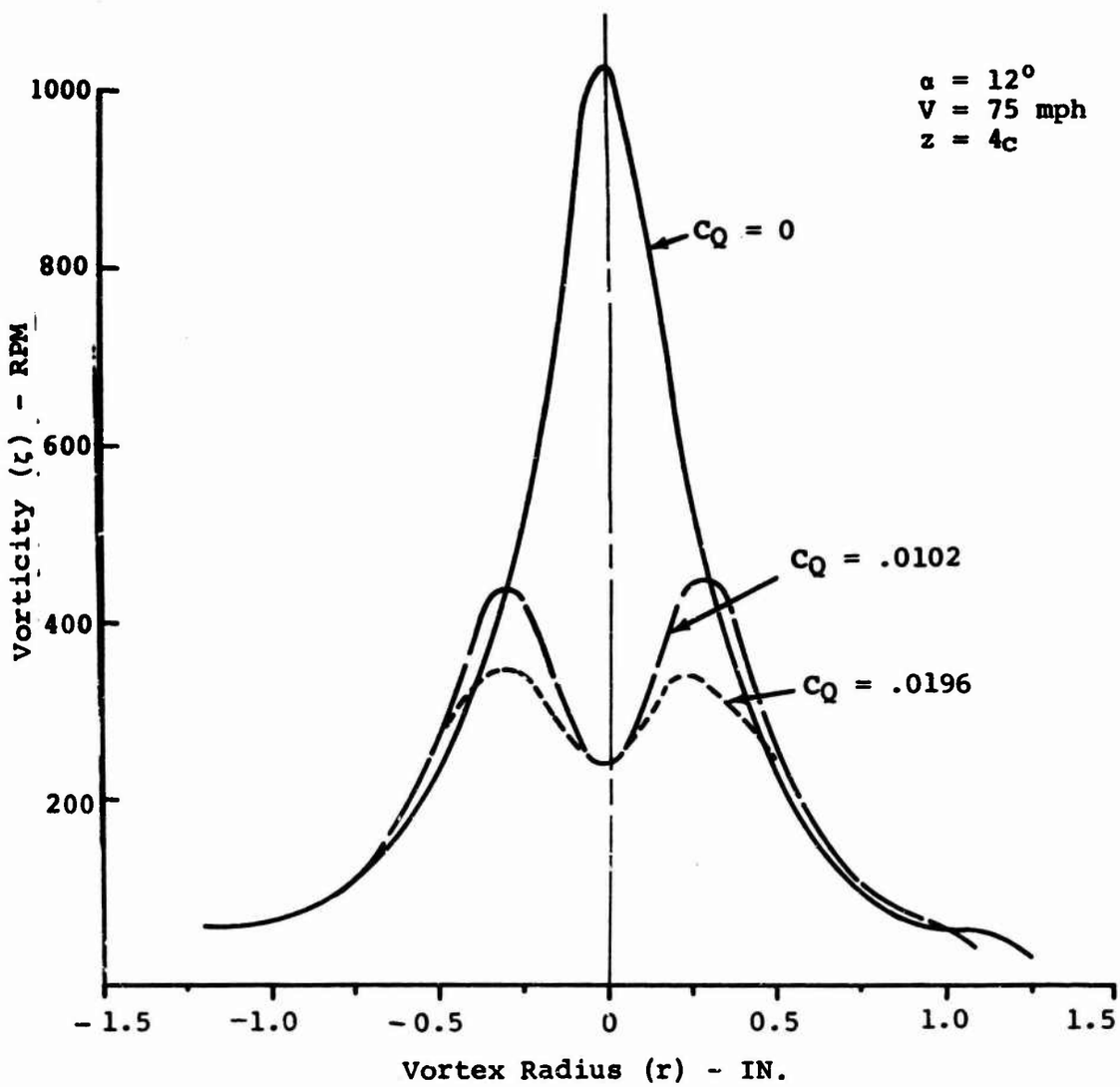

Figure 22. Effect of Blowing on Vorticity Distribution
(α = 12°)

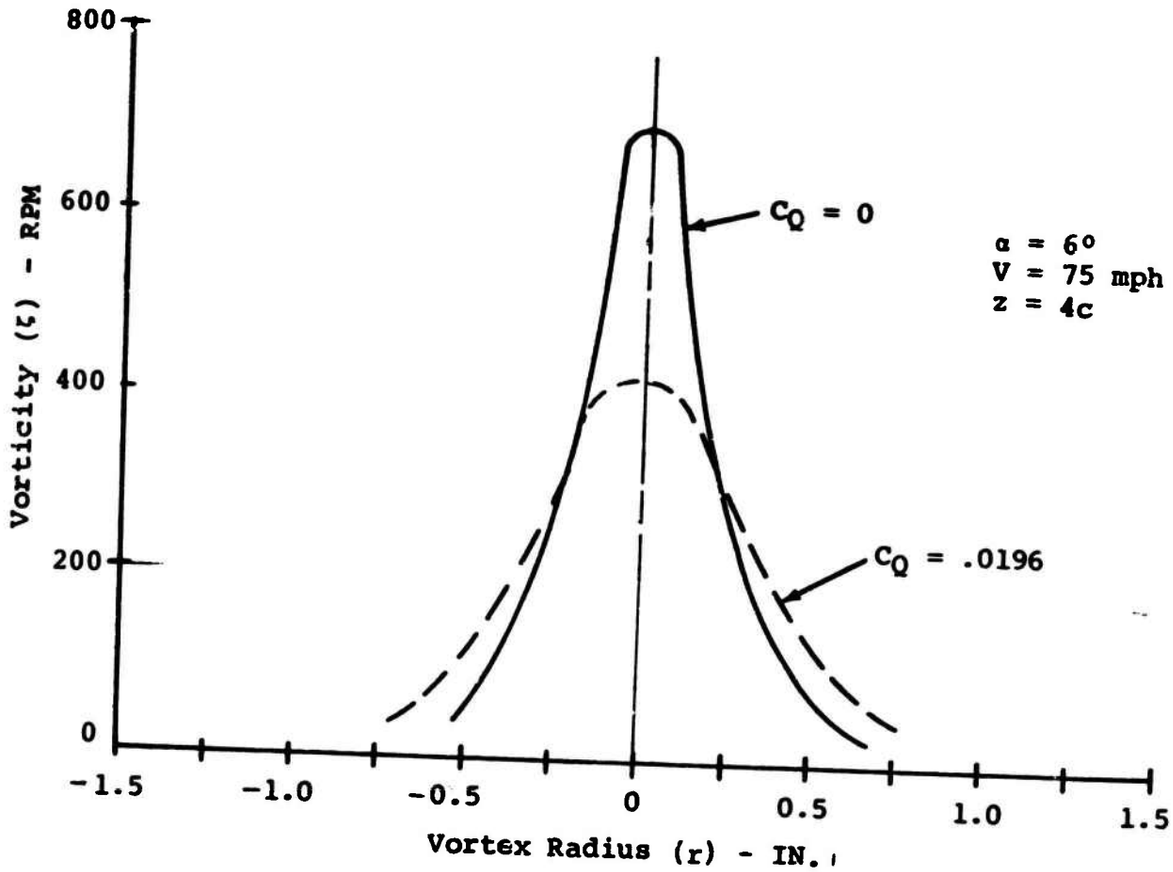

Figure 23. Effect of Blowing on Vorticity Distribution ($\alpha = 6^{o}$)

The numerator in Equation 14 was evaluated by measuring the jet reaction as a function of the gage pressure in the wing tip cavity just ahead of the slot. For the geometry tested, the jet reaction is related to gage pressure by

$$R_j = 0.0355\Delta_p \tag{16}$$

where

R_j is the jet reaction in pounds.

Δ_p is the gage pressure in inches of mercury.

Figure 24 shows that blowing has only a slight effect on the maximum induced velocity, even though the velocity-versus-radius curve is altered appreciably for an α of 12 degrees.

PHOTOGRAPHIC TUFT-GRID STUDIES

Photographs were made of 6-inch-square tuft grid mounted two chord-lengths behind the trailing edge of each wing tip. The results are shown in Figures 25 through 28. The tufts are light plastic strips, 0.5 inch long, spaced 0.375 inch apart. The angle of attack and tip configuration are noted on each photograph.

In Figure 25, the vorticity and velocity distributions for the standard tip at 12 degrees are superimposed to the same distance scale on a photograph of the tuft grid. Tuft deflections correspond with the velocity distribution, and the blurred tufts are limited to the area where vorticity is concentrated.

Figure 26 compares the standard, honeycomb, and 40-percent-open-porous tip, all at a 12-degree angle of attack.

In Figure 27, a series of photographs taken at 1/60 of a second illustrates the effect of angle of attack on the trailed vorticity of each tip. With the exception of the porous tips, a well-defined circular area can be seen increasing in diameter with increasing angle of attack; the projected length of the tufts indicates a high tangential velocity in the vortex. Also, for several of the tips, blurring of the tufts indicates the severity and extent of rotation in the center of the vortex. The 10-percent-porous tip displays a rather weak circular pattern for 8 degrees and 10 degrees which becomes blurred at 12 degrees. The other two porous tips do not display any

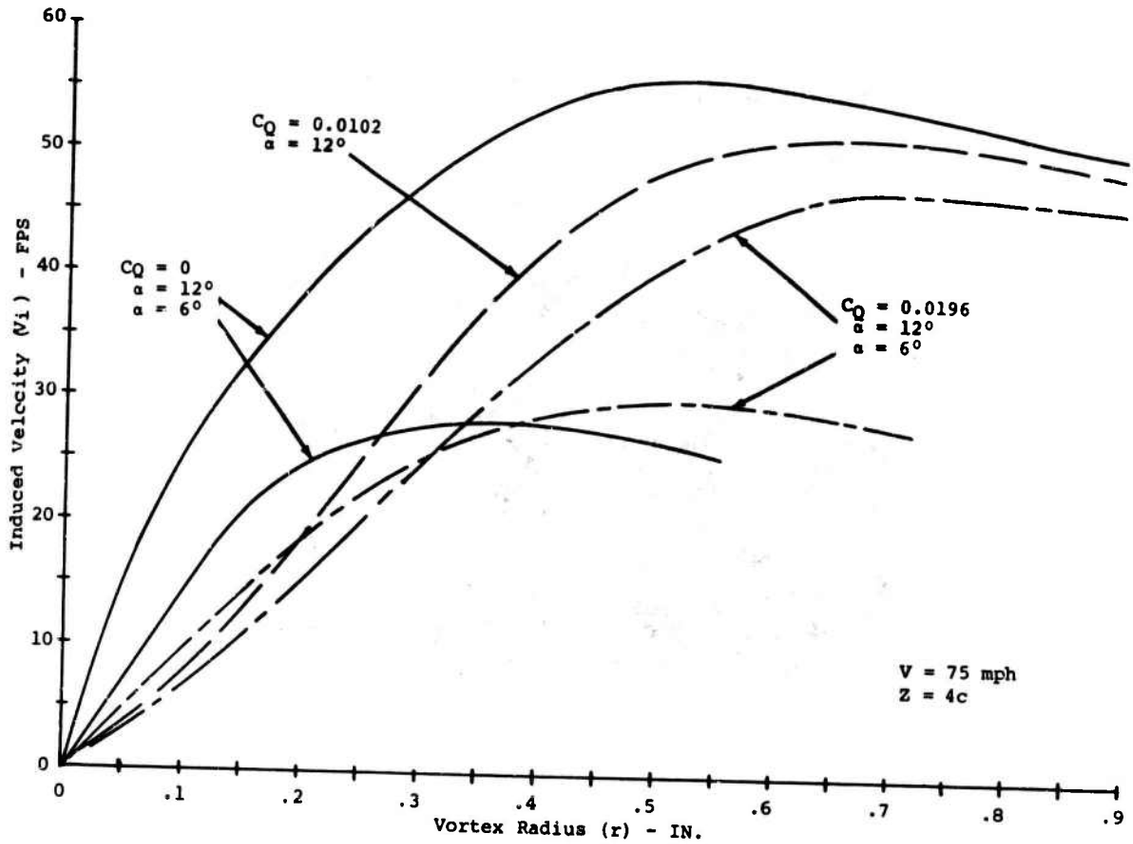

Figure 24. Effect of Blowing on Velocity Distribution

Standard Tip $\alpha = 12°$ V = 75 mph

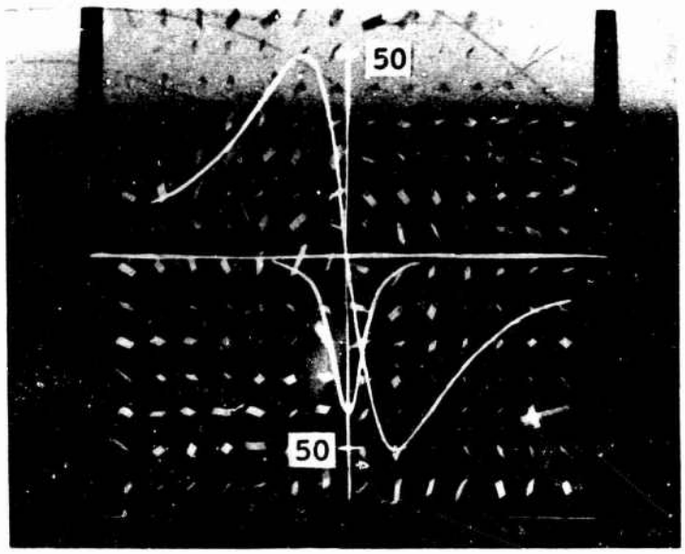

Relative Vorticity and Velocity Distributions

Figure 25. Comparison of Photographic Tuft-Grid Study With Vortex Measurements

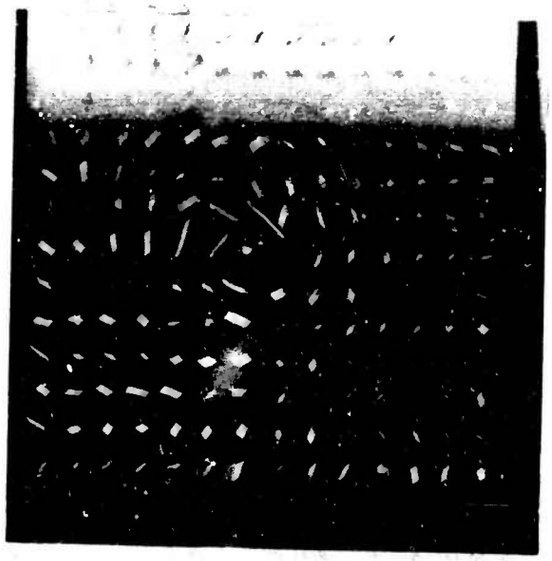

Standard Tip

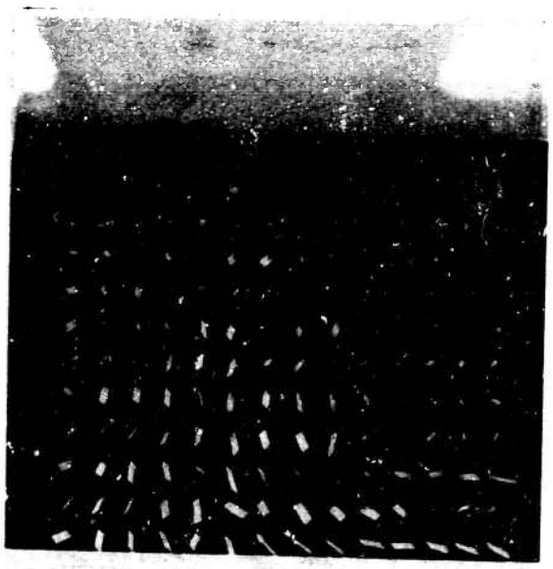

Honeycomb Tip

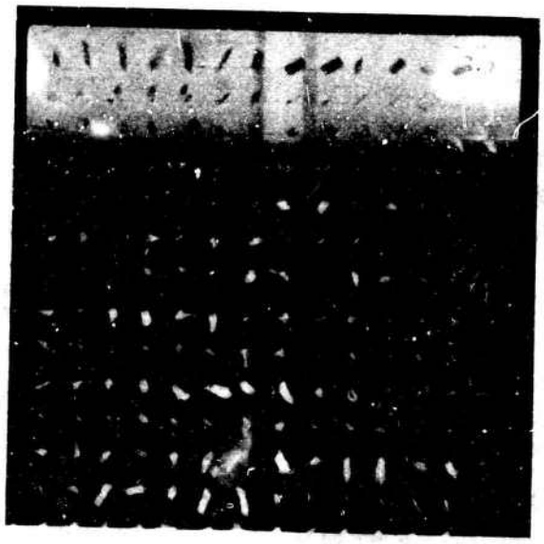

40%-Porous Tip

Figure 26. Tuft-Grid Study: Standard, Honeycomb, and 40%-Porous Tips at 12° Angle of Attack, $z = 2c$, $V = 75$ mph.

Standard Tip

V = 75 mph
z = 2c

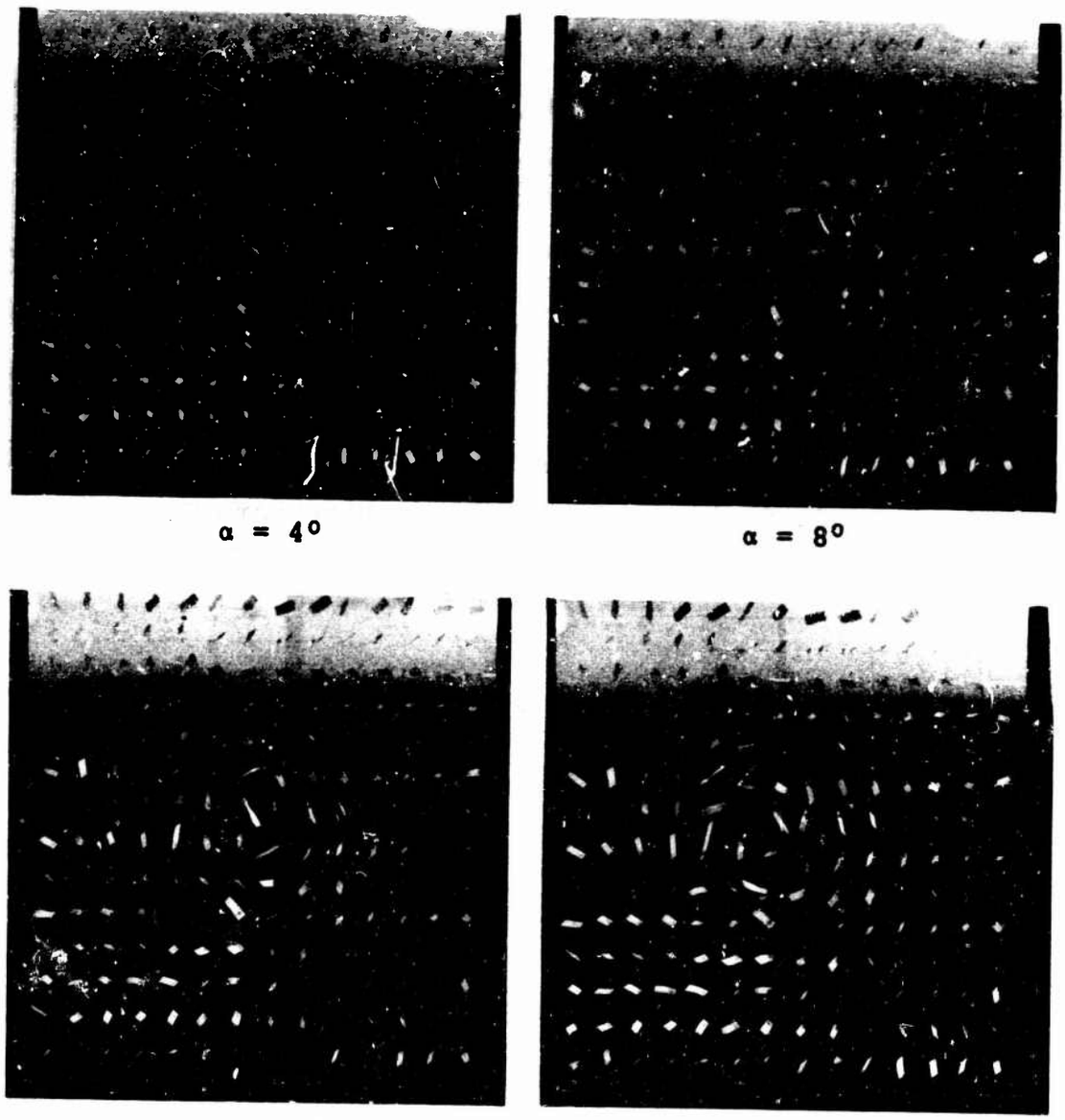

$\alpha = 4^{\circ}$ $\alpha = 8^{\circ}$

$\alpha = 12^{\circ}$ $\alpha = 14^{\circ}$

Figure 27. Tuft-Grid Study: Effect of Angle of Attack and Tip Shape on Vorticity (Sheet 1 of 8)

60°-Sweptback Tip

V = 75 mph
z = 2c

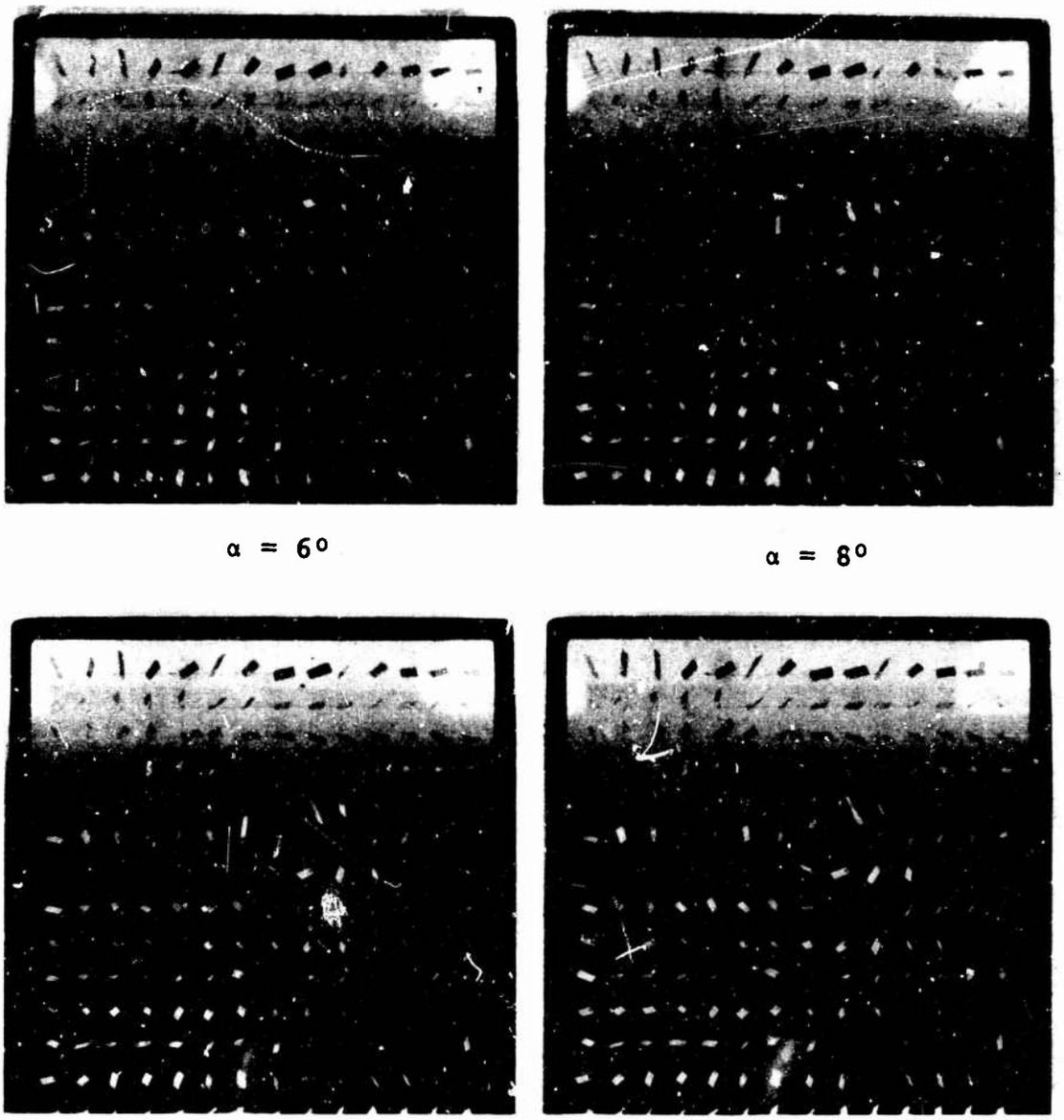

α = 6°

α = 8°

α = 10°

α = 12°

Figure 27. Tuft-Grid Study: Effect of Angle of Attack and Tip Shape on Vorticity (Sheet 2 of 8)

Honeycomb Tip

V = 75 mph
z = 2c

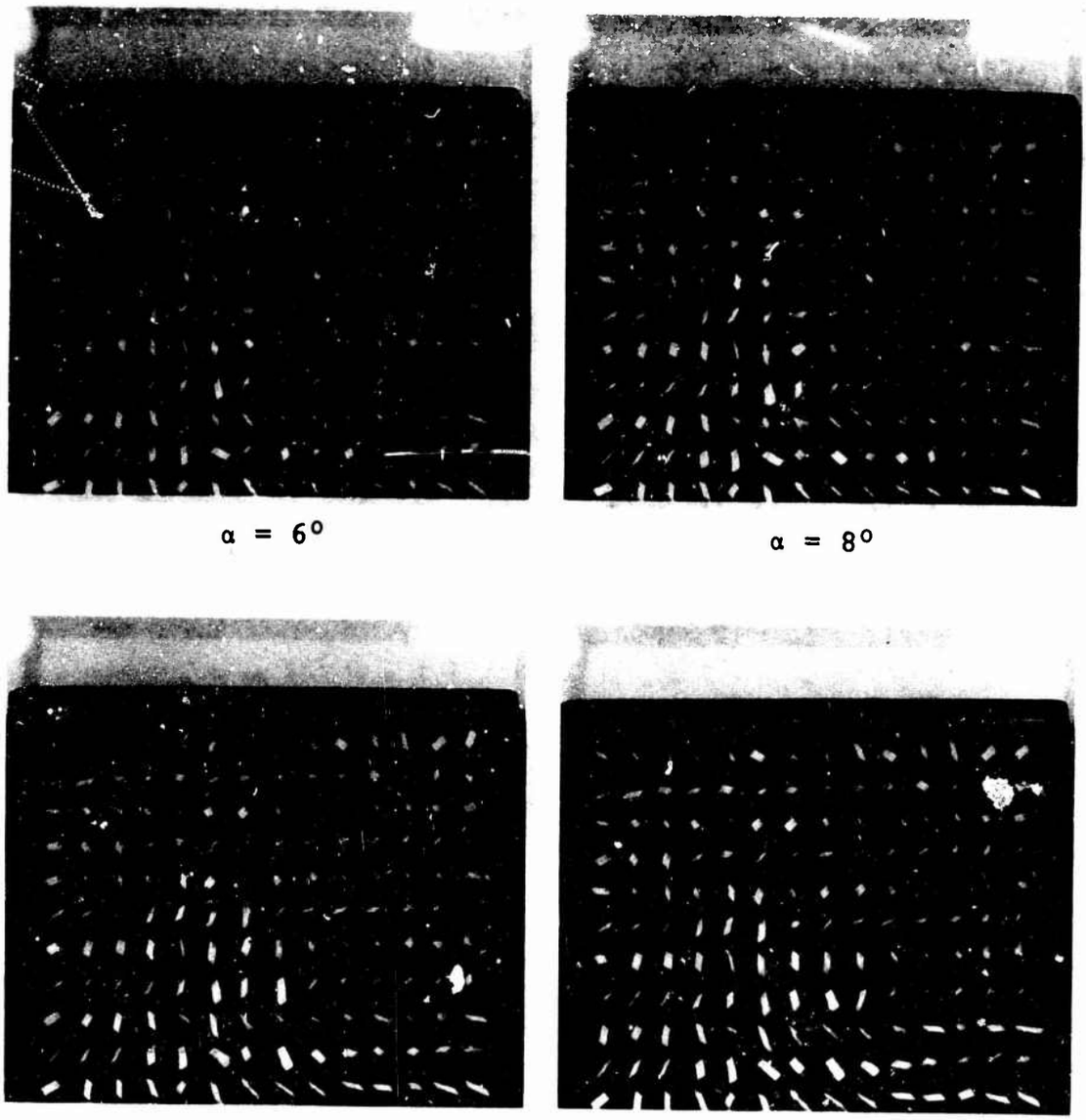

$\alpha = 6^{\circ}$ $\alpha = 8^{\circ}$

$\alpha = 10^{\circ}$ $\alpha = 12^{\circ}$

Figure 27. Tuft-Grid Study: Effect of Angle of Attack and Tip Shape on Vorticity (Sheet 3 of 8)

Duct/Vanes Tip

V = 75 mph
z = 2c

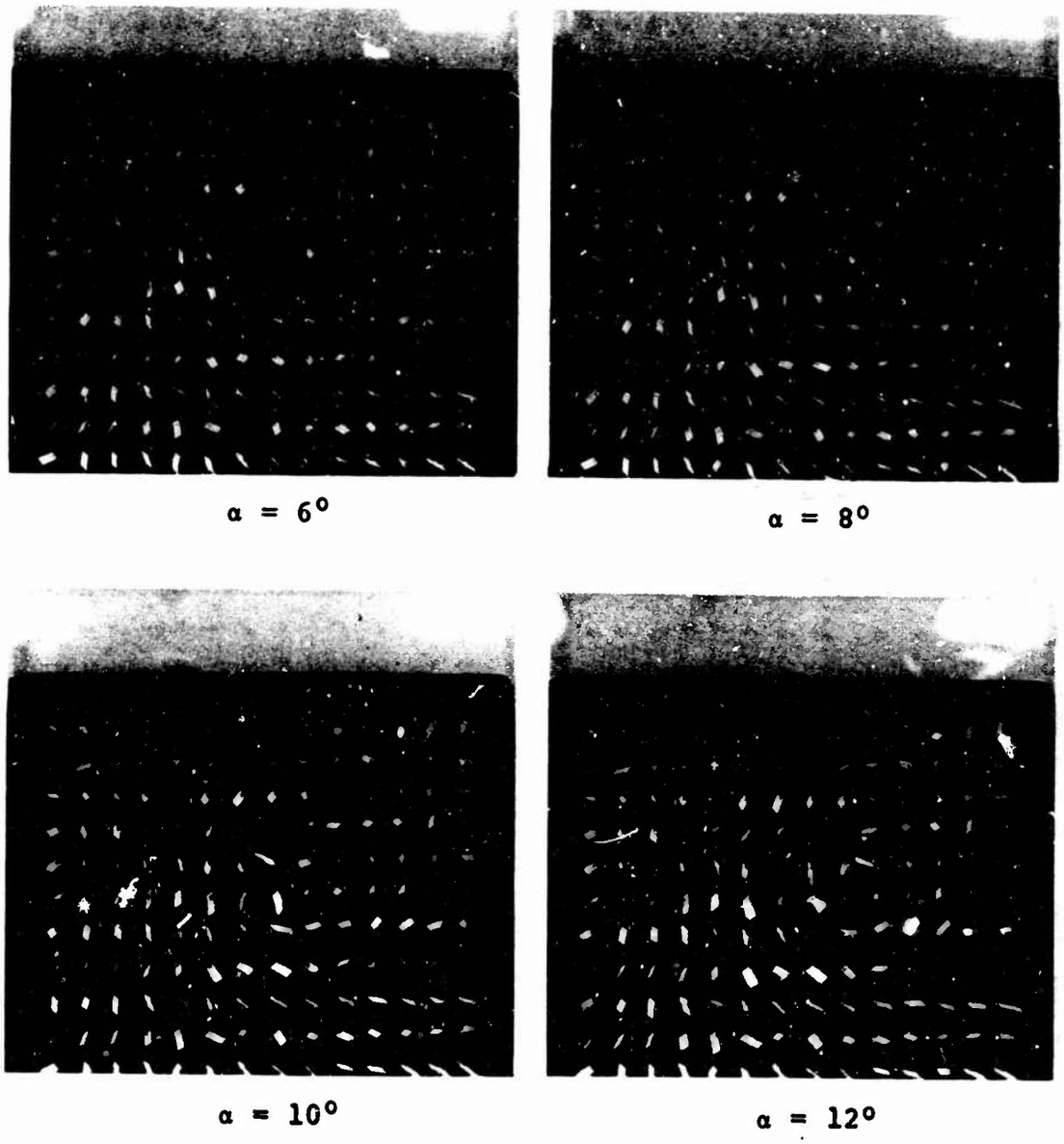

Figure 27. Tuft-Grid Study: Effect of Angle of Attack and Tip Shape on Vorticity (Sheet 4 of 8)

Contravanes Tip

V = 75 mph
z = 2c

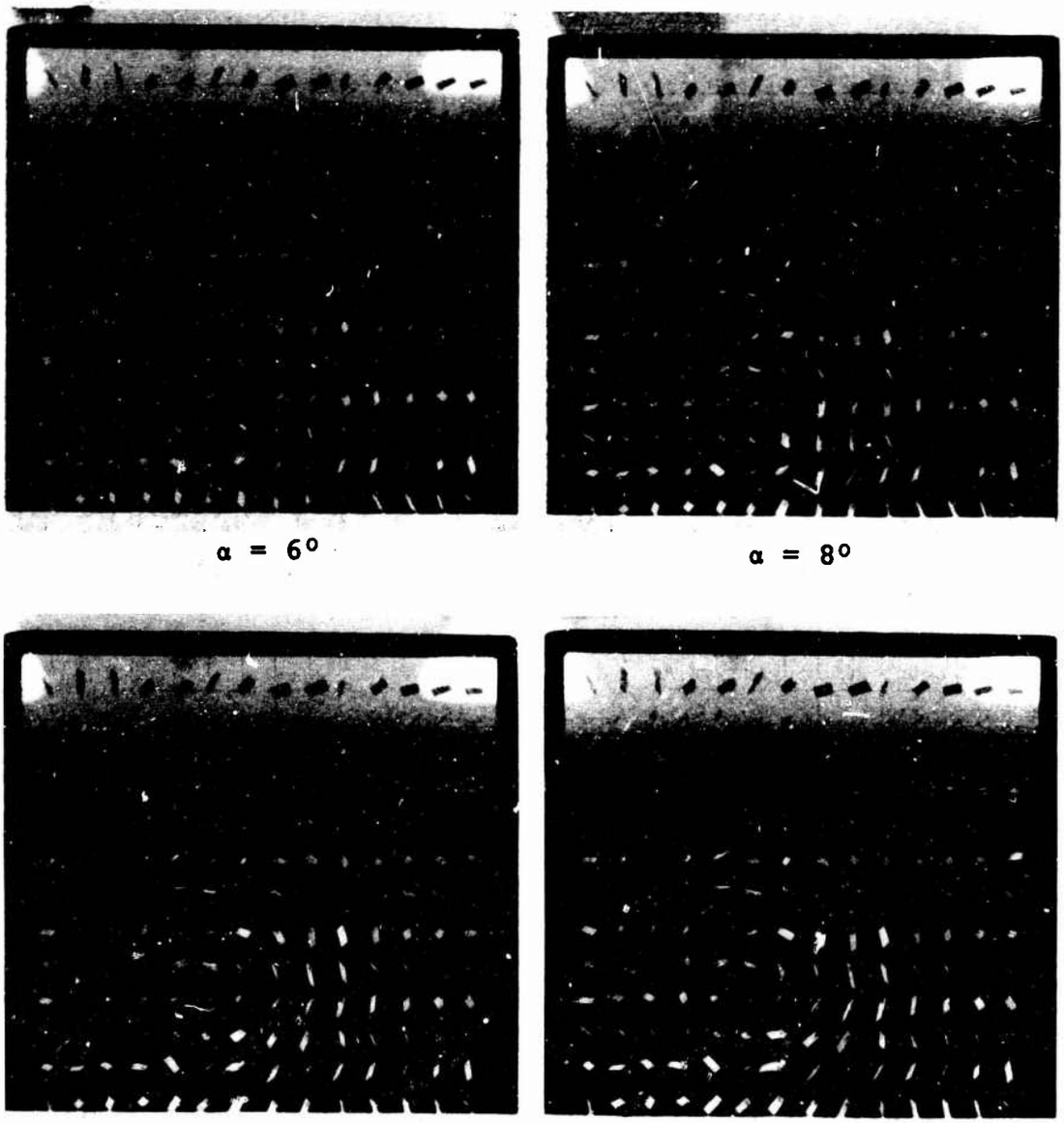

$\alpha = 6^{\circ}$ $\alpha = 8^{\circ}$

$\alpha = 10^{\circ}$ $\alpha = 12^{\circ}$

Figure 27. Tuft-Grid Study: Effect of Angle of Attack and Tip Shape on Vorticity (Sheet 5 of 8)

10%-Porous Tip

V = 75 mph
z = 2c

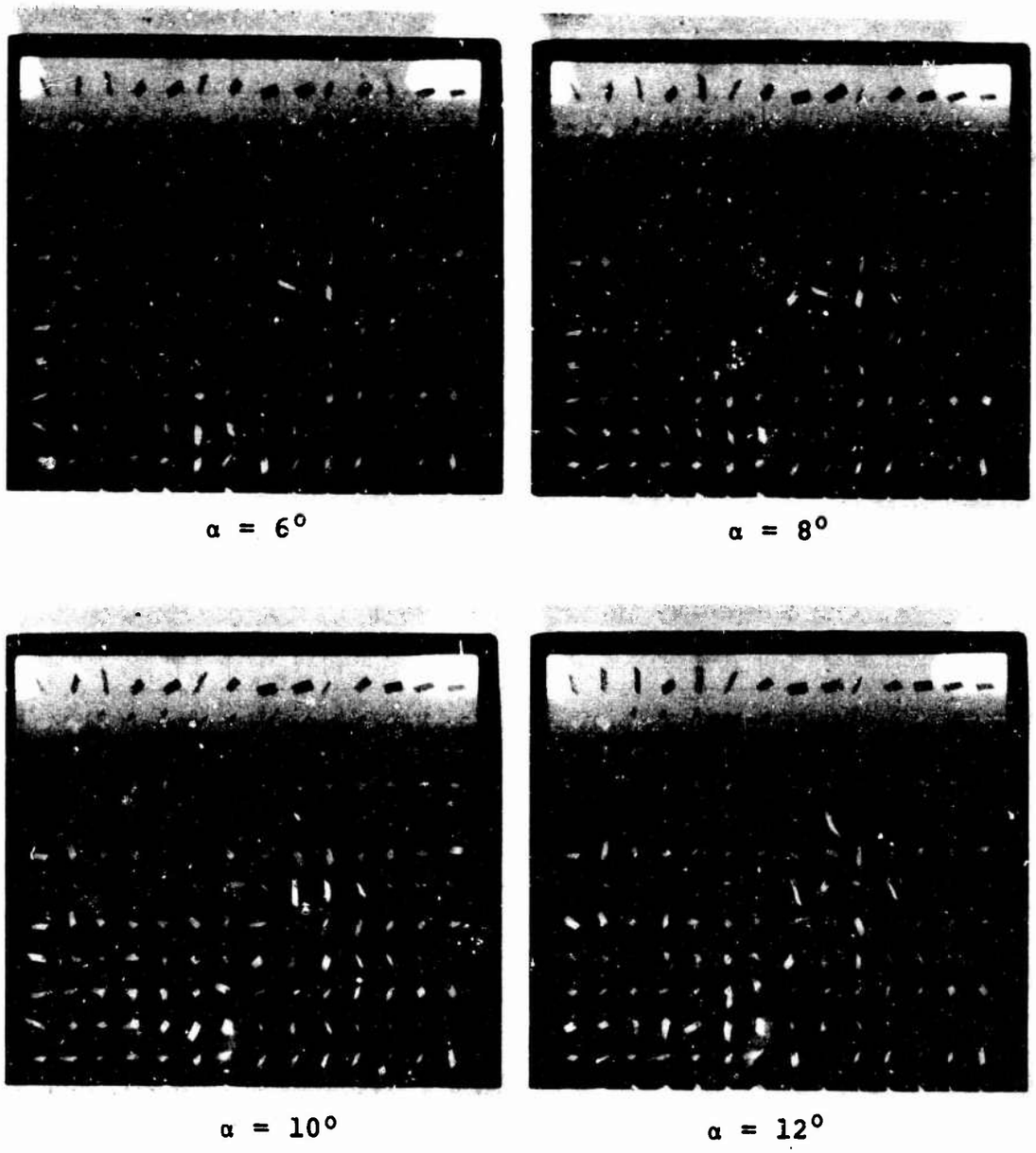

$\alpha = 6^{\circ}$ $\alpha = 8^{\circ}$

$\alpha = 10^{\circ}$ $\alpha = 12^{\circ}$

Figure 27. Tuft-Grid Study: Effect of Angle of Attack and Tip Shape on Vorticity (Sheet 6 of 8)

20%-Porous Tip

V = 75 mph
z = 2c

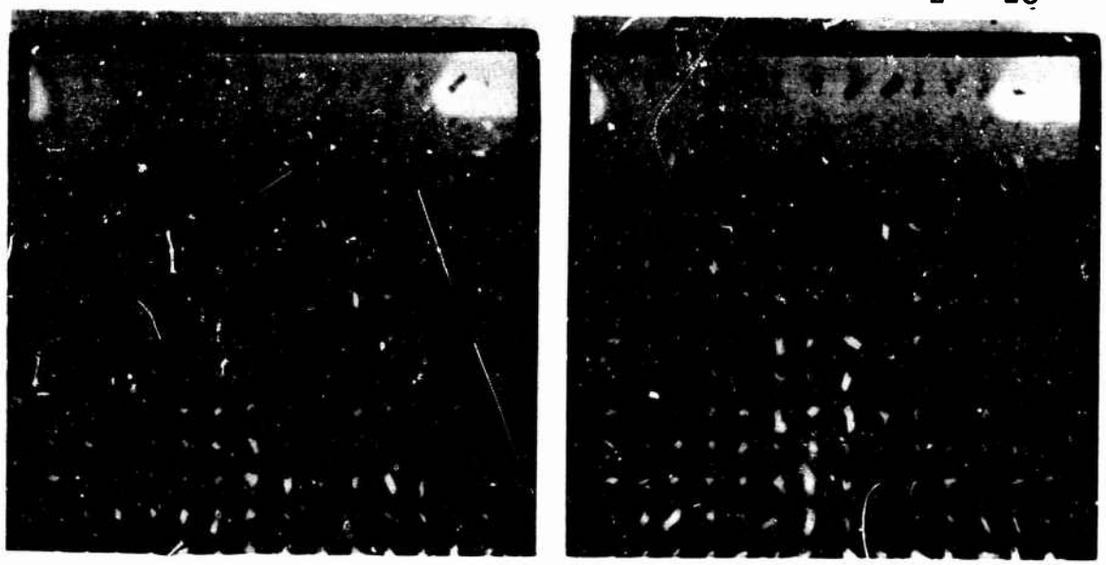

$\alpha = 6^{\circ}$

$\alpha = 8^{\circ}$

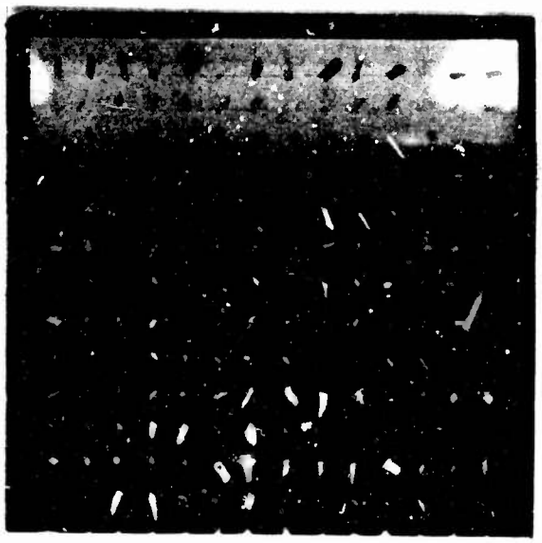

$\alpha = 10^{\circ}$

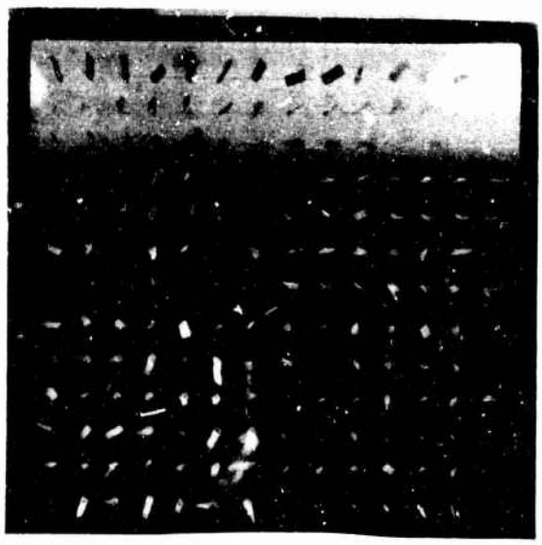

$\alpha = 12^{\circ}$

Figure 27. Tuft-Grid Study: Effect of Angle of Attack and Tip Shape on Vorticity (Sheet 7 of 8)

40%-Porous Tip

V = 75 mph
z = 2c

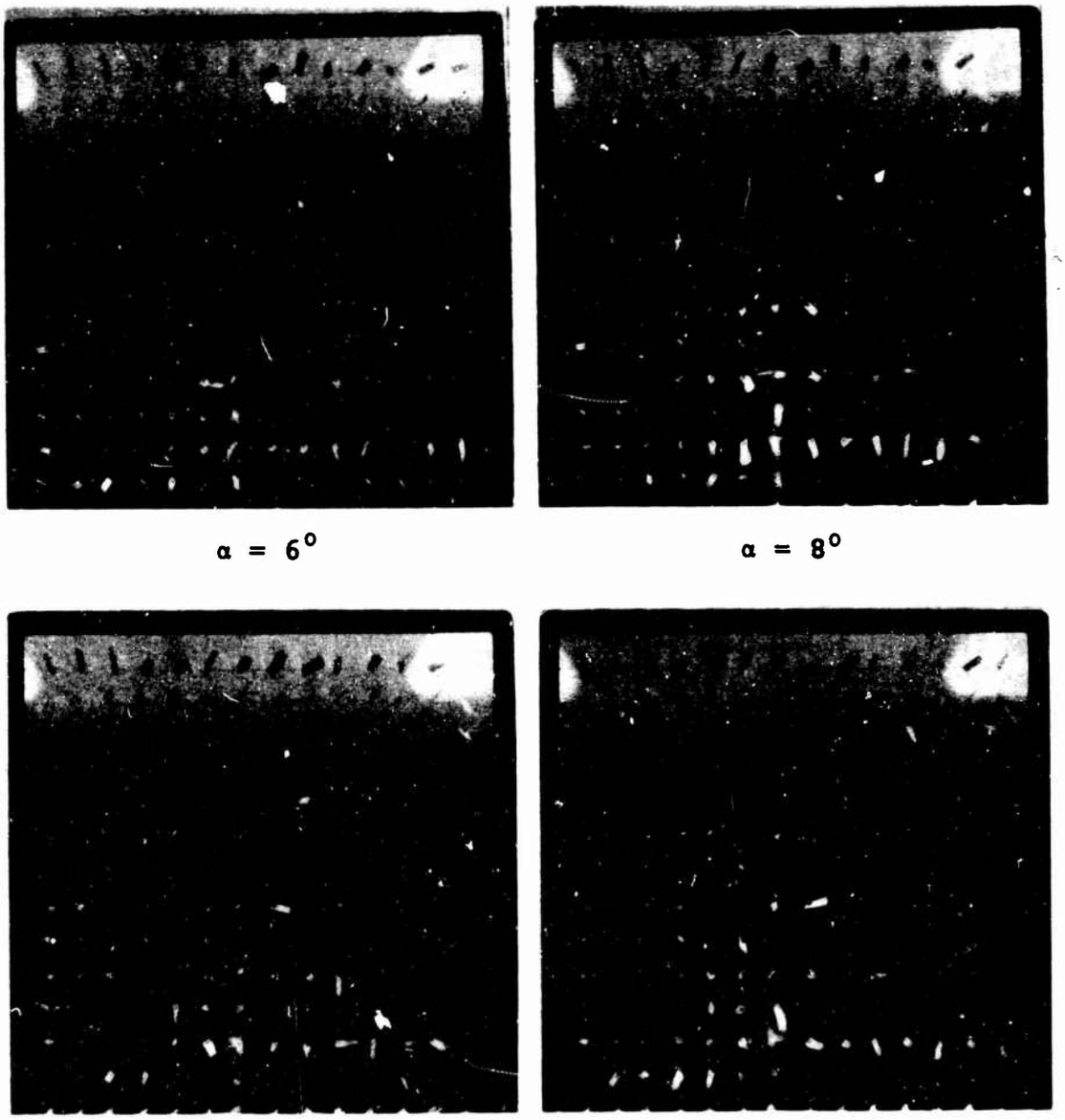

$\alpha = 6^{\circ}$ $\alpha = 8^{\circ}$

$\alpha = 10^{\circ}$ $\alpha = 12^{\circ}$

Figure 27. Tuft-Grid Study: Effect of Angle of Attack and Tip Shape on Vorticity (Sheet 8 of 8)

Standard Tip

V = 75 mph
$\alpha = 12^{o}$

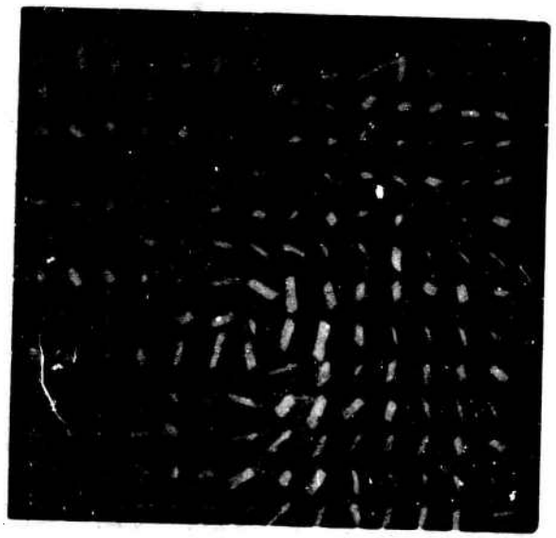

1.5 In. Behind Trailing Edge

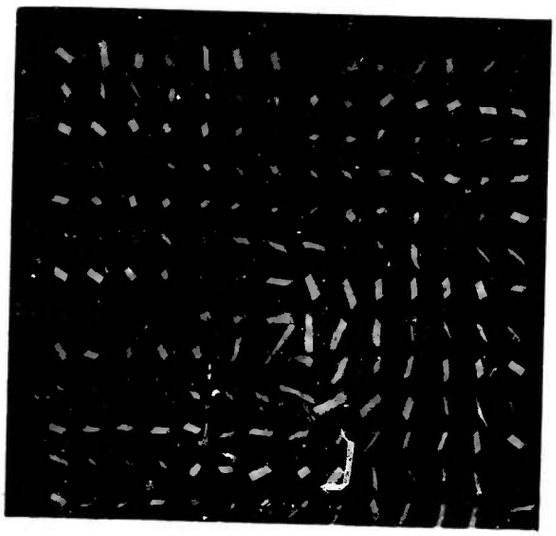

4.0 In. Behind Trailing Edge

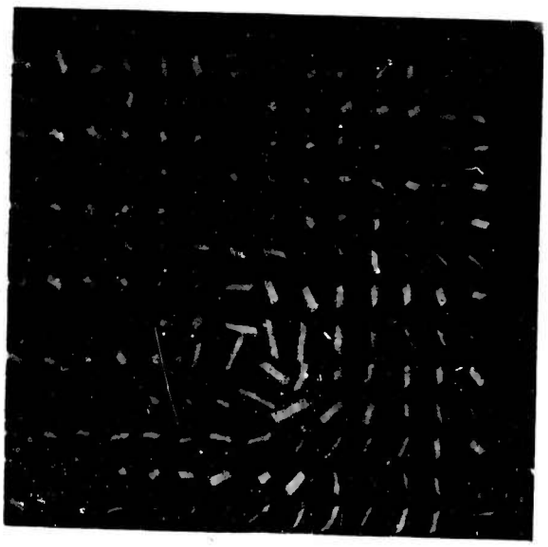

6.0 In. Behind Trailing Edge

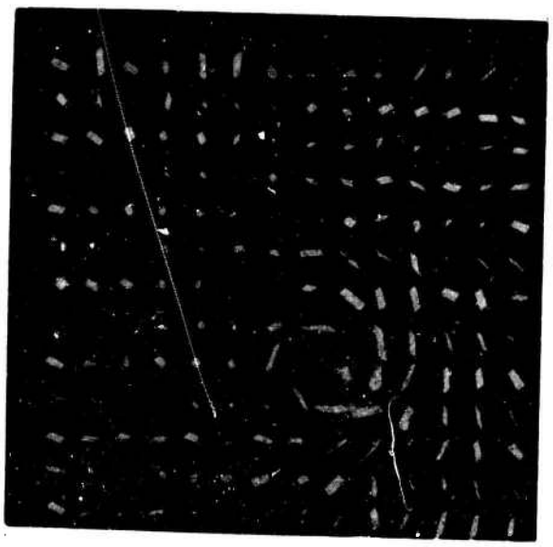

8.0 In. Behind Trailing Edge

Figure 28. Tuft-Grid Study at Varying Distances Downstream From the Standard Tip (Sheet 1 of 2)

Standard Tip

V = 75 mph
α = 12°

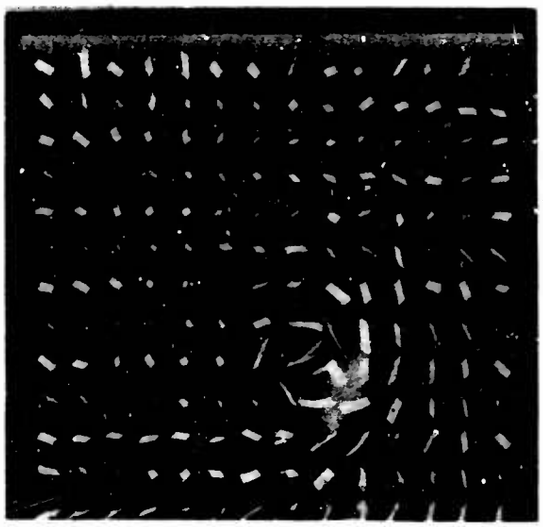

10.0 In. Behind Trailing Edge

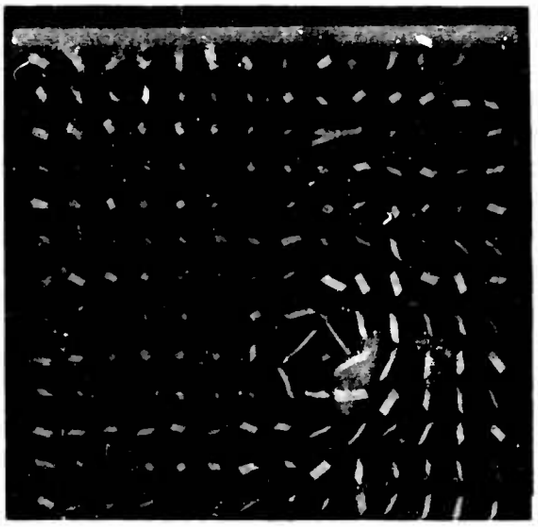

12.0 In. Behind Trailing Edge

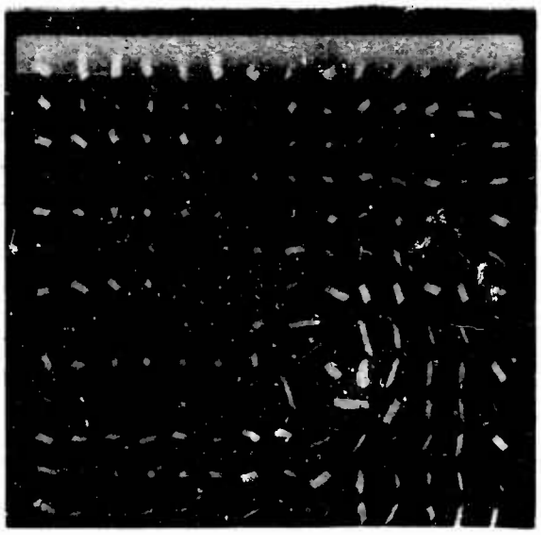

14.0 In. Behind Trailing Edge

Figure 28. Tuft-Grid Study at Varying Distances Downstream From the Standard Tip (Sheet 2 of 2)

definite patterns throughout the angle-of-attack range.

Figure 28, a sequence of pictures taken at various distances downstream from the trailing edge of the standard tip, shows little difference in the tuft-grid patterns of the core.

EVALUATION OF VORTICITY FROM TEST DATA

The contour maps for the standard tip (Figure 29) show the progressive rolling-up of the trailing vortex sheet into a somewhat distorted vortex two chord-lengths downstream of the wing. The measurable rotating fluid extends inboard for approximately 60 percent of the semi-span at one inch behind the trailing edge. This region shortens progressively downstream, but it is interesting to note that it remains essentially plain, distorting only where it feeds into the vortex.

Figure 30 shows similar information for the 40-percent-porous tip. Inboard along the trailing edge of the wing, the contours are similar to those for the standard tip. Outboard, however, the region of rotational flow is much larger, and the maximum vorticity is considerably less than for the standard tip.

These contours from probe data agree well with the tuft photographs shown in Figure 28: both show that the core vortex persists for a long time. This suggests that a rapid decay of vorticity cannot be counted upon to achieve noise reduction.

VORTEX STRENGTHS

It is interesting to consider the vortex strengths which were determined by integrating the vorticity. According to Helmholz's theorem of vortex continuity, the strength of the trailing vortex should equal the midspan value of the bound circulation, given by

$$\Gamma_o = \frac{1}{2} c_o C_L V \frac{C_{\ell_o}}{C_L} \tag{17}$$

where

Γ_o is the bound circulation.

c_o is the midspan chord.

C_{ℓ_o} is the section lift coefficient.

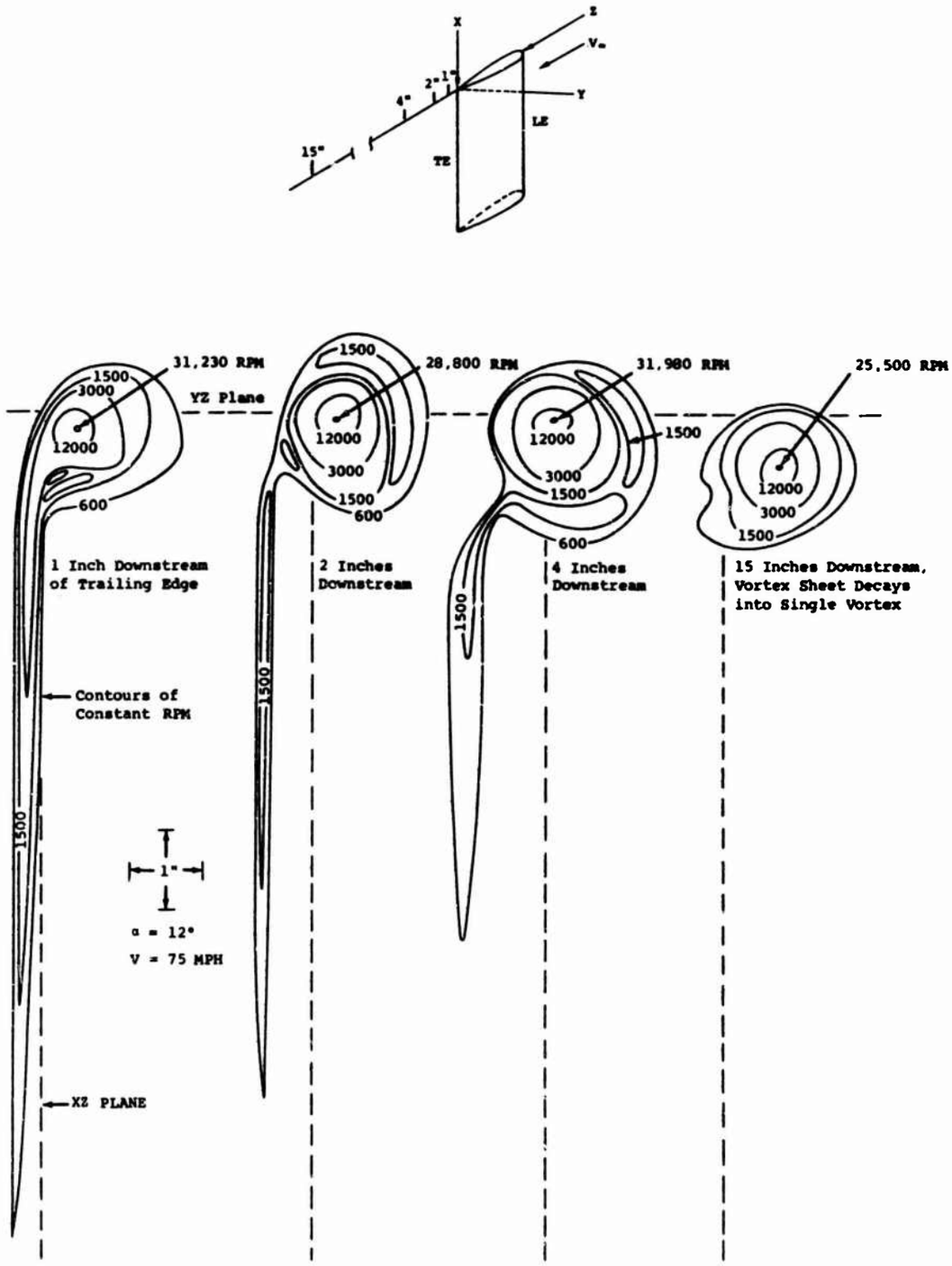

Figure 29. Contours of Constant Rotational Speeds in Four Transverse Planes Downstream From Standard Tip

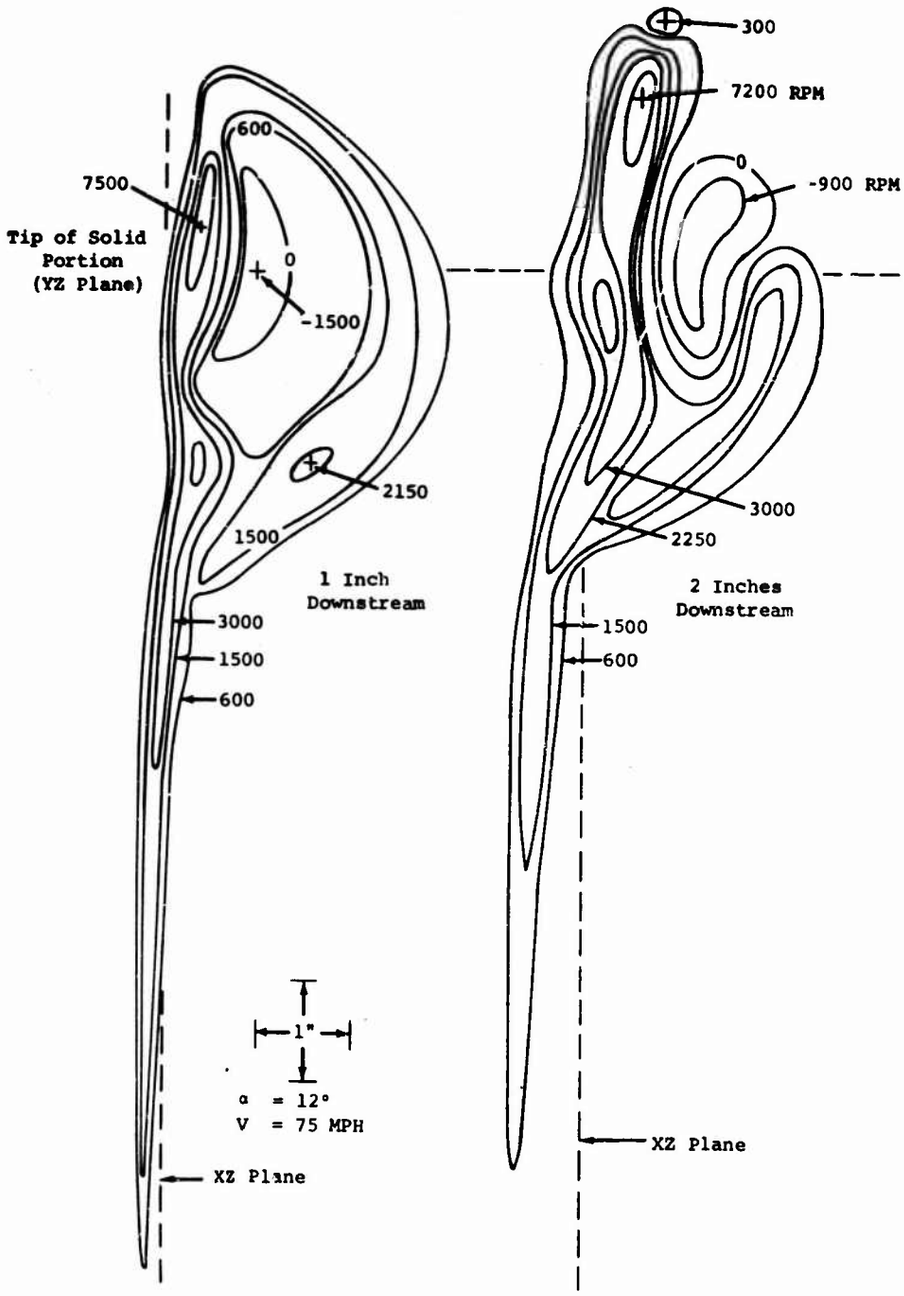

Figure 30. Contours of Constant Rotational Speeds 1 and 2 Inches Downstream From 40%-Porous Tip (Sheet 1 of 2)

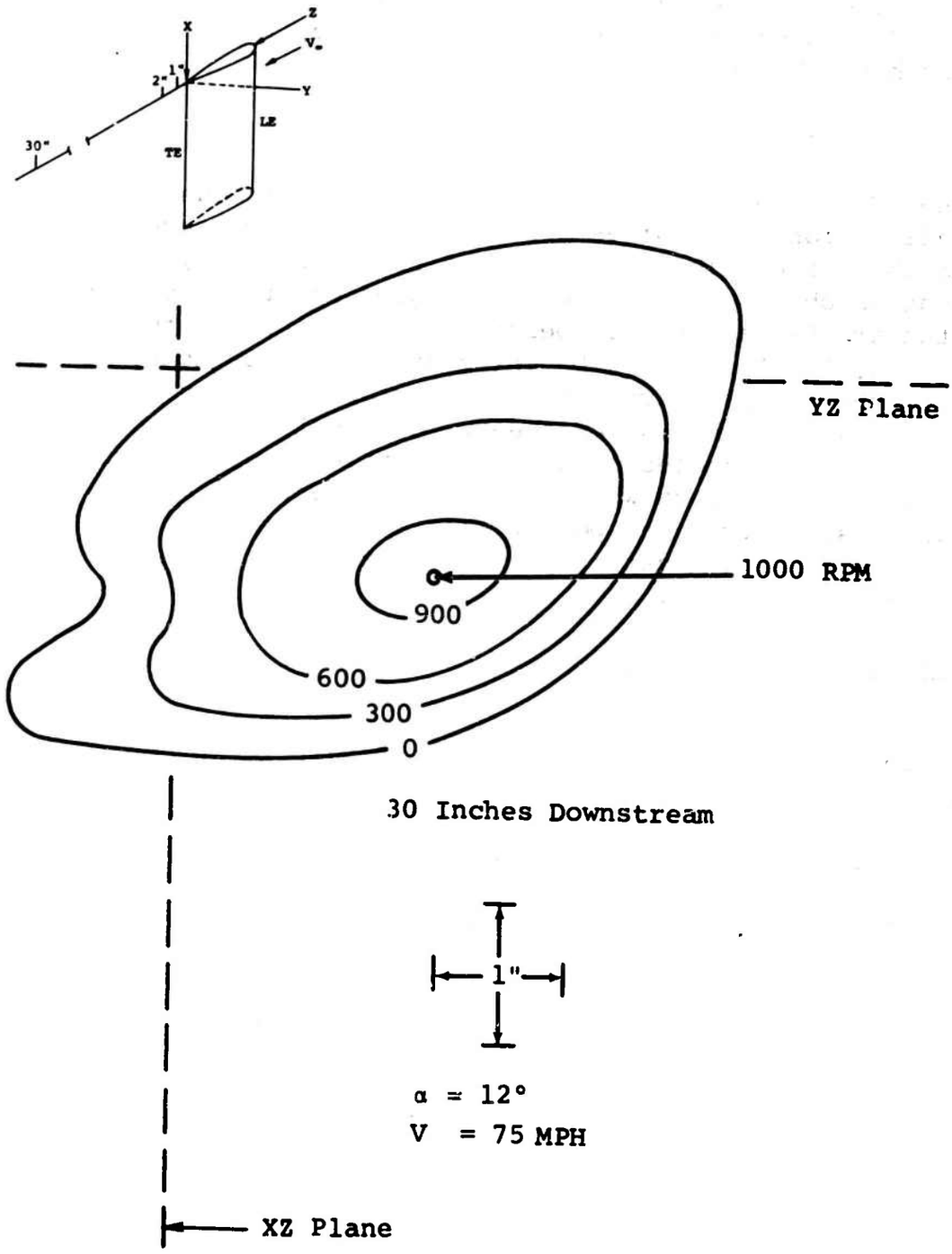

Figure 30. Contours of Constant Rotational Speeds 30 Inches Downstream From 40%-Porous Tip (Sheet 2 of 2)

From the computer program used to design the wing, the ratio $C\ell_0/C_L$ was determined to be 1.08. Hence, for a V of 75 miles per hour, Γ_0 should be

$$\Gamma_0 = 38.0\ C_L\ ft^2/sec. \tag{18}$$

When Equation 18 is reduced 20 percent to account for the probe calibration at 75 miles per hour, and then compared (Figure 31) to the circulation data obtained from vorticity, close agreement is obtained at the higher angles of attack between the standard tip and the 10-percent-porous tip. At the lower angles, the Γ obtained by integrating the vorticity is less than the midspan circulation, due probably to an incomplete rolling-up of the vortex sheet. However, the agreement shown at the higher angles lends considerable support to the creditability of the data which has been presented. Notice that the vortex sheet from the porous tips rolls up more slowly than that from the standard tip, due probably to the graduated loading at the tip.

PERFORMANCE EVALUATION

The decrease in the tangential component of the trailed vortex by core thickening has been achieved with an accompanying increase of the tip drag. This drag is directly realized as an increase in the power required for flight. However, the power required by a "banging" rotor (i.e., one which intersects a trailed vortex) has not been measured quantitatively but could conceivably be of the same order of magnitude as that required by adding tip drag. Thus, while the wind-tunnel measurements indicate an increase in power required for the subject tips, they do not take into account any power loss already inherent in a "banging" rotor, and the accompanying data might indicate a higher than actual value for the performance penalties of the subject tip configurations. An estimate of the power required by the tips in hover is presented below.

The drag coefficient at any angle of attack is related to

C_{D_0}, the zero angle coefficient, by

$$\Delta C_D^*(\alpha) = \Delta C_{D_0}\frac{S}{C^2} + \alpha^2\Delta\left(\frac{dC_{Dp}}{dC_L^2}\right)\left(\frac{dC_{L^2}}{d\alpha}\right)\frac{S}{C^2}$$

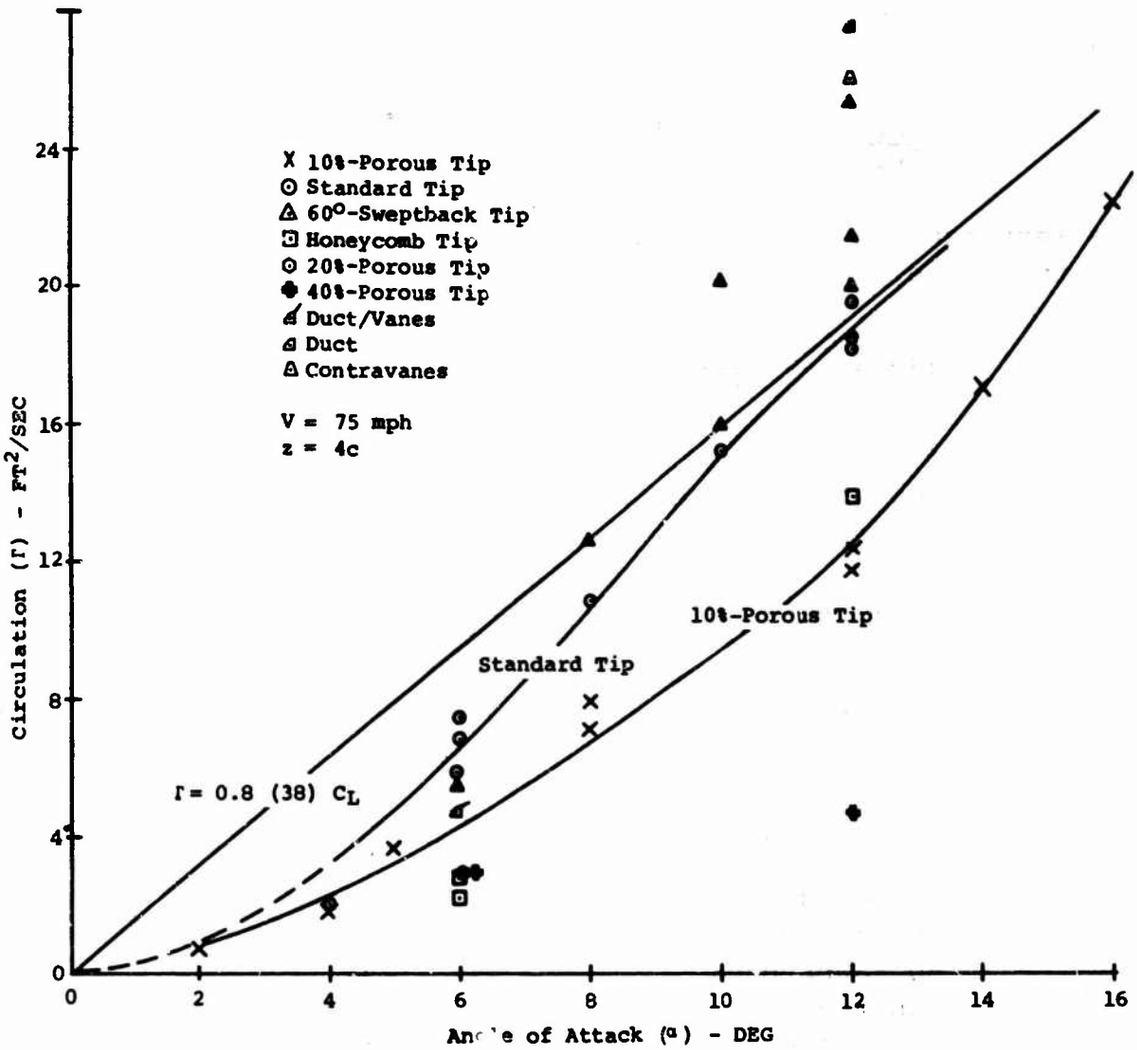

Figure 31. Circulation Determined From Vorticity Compared With Circulation Determined From Lift Measurements

where

$$\Delta C_{D_O} = C_{D_O\ (TIP)} - C_{D_O\ (STD)}$$

$$S = \text{Wing Area}$$

$$c = \text{Wing Chord}$$

$$\frac{dC_L}{d\alpha} = \text{Slope of the Lift Curve}$$

and

$$\frac{dC_{Dp}}{dC_L{}^2} = \frac{1}{\pi AR\varepsilon} - \frac{1}{\pi AR} .$$

The increment in power required relative to the standard tip may then be evaluated from

$$\Delta HP = \frac{\Delta C_D c^2 q\Omega Rb}{550} .$$

Estimates of the power required in hover are presented for a CH-47A helicopter with the following geometry and operating characteristics:

Gross Weight	=	28,500 pounds
Blade Radius	=	29.5 feet
Rotor rpm	=	230
No. of Blades	=	3
C	=	1.92 feet

Tip Configuration	ΔHP re Std Tip
Standard	0
Duct/Vanes	138
60°-Sweptback	-54
Contravanes	194
Honeycomb	689
10%-Porous	32
20%-Porous	120
40%-Porous	435

In forward flight, the power required will be the result of the added torque at the tip plus the increased drag of the rotor. This method has not been developed for the case of added rotor blade tips.

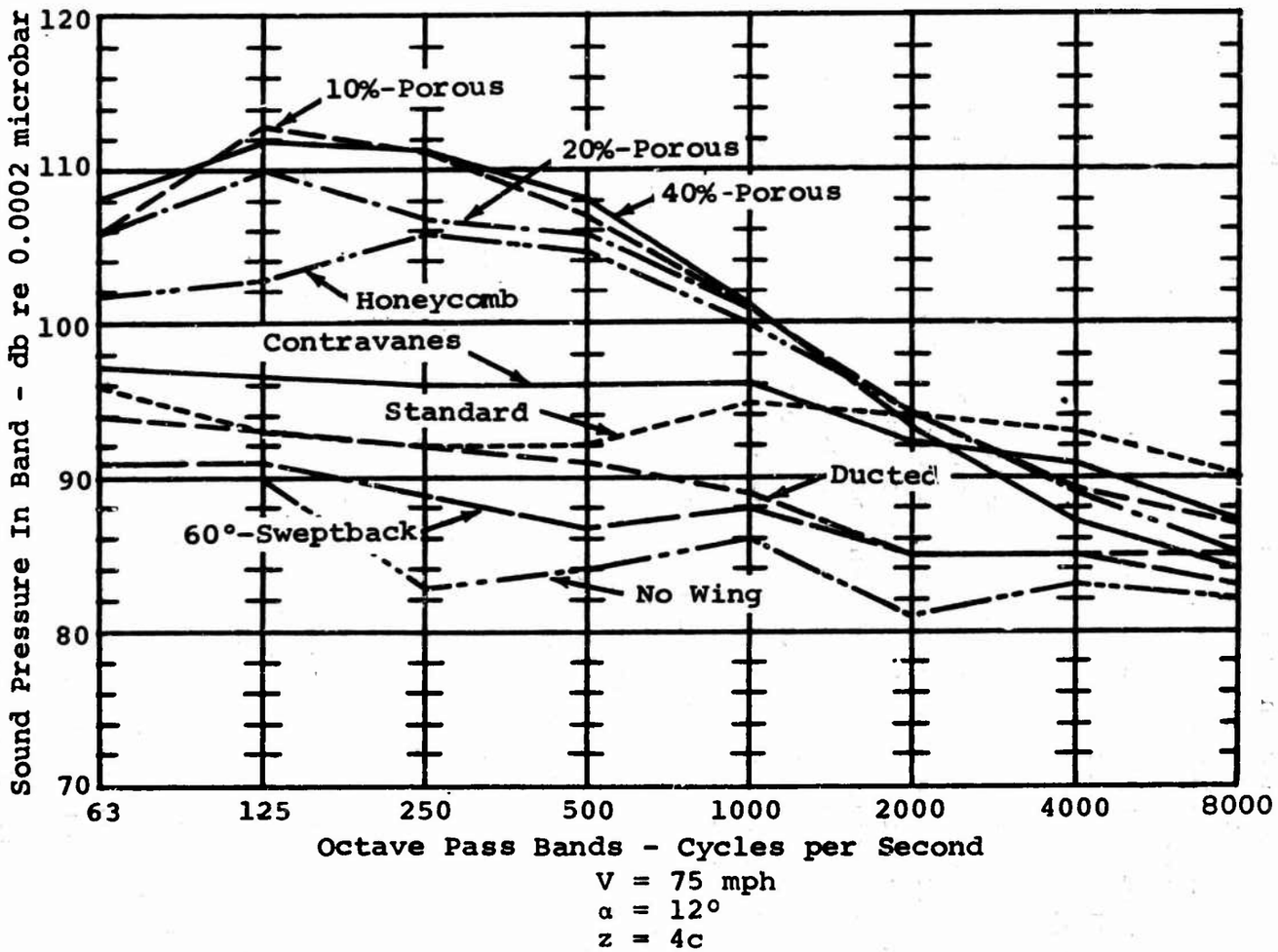

Figure 32. Sound Levels in Wakes of Flight Tip Configurations

NOISE-LEVEL MEASUREMENTS

Measurements of noise level were made in the wake of eight tip configurations at 75 mph and α = 12 degrees to evaluate the effect of vorticity on the generated sound levels (Figure 32). The noise obtained in the tunnel is of a continuous broad-band nature and not the sharp rotor bang which would be experienced by the interaction between the vortex and an intersecting rotor blade at speeds sufficient to cause shock wave formation. While no direct correlation with full-scale rotors was anticipated, it was felt that noise could be a measure of tip vortex strength.

Introduction of the wing into the tunnel causes boundary layer turbulence and tip vortex formation, both of which result in noise. The higher noise levels associated with the porous tips are probably due to increased boundary layer turbulence caused by surface roughness and may indicate that the general broad-band type of blade noise may increase. This, however, would be of secondary importance. The noise data do not always appear consistent; this may be due to the proximity of the microphone with respect to the vortex, which is an important factor in the measured noise level, and also due to shift in the path which the shed vortex takes with each tip configuration. In addition, for some configurations, the vorticity is concentrated over a small area; for other shapes, it is distributed over a large area. Thus the noise measured by a microphone in the wake of a weak vortex might be higher than the level measured by the same microphone located out of the wake of a strong vortex. No attempt was made to center the microphone in the wake of each tip configuration.

Figure 33 presents the sound level measurements for the 20-percent-porous tip at several angles of attack. A large increase in level is noted until an α of 6 degrees, above which the level remains essentially constant.

Figure 17 shows a similar relationship between vorticity and angle of attack, where a maximum vortex velocity is attained at some α below stall and may remain level, or even decrease, at still higher angles.

INTERPRETATION OF RESULTS

This program has investigated the maximum induced velocities in the trailed vortex for each wing tip by integrating the

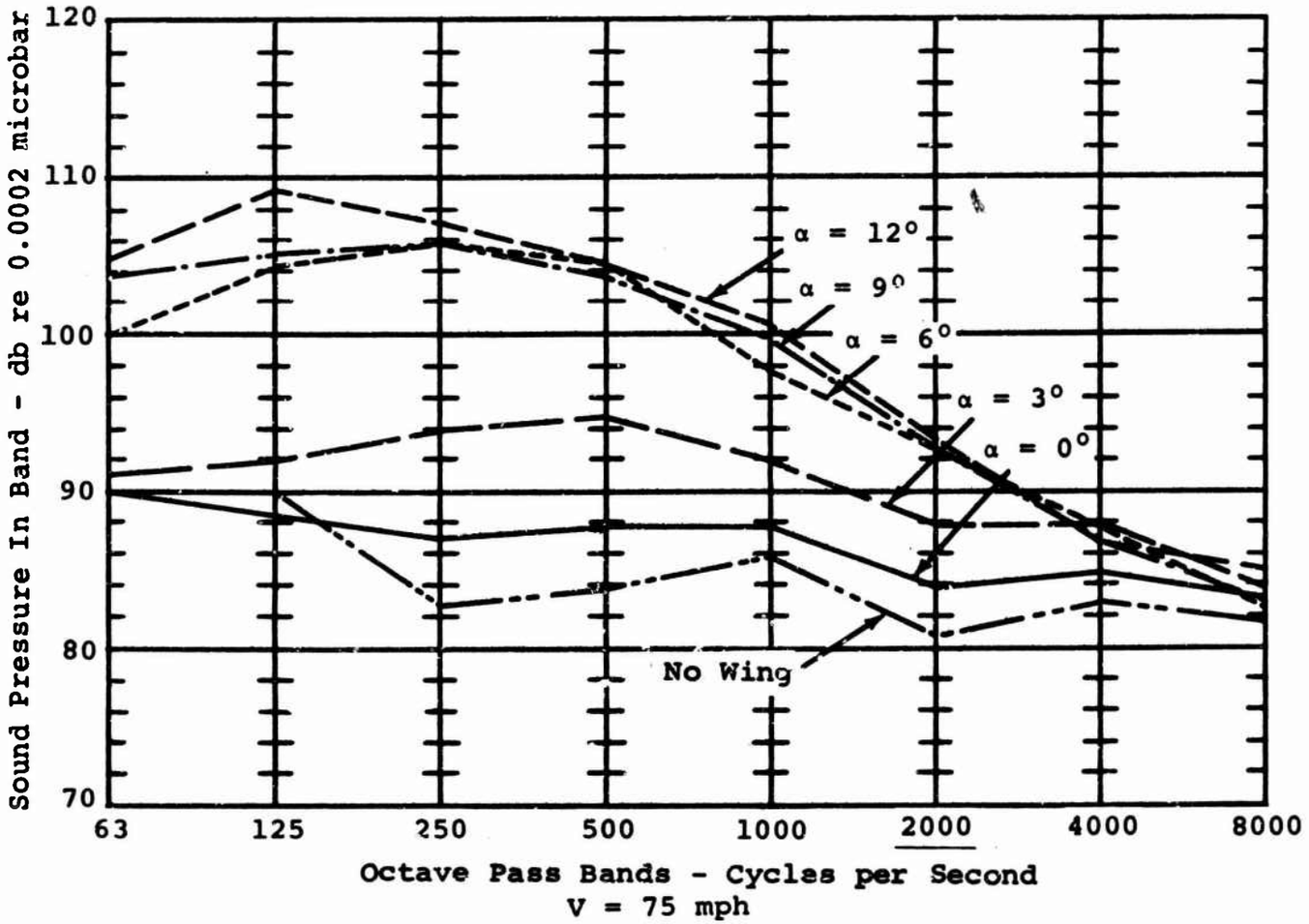

Figure 33. Effect of Angle of Attack on Noise Level of 20%-Porous Tip

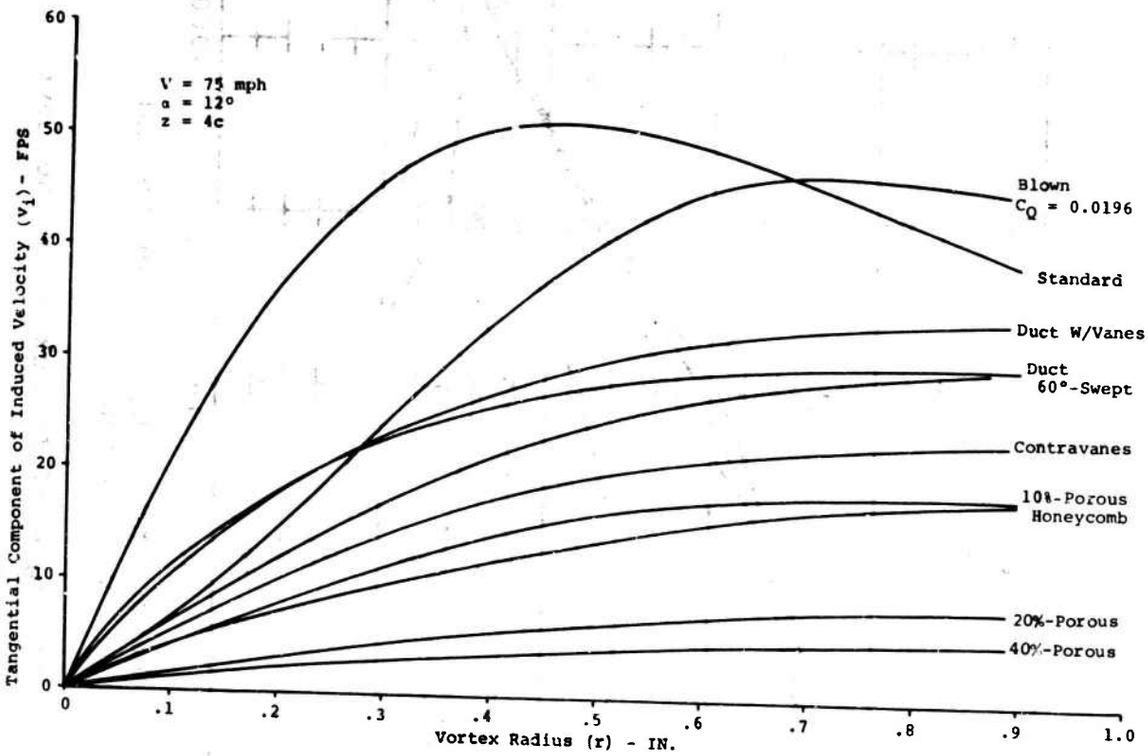

Figure 34. Tangential Component of Induced Velocity Variation for Ten Tip Configurations

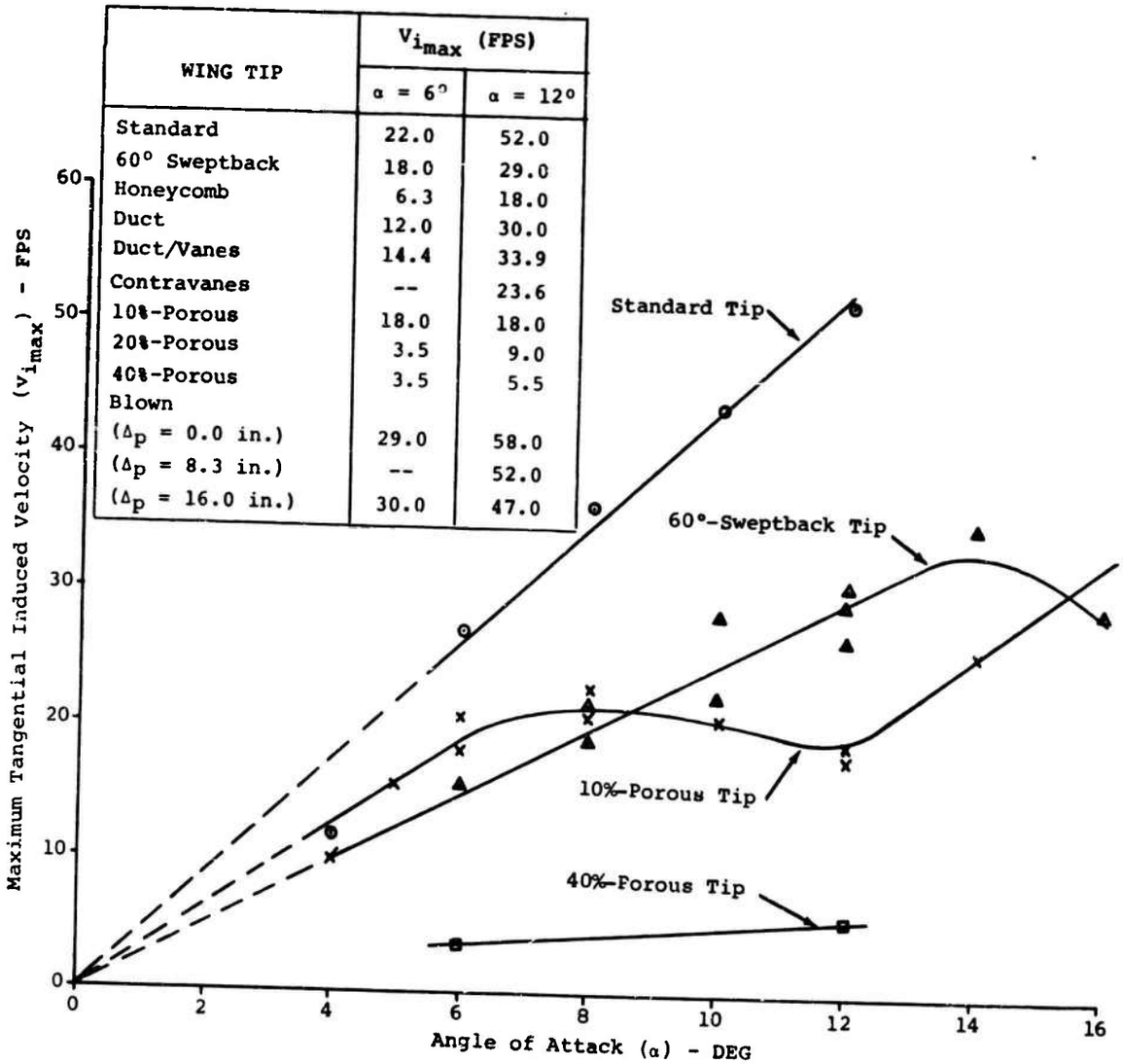

WING TIP	$V_{i_{max}}$ (FPS)	
	α = 6°	α = 12°
Standard	22.0	52.0
60° Sweptback	18.0	29.0
Honeycomb	6.3	18.0
Duct	12.0	30.0
Duct/Vanes	14.4	33.9
Contravanes	--	23.6
10%-Porous	18.0	18.0
20%-Porous	3.5	9.0
40%-Porous	3.5	5.5
Blown		
(Δ_p = 0.0 in.)	29.0	58.0
(Δ_p = 8.3 in.)	--	52.0
(Δ_p = 16.0 in.)	30.0	47.0

Figure 35. Maximum Induced Velocity as a Function of α

vorticity, as previously described. The results are presented in Figures 34 and 35.

The data have been presented as measured by the probe, without any corrections for calibration or finite size of the probe. With the exception of Figure 21, all of the curves are for 75 miles per hour, so they are directly comparable. Any values of vorticity, velocity or circulation read from these curves must be increased by 20 percent to obtain true values. The width of the vortices is not affected by the calibration. The calculated value of the exponent n will not depend on the probe calibration, since n is a function of the shape, not magnitude, of the vorticity distribution, and therefore does not depend on the correction for finite size of the probe. Generally, the wings with the more "pointed" vorticity distributions produced the lower n values. In fact, correcting a few selected distributions for finite size brought their values of n very close to the theoretical value of 2. Therefore, it seems that Equations 12 and 13, for the case where n = 2, are truly descriptive of the trailing vortex geometry. In this case the maximum tangential velocity can be obtained directly from Equation 13, as

$$v_{i_{max}} = .384\ w\zeta_o$$

$$v_{i_{max}} = .0846\ \frac{\gamma}{w}.$$

This occurs at a radius of 1.35 w.

Figure 34 shows the magnitude of velocity reduction achieved by core thickening due to the tips tested. Note that, in general, the lower maximum induced velocity curves peak at larger vortex radii, indicative of core thickening.

Figure 35 shows that, for the standard tips, velocity increases almost linearly with angle of attack, attaining its maximum value of over 52 feet per second at 12 degrees. For the 10-percent-porous tip and the 60-degree-sweptback tip, v_i again increases almost linearly with α; but for the 10-percent-porous tip, v_i is nearly constant between 6 degrees and 12 degrees, and actually decreases slightly at 12 degrees. The 40-percent-porous tip induces velocities about 1/10 those of the standard tip. Thus the porous tip seems to be a promising means of reducing the velocities associated with a trailing vortex system. A comparison of maximum induced velocities for the porous tips at 12-degree angle of attack is shown in Figure 36.

WING TIP	C_{D_O}	ε	$\frac{dC_l}{d\alpha}$	SEMI- WING AREA ($In.^2$)	AR
Standard	.015	.84	.053	138	4.70
60°-Sweptback	.015	.90	.062	148	5.82
Honeycomb	.025	.55	.059	138	4.70
Duct/Vanes	.017	.75	.056	146	4.95
Contravanes	.020	.90	.051	159	5.41
10%-Porous	.015	.77	.055	159	5.41
20%-Porous	.017	.77	.052	159	5.41
40%-Porous	.024	.51	.045	159	5.41
Duct	Data Not Available				
Blown	Data Not Available				

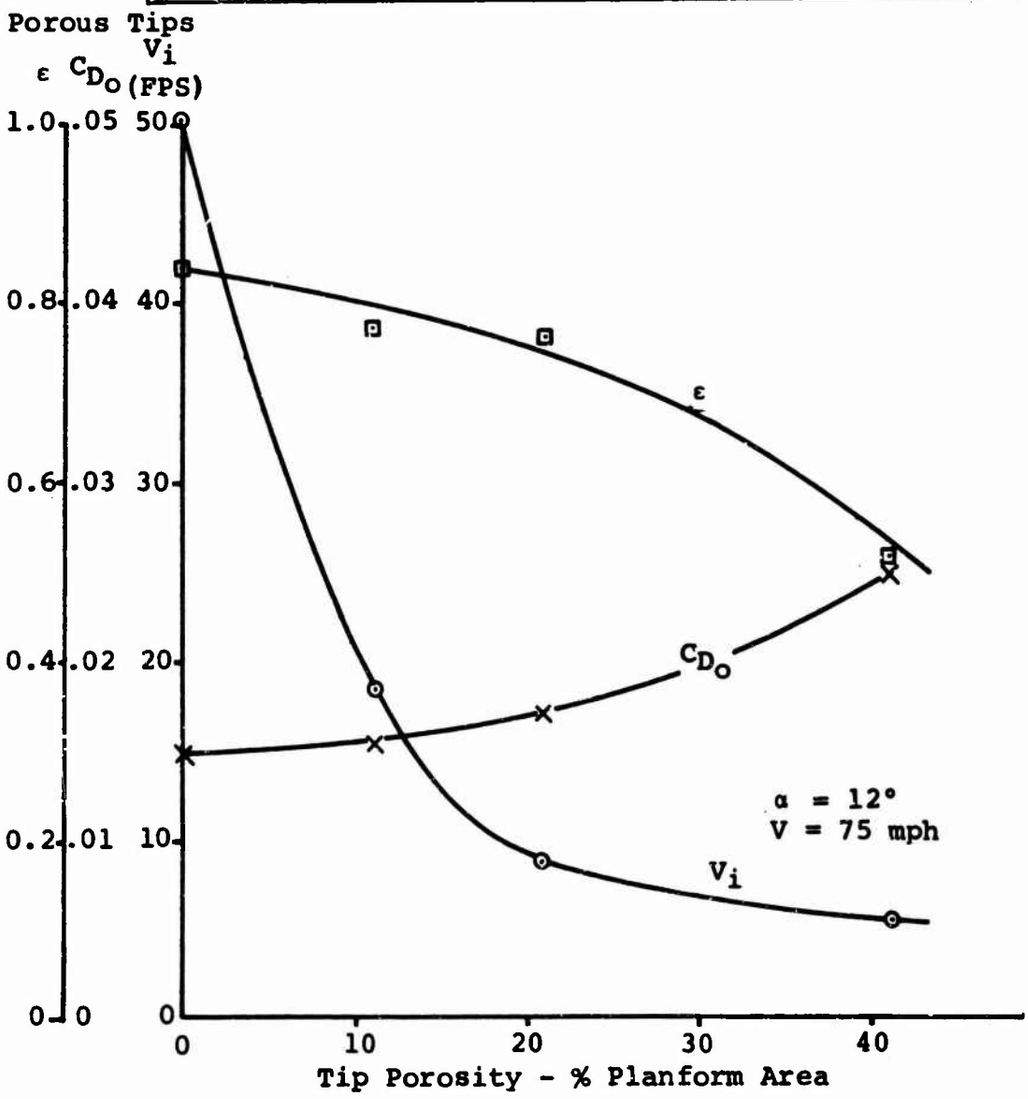

Figure 36. Lift and Drag Data

This reduction in v_i, however, is not gained without a penalty of increased drag. Lift and drag data for eight of the wing tips are given in Figure 36. C_{D_o} is the drag coefficient for $C_L = 0$, while ε is Oswald's span efficiency factor defined by

$$\varepsilon = \frac{C_L^2}{\pi AR\ (C_o - C_{D_o})} .$$

Plotting C_{D_o}, ε, and $v_{i_{max}}$ against porosity reveals that a porosity between 10 and 20 percent is probably the optimum; above 20 percent the rate of increase of C_{D_o} with respect to v_i appears to be prohibitive.

CONCLUSIONS

Conclusions which can be drawn from this program are:

1. Tangential velocities around trailing vortices can be at least as high as 57 percent of the free-stream velocity and can be significantly reduced by altering the tip shape.

2. The vorticity decreases exponentially with the square of the radius.

3. The width of the vortex increases nearly linearly with angle of attack. Depending on the tip configuration, the width may be from 5 to 10 percent of the chord.

4. The vorticity increases with α up to some α which is less than the stalling angle of attack, and then decreases for higher α. The α for maximum vorticity depends upon the tip shape and is apparently related to the tendency of the flow to separate locally. Vortex induced noise appears to follow a similar trend.

5. Thickening the vortex core to reduce the tangential velocity increases the drag and may increase the boundary layer noise.

6. The most promising means of reducing v_i seems to be the use of a porous tip. Compared to a standard tip, the induced velocity can be reduced by a factor of 10. This should lead to the elimination of blade bang, which, when it occurs, is the predominant rotor noise source.

7. Performance penalties are not clearly calculable, since the increase in drag predicted for the blade tips may be offset by a decrease in the power required for trailing rotor blades to intercept significantly reduced vortex core velocities.

REFERENCES

1. McCormick, B. W., On Cavitation Produced by a Vortex Trailing from a Lifting Surface, ASME Jour. of Basic Eng., September 1962, pp. 369-379.

2. May, D. M., The Development of a Vortex Meter, M. S. Thesis, The Pennsylvania State University, 1964.

3. Lamb, H., Hydrodynamics, London, New York, Cambridge University Press, 1932. Also published by Dover, 6th edition, pp. 590-592.

4. Rouse, H., and Hsu, H. C., On the Growth and Decay of a Vortex Filament, Proceedings, First National Congress of Applied Mechanics, 1951.

Unclassified
Security Classification

DOCUMENT CONTROL DATA - R&D
(Security classification of title, body of abstract and indexing annotation must be entered when the overall report is classified)

1. ORIGINATING ACTIVITY *(Corporate author)* Vertol Division The Boeing Company Morton, Pennsylvania	2a. REPORT SECURITY CLASSIFICATION Unclassified 2b. GROUP

3. REPORT TITLE

Tip Vortex Core Thickening for Application to Helicopter Rotor Noise Reduction

4. DESCRIPTIVE NOTES *(Type of report and inclusive dates)*

Final Report

5. AUTHOR(S) *(Last name, first name, initial)*

Spencer, Robert H. McCormick, Bernard W.
Sternfeld, Henry, Jr.

6. REPORT DATE	7a. TOTAL NO. OF PAGES	7b. NO. OF REFS
September 1966	89	4

8a. CONTRACT OR GRANT NO. DA 44-177-AMC-215(T) b. PROJECT NO. c. Task 1P121401A14801 d.	9a. ORIGINATOR'S REPORT NUMBER(S) USAAVLABS Technical Report 66-1 9b. OTHER REPORT NO(S) *(Any other numbers that may be assigned this report)* R-403A

10. AVAILABILITY/LIMITATION NOTICES

Distribution of this document is unlimited.

11. SUPPLEMENTARY NOTES	12. SPONSORING MILITARY ACTIVITY US Army Aviation Materiel Laboratories Fort Eustis, Virginia

13. ABSTRACT

Helicopter rotor noise levels are sharply increased when a rotor blade intercepts the rolled-up tip vortex trailed by a previous blade. This study deals with modification of the induced velocity structure of the vortex from both an analytical and an experimental standpoint. Ten tip configurations were evaluated in wind tunnel, to determine the magnitude of velocity reduction achievable. Results indicated that the maximum velocities induced within the vortex core could be reduced to about 12 percent of those for a standard tip (formed by revolving the tip airfoil section about the chordline and typical for many present generation helicopters). Drag data measured on the model wing for each blade tip indicate that most configurations adversely affect performance.

DD FORM 1 JAN 64 1473

Unclassified
Security Classification

Unclassified
Security Classification

14. KEY WORDS	LINK A ROLE	LINK A WT	LINK B ROLE	LINK B WT	LINK C ROLE	LINK C WT
Helicopter Rotor Noise Reduction						
Tip Vortex Core Thickening						

INSTRUCTIONS

1. ORIGINATING ACTIVITY: Enter the name and address of the contractor, subcontractor, grantee, Department of Defense activity or other organization *(corporate author)* issuing the report.

2a. REPORT SECURITY CLASSIFICATION: Enter the overall security classification of the report. Indicate whether "Restricted Data" is included. Marking is to be in accordance with appropriate security regulations.

2b. GROUP: Automatic downgrading is specified in DoD Directive 5200.10 and Armed Forces Industrial Manual. Enter the group number. Also, when applicable, show that optional markings have been used for Group 3 and Group 4 as authorized.

3. REPORT TITLE: Enter the complete report title in all capital letters. Titles in all cases should be unclassified. If a meaningful title cannot be selected without classification, show title classification in all capitals in parenthesis immediately following the title.

4. DESCRIPTIVE NOTES: If appropriate, enter the type of report, e.g., interim, progress, summary, annual, or final. Give the inclusive dates when a specific reporting period is covered.

5. AUTHOR(S): Enter the name(s) of author(s) as shown on or in the report. Enter last name, first name, middle initial. If military, show rank and branch of service. The name of the principal author is an absolute minimum requirement.

6. REPORT DATE: Enter the date of the report as day, month, year; or month, year. If more than one date appears on the report, use date of publication.

7a. TOTAL NUMBER OF PAGES: The total page count should follow normal pagination procedures, i.e., enter the number of pages containing information.

7b. NUMBER OF REFERENCES: Enter the total number of references cited in the report.

8a. CONTRACT OR GRANT NUMBER: If appropriate, enter the applicable number of the contract or grant under which the report was written.

8b, 8c, & 8d. PROJECT NUMBER: Enter the appropriate military department identification, such as project number, subproject number, system numbers, task number, etc.

9a. ORIGINATOR'S REPORT NUMBER(S): Enter the official report number by which the document will be identified and controlled by the originating activity. This number must be unique to this report.

9b. OTHER REPORT NUMBER(S): If the report has been assigned any other report numbers *(either by the originator or by the sponsor)*, also enter this number(s).

10. AVAILABILITY/LIMITATION NOTICES: Enter any limitations on further dissemination of the report, other than those imposed by security classification, using standard statements such as:

(1) "Qualified requesters may obtain copies of this report from DDC."

(2) "Foreign announcement and dissemination of this report by DDC is not authorized."

(3) "U. S. Government agencies may obtain copies of this report directly from DDC. Other qualified DDC users shall request through _____."

(4) "U. S. military agencies may obtain copies of this report directly from DDC. Other qualified users shall request through _____."

(5) "All distribution of this report is controlled. Qualified DDC users shall request through _____."

If the report has been furnished to the Office of Technical Services, Department of Commerce, for sale to the public, indicate this fact and enter the price, if known.

11. SUPPLEMENTARY NOTES: Use for additional explanatory notes.

12. SPONSORING MILITARY ACTIVITY: Enter the name of the departmental project office or laboratory sponsoring *(paying for)* the research and development. Include address.

13. ABSTRACT: Enter an abstract giving a brief and factual summary of the document indicative of the report, even though it may also appear elsewhere in the body of the technical report. If additional space is required, a continuation sheet shall be attached.

It is highly desirable that the abstract of classified reports be unclassified. Each paragraph of the abstract shall end with an indication of the military security classification of the information in the paragraph, represented as *(TS)*, *(S)*, *(C)*, or *(U)*.

There is no limitation on the length of the abstract. However, the suggested length is from 150 to 225 words.

14. KEY WORDS: Key words are technically meaningful terms or short phrases that characterize a report and may be used as index entries for cataloging the report. Key words must be selected so that no security classification is required. Identifiers, such as equipment model designation, trade name, military project code name, geographic location, may be used as key words but will be followed by an indication of technical context. The assignment of links, rules, and weights is optional.

Unclassified
Security Classification

6011-66